Numerical and deterministic analyses of rainfall-induced slope failures in small catchment scale

Ehime University
Graduate School of Science & Engineering

Kiran Prasad Acharya

Numerical and deterministic analyses of rainfall-induced slope failures in small catchment scale

by

Kiran Prasad Acharya

A Dissertation

Submitted in Partial Fulfillment of the Requirements for the Degree of

Doctor of Engineering

In

Graduate School of Science and Engineering,

Ehime University

3 Bunkyo-Cho Matsuyama, Ehime, Japan

March 2014

Numerical and deterministic analyses of rainfall-induced slope failures in small catchment scale

Supervisor
***Professor* Dr. Ryuichi YATABE**

Dissertation Committee
***Professor* Dr. Ryuichi YATABE**
***Professor* Dr. Mitsu OKAMURA**
***Associate Professor* Dr. Hideaki YASUHARA**

Certificate

This is to certify that the dissertation entitled, "Numerical and deterministic analyses of rainfall-induced slope failures in small catchment scale" presented by Mr. Kiran Prasad Acharya in partial fulfillment of the academic requirement of the Doctoral degree in Engineering of Special Graduate Course on Disaster Mitigation studies for Asian Students has been examined and accepted by the evaluation committee at Graduate School of Science and Engineering of Ehime University.

Dr. Ryuichi Yatabe
Professor
Graduate School of Science and Engineering
Ehime University
Supervisor

Dr. Mitsu Okamura
Professor
Graduate School of Science and Engineering
Ehime University
Sub-supervisor

Dr. Hideaki Yasuhara
Associate Professor
Graduate School of Science and Engineering
Ehime University
Sub-supervisor

This Ph.D. thesis is dedicated to my parents, brothers Ananda and Sushil, and wife Bimala

Abstract

The objective of this Ph.D. research was to evaluate rainfall-induced slope failure and potential instability in small catchment scale. For this, a tertiary sedimentary terrain in northeastern hills of Niihama city in Ehime prefecture of Japan was selected as study area. In 2004, this area suffered an extensive slope failure damage due to extreme typhoon rainfalls. To fulfill the objective, the research was carried out in three parts: i) seepage and slope stability modeling of rainfall-induced slope failures in topographic hollows, ii) deterministic slope failure hazard assessment in a catchment and its replication in neighborhood catchments, and iii) numerical analysis on influence of basic parameters of topography on hillslope instability in catchment scale.

With rainfall infiltration, subsurface hydrology of hillslopes changes through saturated-unsaturated interactions. This leads to triggering of slope failure. The subsurface hydrologic response to rainfall and triggering mechanism in medium to steep slopes of topographic hollow are complex/dynamic phenomena as the topographic hollows undergo continuous morphological change through various processes (i.e., surface wash, soil creep, windthrow, surface ravel of soil and organic material, sloughing of material around the perimeter of the scar, and detrital deposits from established vegetation). The build up of porewater pressure and instability repeat cyclically in topographic hollows which is the main cause for complex/dynamic nature of slope failure triggering in topographic hollows. However, the research on subsurface hydrology and instability in topographic hollows is not getting much attention in recent landslide studies. In this regard, the first part of this research performs two-dimensional numerical modeling of slope failures in topographic hollows so as to investigate contribution of hollow hydrology in causing slope failure. For this, a small catchment, known as Higashifukubegawa of Niihama of tertiary sedimentary terrain, western Japan was selected. In this catchment, a total of seven slope failures occurred in seven topographic hollows during 2004 extreme typhoon rainfall events of various intensitues. Numerical modeling of seepage and slope stability was performed in hillslope profiles passing through the seven slope failure locations and topographic hollows in GeoStudio (2005). The results of numerical modeling were interpreted in terms of transient porewater pressure distribution and factors of safety within the predefined slip surfaces at various typhoon rainfall hours. The innovative element in the first part of this research was that a threshold relationship between topographic hollow area and maximum porewater pressure was established based on two-dimensional seepage analysis. This

relation is thought to be helpful in prediction of maximum porewater pressure in topographic hollows.

The second part of this research highlights problems in current approaches of slope failure hazard assessment and replication in catchment scale, and then focuses on a methodology for preparation as well as replication of catchment-scale deterministic slope failure hazard model. For small areas, like a small catchment, hydrological and geo-mechanical parameters of soil, required for deterministic slope failure hazard modeling, can be prepared. However, replication of deterministic hazard model from one catchment to other catchments is almost impossible since similar set of hydrological and geo-mechanical parameters are also required in other catchments. To solve this problem, the second part of study couples deterministic and statistical regression methods. In result, the slope failure hazard maps were obtained in forty test catchments in the selected area through replication of deterministic model prepared in Higashifukubegawa which showed a moderate to good prediction accuracy with existing slope failures inventories of test catchments. The novelty of the second part of research is successful replication of the deterministic model through parameters-based regression modeling or without using geo-mechanical and hydrological parameters.

Hundreds of studies could be reviewed in literatures which have investigated the influence of parameters and boundary conditions affecting hydrological and geo-mechanical processes occurring in soil through field/laboratory investigation and numerical modeling. However, influence of basic parameters of topography could be found only partially investigated/presented in a few of them. In this context, the third part of research thoroughly investigates hydrological and instability phenomena in GeoStudio (2005) platform in relation to variation in values of basic parameters of topography within their range of variation in Higashifukubegawa catchment. In result, porewater pressure and factor of safety were found varying regularly and with parallel trend. The change in porewater pressure and slope mass weight due to variation in values of basic parameters was used to interpret the change in the determined factors of safety. So, this part of research demonstrates how subsurface hydrology and hillslope instability change with change in values of basic parameters of topography under the same simulating conditions of hydrological and geo-mechanical parameters.

Overall, how the hydrological (subsurface storm flow and water table dynamics) and geo-mechanical influence the slope failure occurrence or slope instability phenomena in less cohesive shallow soil-mantled hillslopes of topographic hollows and slope failure

hazard assessment in small scale catchments, can be understood from this thesis. The rainfall induced slope failures were evaluated realistically through hydro-geo-mechanical approach.

Acknowledgements

I should express my deepest gratitude and sincere thanks to a number of people who inspired and supported me to complete Ph.D. research. First and foremost, I would like to express my profound gratitude to my Professor Dr. Ryuichi Yatabe for his supervision and many fruitful discussions during my study. Without his continuous and invaluable support, this research would not have been possible. I found lucky myself to work with a supervisor like Professor Yatabe.

Next, I would like to extend my gratitude to Professor Dr. Mitsu Okamura and Associate Professor Dr. Hideaki Yasuhara for their encouragement and suggestion in research.

I gratefully acknowledge Assistant Professor Dr. Netra Prakash Bhandary for his excellent suggestions, kind support, and constant interest on me through out the Ph.D. period. He is my one of the inspirations I follow this topic of research. More importantly, his insightful comments during the Ph.D. seminars and study period were really helpful to refine my work. Appreciation by words is insufficient for him.

I would like to express my sincere gratitude to Associate Professor Dr. Ranjan Kumar Dahal, of Tribhuvan University, Nepal for sharing some of his expert knowledge with me. He was always available for me when I needed his help.

I am thankful to Mr. Masatoshi Anakura and Dr. Manita Timilsina (former graduate students of Ehime University) for their help in data preparation required for this research. Without their cooperation, this study would not have been completed.

My eternal gratitude goes to my father, mother, and brothers (Ananda and Sushil) for their encouragement through out the study period despite their physical absence.

Last but not least, I want to thank to my faithful wife Bimala whose unconditional infinite love, dedication, sacrifice, companionship, and invaluable backing helped in the successful completion of my Ph.D. study.

Contents

List of Tables

List of Figures

Chapter 1

Introduction

1.1 Background and research problem statement

Consideration of saturated soil conditions in design of geotechnical structures is fundamental in soil mechanics as the designs are aimed at weakest soil strength. The pioneer studies in soil mechanics, like Terzaghi (1943), Skempton et al. (1960), Bishop (1955), Fredlund and Morgenstern (1977) etc. have tackled slope stability problems treating soil at saturated state. Also in most of the previous studies of shallow landslide, landslide initiation has been presented as to occur under only saturated state. The concept that soil slope can fail in unsaturated condition was highlighted in soil mechanics after Fredlund 1973. The studies before 1973 were, therefore, incomplete to describe slope stability, landslide triggering mechanism and spatial occurrence of landslide hazard. The unsaturated soil mechanics has been receiving sufficient acceptance worldwide after a first text book on unsaturated soils `Soil Mechanics for Unsaturated Soils` was published by DG Fredlund and H Rahardjo in 1993. Some studies, like Brand (1984), Fourie 1996 etc. have concluded that design and construction of saturated soil slopes can not be applied successfully for the slopes under unsaturated condition. In recent decades, extensive studies were performed through geomorphological, hydrological and geo-mechanical approaches relating rainfall, saturated/unsaturated soil properties, and subsurface hydrology so as to understand landslide triggering phenomena. But, the existing studies were case studies from different geographical locations of the world and they have suggested fairly different conclusions on the same problem of landslide triggering (Gofar et al. 2009).

There exists complex dynamic interaction between climatic conditions and various parameters forming topography which govern two particular mechanisms occurring in soil: subsurface hydrological and geo-mechanical change. Several other mechanisms are associated these two mechanisms which must be treated as integrated mechanism. The main problem in existing studies is that they have treated each mechanism separately (Gofar et al. 2009). Majority of the methodologies were developed based on laboratory and field test. The methodologies have their own limitations in term of sample size and the target area. Furthermore, most of the methodologies involve numbers of parameters which are problematic to estimate accurately. Even with the use of exixting

software, it has not been possible to treat different mechanisms singly or in integrated form (Gofar et al. 2009).

Global warming is continuously increasing in recent years and climatic conditions are changing worldwide. Change in climatic conditions cause variation in geomorphology and soil properties. This directly affects rainfall infiltration through soil. Estimating subsurface zone moisture storage change with rainfall infiltration is complex problem since variation in soil properties alters seepage path, and therefore groundwater level. Due to these reasons, to predict where and when a slope will fail or how big a slope failure will be has become more complex. On the other hand, subsurface mechanisms trying to cause failure in a slope may not be exactly same to that in other slope within the same area. Nature of failure might differ in the same location after many landslides had occurred in the past. The depth, length, and width of landslide have not yet been possible to predict through available numerical modeling programs. Therefore, previous studies on mechanism of landslide triggering employing historical record of landslide and rainfall are still considered to be insufficient to fully describe dynamic nature of landslide triggering. Mechanism of landslide triggering has still been an inadequately explored topic of research. In this context, some more studies are necessary with time to explore dynamic mechanism of landslide triggering.

Landslides most commonly occur on unchanneled topography or topographic hollows as evidence of ongoing geomorphic development of valley heads. They mainly take place on uppermost part of hollows i.e., near slope crests. With repetition of landslides, there is sustaining growth of hillslope depression which, in turn, determines the persistent spacing of topographic hollows in drainage basins (Tsukamoto 1973, Matshushi 2006). The subsurface storm flow on steep soil-mantled hillslopes of topographic hollows is first order control on landslide initiation. Investigating dynamic subsurface storm flow in topographic hollows is much more complex. However, topographic hollows are poorly reflected in recent landslide research and hydrologic regime in topographic hollows has not been so well investigated except in some good studies.

There has been a problem in catchment-scale shallow landslide hazard assessment as well as replication. In literature, this problem has been fairly acknowledged. The three methods: heuristic, statistical and deterministic have been used worldwide for landslide hazard assessment. However, in many past studies, hazard assessment has been done without considering appropriateness of method. Heuristic methods can be used for landslide hazard assessment, but replication of heuristic hazard models is almost

impossible as these are fully based on expert's opinion on conditions of employed parameters, and therefore degree of hazard. Different from heuristic method, statistical methods are suitable for both landslide hazard assessment and replication. These are considered robust for hazard assessment mainly in larger areas because these need significant variation in geological and geomorphological parameters which is generally found in larger areas. But, for smaller areas, like catchments, geological and geomorphological conditions are fairly homogenous and accurate results on spatial prediction of landslide hazard may not be obtained by applying statistical methods. In such condition, landslide hazard analyses can be done with deterministic methods. Deterministic analyses are performed through geo-mechanical and hydrological parameters of soils determined from laboratory experiments on soil samples retrieved from field rather than geological and geo-morphological parameters. A detailed variation in geo-mechanical and hydrological parameters can be found and a large amount of data can be collected even from small catchments. However, replication of deterministic models from one catchment to other catchments is problematic since exactly similar geo-mechanical and hydrological parameters also have to be prepared in other catchment which is much costly and difficult. Therefore, any of the methods described above can not be used with ease for both landslide hazard assessment and replication of landslide hazard model in small catchment scale.

Knowledge on influence of parameters affecting failure or hillslope instability becomes primary for both slope stability and landslide hazard study. Influence of various hydrological (soil permeability, porosity) and geo-mechanical parameters (soil cohesion, root cohesion, and unit weight of soil) have been studied and well discussed in hundreds of past studies under various boundary conditions. However, the influence of basic parameters forming topography could be found only partially acknowledged in a few of them. Basic parameters of topography, such as slope inclination, slope length, and soil depth are proxy to describe subsurface porewater pressures and flow path dynamics or to characterize initial conditions for soil water storage prior to rainfall events. However, no earlier to recent study has presented detail investigation on influence of these parameters on hillslope subsurface hydrology and instability.

1.2 Research objectives

Understanding various problems, this Ph.D. research mainly focuses on subsurface hydrology and instability in topographic hollows, slope failure hazard assessment and replication in small catchments, and analysis of basic parameters of topography affecting

hillslope instability. The aim of this study is to evaluate rainfall-induced slope failure and potential instability during extreme rainfall under the influence of topographical, hydrological and geo-mechanical parameters. For this, extreme typhoon rainfall region of Shikoku Island of Japan was considered. Figure 1.1 shows the conceptual research flow of this study.

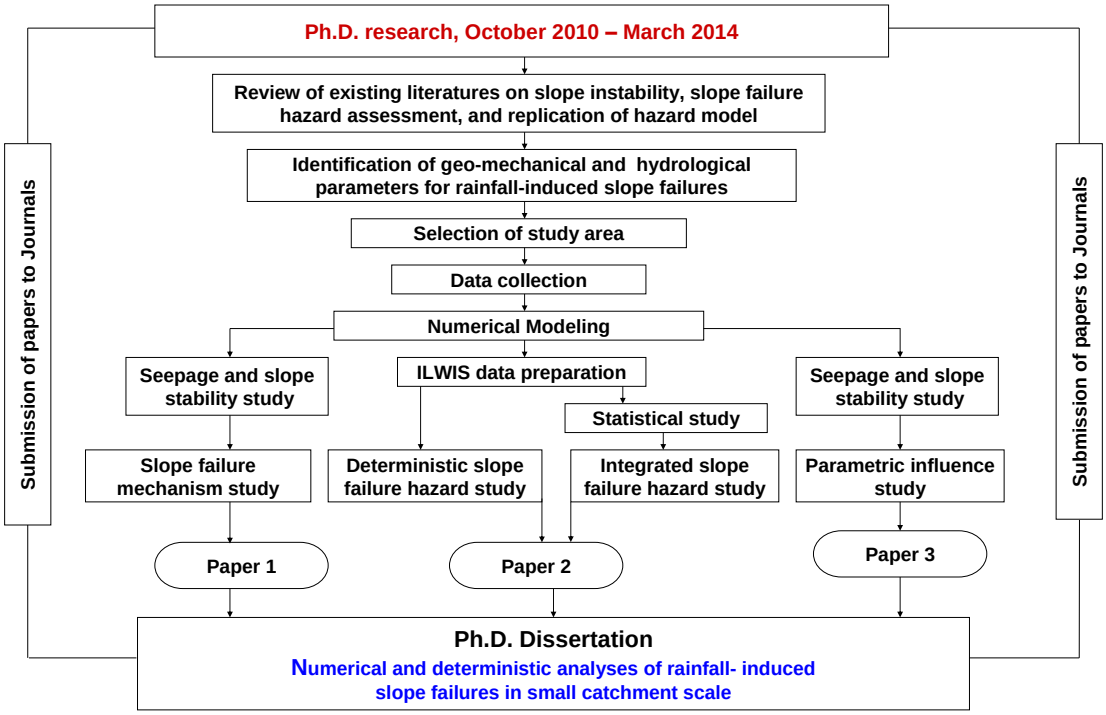

Figure 1.1 Research flow of this study

The objectives of this study can be given as below.

Objective 1

To explore triggering mechanism of rainfall-induced slope failures in topographic hollows. This objective is divided into several sub-objectives:

(i) to understand geological, geo-morphological and climatic conditions on selected area which had favored slope failures in the past during extreme typhoon rainfall,

(ii) to understand hydrological and geo-mechanical properties of soil in slope failure spots,

(iii) to perform transient hydrological modeling along failed mass in topographic hollows so as to bridge different mechanisms favoring slope failure,

(iv) to link topographic hollow parameters with dynamic subsurface hollow hydrology, and

(v) to investigate variation of porewater pressure as well as factor of safety in various hours of typhoon rainfall to know the time of occurrence of slope failure.

Objective 2

To present replication procedure for a slope failure hazard model in small catchments. In specific, it studies

(i) to prepare a deterministic slope failure hazard model in a catchment based on the geo-mechanical and hydrological properties of soils obtained from various field/laboratory experiments,

(ii) to replicate the deterministic slope failure hazard model in other catchments without using geo-mechanical and hydrological properties, and

(iii) to replicate the slope failure hazard model with high accuracy.

Objective 3

To evaluate effect of basic parameters of topography on hillslope instability. For simplicity, it can be divided into following.

(i) To understand hydrologic response of shallow coarse-grained unsaturated soil slopes of a catchment to heavy rainfall, and

(ii) to thoroughly investigate change in factor of safety and porewater pressure in hillslope profiles by varying values of basic parameters of hillslopes under same simulating conditions of hydrological and geo-mechanical parameters.

1.3 Organization of thesis

Including this introductory chapter about research problems and research objectives, this thesis contains seven more chapters. **Chapter 2** presents a comprehensive review on shallow landslide triggering. It discusses past studies on rainfall threshold, positive porewater pressure, negative porewater pressure, and perched ground water table for shallow landslide initiation. This chapter also covers various landslide modeling programs and approaches in both local and regional scale. Brief information about geology, geomorphology, and climate of Shikoku Island, where study areas for this research were selected, is given in **Chapter 3**. **Chapter 4** presents an overview of slope failures that occurred in four prefectures of Shikoku Island during extreme typhoon rainfalls of 2004.

Chapter 5, **6** and **7** address objective 1, 2, and 3 respectively. These chapters are based on papers published and/or submitted to peer reviewed journals (introduction, study area, methodology, results, discussion, and conclusions). Numerical simulation using limit equilibrium and finite element methods for slope instability analyses and slope failure

hazard assessment are highlighted in these chapters. In detail, coupled hydrological-slope stability model [SEEP/W, SLOPE/W (GeoStudio 2005)] was applied to investigate triggering of slope failures within topographic hollows in a small catchment in **Chapter 5**. The contribution of hollow subsurface hydrology on instability was well studied and discussed through two-dimensional hydrological-slope stability modeling in this chapter. The detail about preparation of a deterministic slope failure hazard model in a catchment and its replication in neighborhood catchments coupling three models: dynamic hydrological model, infinite slope model, and statistical regression model is presented in **Chapter 6**. In **Chapter 7**, how hillslope subsurface hydrology and instability change with variation in values of basic parameters of topography was thoroughly investigated and presented.

In **Chapter 8**, the major findings/conclusions of this thesis are summarized, together with limitations and recommendations for future research.

Chapter 2

Literature review

2.1 Introduction

This Chapter provides a comprehensive review on literatures which are relevant to this research. It presents those significant case studies reported from various regions of the world which studied landslide triggering phenomena and landslide hazard assessment. Particular attention has been paid to various modeling programs and approaches used by past researchers for local- and regional-scale landslide modeling.

2.2 Landslide triggering scenario

Landslides are geomorphic processes that shape landscape evolution. In mountainous topographies, they represent the most important hazard. Various hydrological and geo-mechanical parameters of soil play role in causing landslide. But, for initiation of landslide, triggering agent is necessary. Examples of triggering agents are geological events (seismic shaking due to volcanic eruption, earthquake), hydrological events (e.g., rainfall, snow melt or water level change in rivers or lakes at the foot of slopes), and human interventions (excessive loading and improper slope cutting). It is almost impossible to predict triggering events. The most common trigger is rainfall. Rainfall is important for occurrence of both shallow and deep-seated landslides. In the following, first the rainfall threshold for triggering landslide is described.

Rainfall threshold can be defined as the minimum amount of rainfall after crossing which landslide is sure to occur (Dahal 2008). Significance of defining rainfall threshold is that it can be used in early warning system (Clark 1987). Rainfall threshold for triggering landslide differs from one region to another based on hydro-climatological and geophysical properties, such as regional and local rainfall characteristics and patterns, lithology, slope morphometry, soil characteristics, lithology, morphology, climate, geological history, time, and change in vegetation pattern (Crosta 1998, Crozier 1999). Crozier and Preston (1999) observed that resistance to further triggering may occur after many movements had occurred. The Rainfall threshold can be broadly divided into two types: empirical or statistical and physical threshold.

Empirical rainfall threshold: Empirical or statistical methods are used to determine rainfall threshold when sufficient data on landslide occurrence and rainfall conditions are available (Thiebes 2011). Empirical thresholds are expressed as rainfall intensity and duration or cumulative and antecedent rainfall. These are defined as the line fitting minimum intensity of rainfall associated with the occurrence of landslide in various areas (Caine 1980). But according to Terlien (1998), the rainfall events that do not cause failure should also be noted. Therefore, minimum and maximum probability thresholds should be acquired. The rainfalls below the minimum probability threshold never trigger failure, but the rainfalls above maximum probability threshold always cause failure (Glade 1997, Glade 1998). Between minimum and maximum value of thresholds, failure may occur under certain circumstances. Caine (1980) is pioneer study in the field of empirical rainfall threshold determination. Rainfall threshold determined in this study is based on rainfall intensity and duration analyses. After Caine (1980), many researches were projected which defined rainfall threshold for triggering landslide (Jakob and Weatherly 2003, Gabet et al. 2004, Matshushi 2006, Chang et al. 2007, Dahal and Hasegawa 2008, Frattini et al. 2009, Guzzetti et al. 2007, 2008).

Empirical threshold for initiation of landslide has been broadly discussed into three types: global, regional, and local thresholds by Guzzetti et al. 2007. Global threshold (Caine 1980, Innes 1983, Clarizia et al. 1996, Cannon and Gartner 2005, Guzzeti et al. 2008) includes a general minimum level below which landslides do not occur. Local morphological, lithological and land use conditions and local or regional rainfall pattern/history are not considered while defining global threshold. Regional thresholds cover areas extending from a few to several thousand square kilometers of similar meteorological, climatic, and physiographic characteristics. These are potentially suitable to use in landslide warning systems based on quantitative spatial rainfall forecasts, estimates, or measurements (Guzzetti et al. 2007). Local thresholds are applicable to single landslides or to group of landslides in areas extending from a few to some hundreds of square kilometers. These consider local climatic unit and geomorphological setting. Regional and local thresholds can be well implemented in the area where they were developed, but cannot be easily extrapolated to adjacent regions (Crosta 1998). Giannecchini et al. 2012 defined the critical rainfall thresholds for the Middle Serchio River Valley and compared it with the local, regional and global curves proposed by various authors. The results of their analysis suggested that landslide activity initiation requires a higher amount of rainfall and greater intensity in their study area than elsewhere.

Antecedent rainfalls also play important role in determining empirical rainfall threshold (Johnson and Sitar 1990, Crozier 1999, Godt et al. 2006). Antecedent Daily Rainfall method to determine rainfall thresholds based on antecedent and daily rainfall was developed by Crozier and Eyles (1980). In this method, the influence of antecedent soil water is controlled by a decay factor obtained from discharge hydrographs. Based on Crozier and Eyles (1980), several studies were performed and presented incorporating antecedent rainfall (e.g., Kim et al. 1992, Glade et al. 2000, Xiao-jun et al. 2009, Huang 2013, Lee et al. 2014 etc.). Kim et al. 1992 concluded that the major parameters affecting empirical threshold differs from one region to another. Glade et al. 2000 presented the antecedent soil water status model to define rainfall threshold. Overall, empirical thresholds are obtained by analyzing distribution of landslides and rainfall patterns. However, these do not take underlying physical processes into account. Therefore, such thresholds are considered more suitable for predicting triggering shallow landslides and debris flow during short and intense rainfall.

Physical rainfall threshold: When data on landslide occurrences and rainfall conditions are limited, rainfall thresholds are determined in deterministic approach, known as physical rainfall threshold. To determine such rainfall thresholds, underlying physical processes involved in triggering landslide are taken into account. The major underlying physical processes are the processes associated with subsurface hydrologic response to rainfall or porewater pressure and geo-mechanical parameters. The porewater pressure required for such rainfall threshold determination is either obtained from hydrological modeling or measured in field. Physical rainfall thresholds are considered to be very strong since these are based on physical laws of mass, energy, and momentum. Small areas are more suitable compared to the large areas for determination of physical rainfall threshold since a large amount of detailed data can be obtained from small areas. However, no uniformity in methodology can be found in past literature for calculation of porewater pressure in relation to rainfall events (Persson et al. 2007). The most common method is to compute subsurface hydrologic response to rainfall or porewater pressure required for slope instability which are then compared with observed porewater pressures and checked for accuracy (Thiebes 2011). The heterogeneity in topographical and geological conditions can generate areas of high porewater pressures (Montgomery et al. 1997). Physical rainfall threshold for triggering landslide can be obtained by combining hillslope subsurface hydrologic response to rainfall with geo-mechanical phenomena in soil. The coupled

hydrological-slope stability models consider both of these phenomena, as in the studies like Wilson and Wieczorek 1995, Crosta 1998, Terlien 1998 etc. Some studies, such as Dietrich et al. 1998, Wieczorek and Glade 2005, Guzzetti et al. 2008 and Brunetti et al. 2010 have described physical threshold as critical rainfall. Other researches utilized various hydrological models to predict pore pressure in response to rainfall events (Reid 1994, Crosta 1998, Ekanayake and Phillips 1999, Iverson 2000, Norbiato et al. 2008, Cole and Moore 2009, Frattini et al. 2009, Alvioli et al. 2014). Deep-seated landslides have complex subsurface hydrology compared to shallow landslides. These are more affected by rainfall of longer duration. Establishing simple statistical correlation between rainfall and deep-seated landslides can not realistically predict triggering of deep-seated landslides (Thiebes 2011). It is necessary to define physical thresholds including rainfall, water infiltration, percolation, slope morphology, bedrock structures. According to Ekanayake and Phillips 1999, these are possible through subsurface hydrological modeling.

Even though, rainfall is considered as the most frequent and the most important factor of triggering of landslide, the change in subsurface zone moisture storage with infiltration is initiating landslide phenomena. The subsurface zone moisture storage change can be categorized into three types: loss of matric suction (directly by rainfall), increase in positive porewater pressure or groundwater table (from the bottom of soil colluvium or bedrock), and development of perched water table. In the following, studies incorporating these phenomena are reviewed.

Loss of matric suction: In unsaturated shallow soil slopes, failure occurs directly by rainfall. This means as the rainwater infiltrates through unsaturated zone to reach bedrock or deep groundwater table, matric suction of unsaturated soil in the path of infiltrating water reduces. When there is sufficient loss of matric suction, failure occurs without increase in groundwater table or positive porewater pressure. Coarse grained unsaturated shallow soil slopes with slope inclination (β) greater than or equal to angle of shearing resistance of soil (ϕ) are considered to be more prone to failure as such slopes are stable only due to matric suction which fully disappears before saturation is achieved. Effect of suction on shallow landslide initiation has been studied in a large number of past researches (Kasim et al. 1998, Ng et al. 1999, Gasmo et al. 2000, Tsaparas et al. 2002, Rahardajo et al. 2007, Tsai 2010, Cascini et al. 2010, Rahardjo et al. 2013, Kassim et al. 2012, Lee et al. 2014). These studies have incorporated how suction varies in unsaturated soil slope with rainfall characteristics/patterns, hydrological properties of soil, boundary

conditions etc. For example, Kasim et al. 1998 performed a numerical modeling in horizontal and inclined unsaturated soil layer to investigate the influence of hydrological properties of soil on steady-state suction distributions. This study concluded that ratio of rainfall flux and saturated soil permeability (q/k_{sat}), and air-entry value of soil primarily control steady-state suction distributions (Gofar et al. 2009). Ng et al. 1999 performed more or less similar kind of study, but including intensity and duration of rainfall, impending layer and conditions of surface cover. Their study concluded that suction response is affected not only by ratio of rainfall flux and saturated soil permeability (q/k_{sat}) but also by the ratio of saturated soil permeability and slope of soil water characteristics curve (k_{sat}/m_w), initial conditions and boundary conditions. Other studies (Brand 1984, Ayalew 1999, Tsaparas e al. 2002, Rahardjo et al. 2001, Roslan and Mohd 2005) have investigated influence of monthly, daily and hourly antecedent rainfall on suction distribution. Studies, like Tofani et al. 2005, Casagli et al. 2006, Muntohar and Liao 2010 have investigated groundwater infiltration process through saturated/unsaturated soil and critical time for failure during extreme events. Kassim et al. 2012 modeled suction distribution in an unsaturated heterogeneous residual soil slope using GeoStudio. Rahardjo et al. 2013 observed the effects of flux boundary conditions on porewater pressure distribution in unsaturated soil slope. Despite these studies, the subsurface hydrological response to rainfall is still a mater of debate due to different and dynamic nature of rainfall in different topographies.

Increase in positive porewater pressure: In case of gentle slopes with deep soil colluviums (generally >2 m), increase in positive porewater pressure or groundwater table occurs with rainfall infiltration. This reduces shear strength at potential slip surface whereby failure occurs. The role of positive porewater pressure in slope stability analysis can be reviewed in detail in basic past studies, like Terzaghi 1943, Skempton et al. 1960, Bishop 1955, Fredlund and Morgestern 1977. These studies treated stability analysis considering saturated state of soil. The approaches in these studies are basically for civil engineering design as man-made slopes are designed for the worst case scenario i.e., completely saturated soil condition. A number of studies have suggested that shallow failures are usually caused by the increased positive pore water pressure (Vaughan 1985, Johnson and Sitar 1990, Campbell 1975, Caine 1980, Reid et al. 1988, Wilson and Wieczorek 1995). Rainfall infiltration reduces shear strength at the slip surface by increasing both positive porewater pressure and soil weight resulting in failure.

Development of perched water table: As described in above paragraph, during landslide triggering, slip surface generally forms at the boundary of soil colluvium and underlain bedrock. However, in unsaturated hillslopes (generally heterogeneous), rainwater gets stored within the low-conductive soil layer above bedrock known as perched water table (Weyman 1973, Weiler et al. 2005). From perched water table, a subsurface flow moves laterally along the upper surface of this layer which helps in causing instability above bedrock or surfacial failure occurs (Dietrich et al. 2007, Lu and Godt 2008, Baum et al. 2010). Lanni et al. 2012 estimated the time for development of perched water table. For this, they simulated vertical rain-water infiltration into unsaturated soil using the concept of drainable porosity (i.e., volume of store soil-water removed/added per unit area per unit decline/growth of water table level) given by Hilbert et al. 2005. Sometimes perched water table is connected to bedrock through fissures. The fissures supply water to bedrock and cause formation of potential slip surface between soil colluvium and bedrock (Van Asch et al. 1999, Spek et al. 2013).

2.3 Modeling landslide occurrence

Landslide modeling is basically done for three purposes, namely (i) back analysis of already failed slopes, (ii) understanding present stability status, and (iii) predicting future occurrence of landslides. Landslide modeling can be broadly divided into two categories which are local- and regional-scale modeling.

2.3.1 Local-scale modeling

It focuses on single landslide processes and the models are called local-scale models. Local-scale models are commonly used in stability analysis of geotechnical structures and natural slopes. Deterministic or physically based local models can be used for detailed investigation of failure processes, influence of triggering events, and assessment of remedial measures (e.g., road side slope stabilization). These are based on either of three methods: limit equilibrium, continuum modeling, and discontinum method (Thiebes 2011) which are described below.

Limit equilibrium method has a long tradition on slope stability analyses practice. Although attention has been paid to finite element-based software for numerical modeling of slope instability in recent studies, limit equilibrium method has still been popularly used and has been incorporated in various programs. To determine the forces that try to slide and resist the slope mass, limit equilibrium method includes a simple mathematical

framework and assesses stability of a slope by discretizing the slope into two-dimensional slices within an assumed slip surface. But, practice of using three-dimensional limit equilibrium approach has also been increasing in recent years. A number of existing methods are used to locate critical slip surfaces or to find lowest factor of safety, such as Bishop's simplified method, Janbu's method, Infinite slope method, Ordinary slice method, General slice method, Spencer's method, and Morgenstern-Price method. However, there are many shortcomings of limit equilibrium method. For example, soil behaviour is not taken into account and complex processes can not be analyzed with a good accuracy (Baba et al. 2012). The forces involved in equilibrium are approximations of forces within the landslides. The computed factor of safety by discretizing the slope into two-dimensional slices is average or global one. Failure is supposed to occur when factor of safety<1.0. However, in reality, displacements may occur upto 1.15 value of factor of safety (Thiebes 2011). Also no information is given about stress distributions in the slope mass and progressiveness of failure by limit equlilibrium method (Krahn 2003, Baba et al. 2012).

Slope stability models in relation to continuum modeling are the software or computer programs. These follow assumptions of either finite difference or finite element method. The common aspect in finite difference and finite element method is that entire slope profile is discretized into finite number of small elements or mesh. The purpose of constructing mesh is to compute stress and strain. Finite difference method yields numerical approximations of differential equations of equilibrium, strain-displacement relations or the stress-strain equations. Compared to limit equilibrium method, continuum modeling permits complex dynamic landslide analyses. Different from limit equilibrium method and continuum modeling, discontinum methods evaluates stability of a slope mass by considering it as a single distinct block. The factor of safety for each block is repeatedly computed so as to explore complex non-linear interaction between deformable elements. In the following, commonly used programs in slope stability analyses which follow the abovementioned three approaches are described.

SEEP/W and SLOPE/W (GeoStudio 2005) represent coupled hydrological-slope stability model. SEEP/W is finite element method based program whereas SLOPE/W is limit equilibrium based program. Both of these programs have been used in this study and a more detailed review on these programs is presented in **Chapter 5** and **7**. SVslope is similar to SLOPE/W; however, it performs three-dimensional limit equilibrium analysis of slopes (Leong and Rahardjo 2012). In latest versions of this program, finite element tools have also been incorporated. Clara-W (Hungr 2001) performs both two- and three-

dimensional limit equilibrium analyses. Various modes of failure such as rotational, non-rotational, ellipsoids, wedges, compound surfaces can be modeled and analyzed. The problem configuration can be directly switched into three-dimensional window from two dimensional one during modeling. CHASM (Combined Hydrology and Stability Model) (Anderson and Lioyd 1991) is another example of coupled hydrological-slope stability model based on limit equilibrium method. It differs from SEEP/W and SLOPE/W in two ways. First it allows using vegetation and stabilization measures in slope stability assessment using Bishop's method and Junbu's method. Second a simple empirical-based run-out simulation can be performed in CHASM. Other examples of coupled hydrological-slope stability modeling programs are HYSWASOR (Van Genuchten 1980), HILLFLOW (Bronstert 1994) or GWFLUCT (Terlien 1996), ASWSM (Crozier 1999) etc.

Plaxis is finite element-based software for analysis of deformation and stability of geotechnical structures in two and three dimensions. It can simulate unsaturated/unsaturated groundwater flow and instability. Static loads; dynamic loads due to earthquakes as well as non-linear, time dependent and anisotropic behaviors of soils/rocks can be assigned as input to this software. Use of Plaxis in landslide research can be found in several studies such as Comegna et al. 2004, Gotman 2007, Singh et al. 2013, and Chandrasekaran et al. 2013 etc.). The water level or porewater pressure required for stability analysis is directly specified as a phreatic line. Below the phreatic line, there is hydrostatic porewater pressure distribution. Strength reduction method along with various advance soil models are used in Plaxis. During analysis, the incremental displacements are taken as the indicators of the likely failure. FLAC (Fast Lagrangian Analysis of continuum) is two-dimensional explicit finite difference program. It can be used in the modeling of geo-material calculation and mechanical behavior geotechnical engineering (e.g., plastic deformation, fluid flow etc.) (Chugh and Stark 2006, He et al. 2008, Gessner 2009, Shuguo et al. 2013). The algorithm used in FLAC solves the governing equation of mass, moment, and saturated flow. The FLAC model is prepared by discritizing the model domain into brick shaped zones which consists of tetrahedral subdomains. DAN was developed by Hungr 1995. It is versatile dynamic software for modeling whole mass movement. It has been widely used for dynamic run-out analysis of rapid landslide processes e.g., rock avalanches (Hungr and Evans 2004, Zhang et al. 2013). DAN follows Lagrangian solution of the equations of unsteady non-uniform flow in an open channel.

GGU is computer aided design-based two-dimensional slope stability analysis program based on limit equilibrium assumptions. Bishop's and Janbu's methods are used

to compute factor of safety in this program. The geotechnical parameters determined from various laboratory experiments are major inputs. GGU is popularly used in German goetechincal engineering. The studies, like Villalobos et al. 2013, Preuth et al. 2010 have used this program in stability assessment of slopes. Galena is also two-dimensional limit equilibrium-based numerical software. It allows for predicting stability using Bishop's method, Spencer-Wright method and Sarma method. This software was developed mainly for slope design in open-pit mines (Moon et al. 2013, Thiebes 2011). Hydrological modeling can not be performed in both GGU and Galena. Xslope (Ballaam 2001) assesses stability status based on Bishop's or Morgenstern-Price method. Soil cohesion, angle of shearing resistance and unit weight of soil are main soil properties used in Xslope. Different from GGU and Galena, porewater pressure simulated in external finite element steady-state seepage model can be integrated in slope stability analysis in Xslope (Hubble et al. 2013).

2.3.2 Regional-scale modeling

Regional-scale modeling focuses on landslide processes on greater spatial extent and the models are known as regional-scale models. With development of powerful computers, and tools, like GIS, ILWIS, Remote sensing, the concept of regional modeling was emerged (or the use of local model has been started to predict landslide processes in larger areas). Regional modeling is performed to investigate landslide susceptibility, hazard and risk. According to Soeters and Van Westen (1996), regional landslide susceptibility and hazard analyses can be classified into four distinct approaches, namely heuristic, statistical, deterministic, and landslide inventory-based approaches.

In heuristic approach, geological and/or geotechnical experts use their knowledge and experience to determine relationship of landslide with the causal factors of landslide. Based on this relationship, certain weight values or ratings are assigned to each factor based on their relative importance and the slope failure hazard map is prepared in a regional scale (Pachauri et al. 1998, Dai et al. 2002, Dakau and Glade 2003). However, assigning the weight values or ratings to each parameter is very subjective (Regmi et al. 2013). The results can vary significantly depending on the experts who prepare the map, knowledge on the study, and the processes present (Guzzetti et al. 2000, Ardizzone et al. 2002).

Statistical approaches are the most common approaches used in regional landslide susceptibility and hazard assessment. Statistical models are also called white box models.

These require detailed identification and mapping of a set of independent causal factors (i.e., geologic and geomorphologic parameters). Then, a relationship between causal factors and slope failure location is established in the form of an empirical parametric function. This function is used for the prediction of future landslide by spatial interpolation. Some of the statistical analysis methods available in literature include multi-variate regression (Dai and Lee 2003), discriminant function modeling (Baeza and Corominas 2001, Santacana et al. 2003, Guzzetti et al. 2005, Jamaludin et al. 2006, Dong et al. 2009, Baeza et al. 2010, He et al. 2012), Conditional analysis (Wu et al. 2004, Duman et al. 2005), and logistic regression (Carrara et al. 1992, Ayalew and Yamagishi 2005).

Deterministic approaches are called black box approaches. These are applicable only when climatic (precipitation), geological (rock types) as well as geomorphological (vegetation, aspect) conditions are fairly homogenous and landslide types are simple (or when statistical approaches are difficult to apply due to lack of heterogeneity in geological and geomorphological parameters). Due to such limitation, regional deterministic models are only suitable for simple landslide processes, such as shallow translational landslide or slope failure. Deterministic modeling is performed employing distributed hydrological model and infinite slope model. Distributed hydrological model simulates to compute soil moisture content above bedrock based on topographical flow routing. Infinite slope model uses computed soil moisture content and geotechnical parameters (cohesion, angle of shearing resistance, unit weight of soil etc.) determined in laboratory to ascertain factor of safety on a cell-by-cell basis, which can be displayed in a grid-based continuous raster map. The computed factor of safety is then ranged to create a slope failure hazard map, which can be used to provide the best quantitative information about slope instability or hazard in a small scale. Finally, the hazard map can be used directly in designing civil engineering structures or in quantitative risk analyses (Jia et al. 2012). The famous regional deterministic models are TOPMODEL (Beven and Kirkby 1979), SINMAP (Pack et al. 1998), and SHALSTAB (Dietrich et al. 1998). Both deterministic and statistical approaches have been used in **Chapter 6.** In this chapter, the deterministic approach was coupled morphometrically with statistical approach to predict slope failure hazard index in small catchments and the approach is so called grey-box or semi-physical.

In landslide inventory-based approach, geo-morphological mapping in field and the detailed analyses of landslide distribution is performed. In case of multi-temporal inventories, activity patterns are also analyzed. These form the basis for regional modeling of landslide hazard and risk.

2.4 Chapter summary

In this chapter, past studies on landslide triggering and landslide modeling were briefly reviewed. First the theory on rainfall threshold for triggering landslide was established. Then, some significant studies on landslide initiation due to various phenomena, such as loss of matric suction, perched water table, and increase in ground water level with rainfall infiltration were presented. Various slope stability and hydrological-slope stability modeling programs for single landslide process were also briefly given. Finally, the common modeling approaches used worldwide for landslide hazard analyses in regional scale were described. This chapter is foundation for the work presented in this thesis.

Chapter 3

Geology, geomorphology and climate of Shikoku Island

3.1 Geology of Shikoku Island

Among the four main Islands of Japan, Shikoku is the smallest Island. It has an area of 18,000 km^2. Geographically, it lies between Seto Inland Sea and the Pacific Ocean. More clearly, it is situated on the south of the Island of Honshu and east of the Island of Kyushu. In the middle part, Shikoku has a few plain areas along the costal lines and elevated peaks. On the contribution of the geological and morphological settings, landslide and flood related to typhoon rainfalls are common in Shikoku. The subduction zone in Shikoku area consists of accretionary complexes and metamorphic rocks which are parallel to the extending direction of the arcs. This zone is divided into five rock belts by tectonic structures (e.g., thrust faults). The rock zones on the side of Japan Sea are older whereas these become younger towards Pacific Ocean. The geology of Shikoku Island can be roughly divided into three major geological Belts: Ryoke Belt, Sambagawa-Chichibu Belt, and Shimanto Belt from north to south (Figure 3.1). These three Belts are bordered by two northerly dipping major faults, the Median Tectonic Line (MTL) and the Butsuzo Tectonic Line (BTL) from north to south respectively. When geological setting is considered in detail, Shikoku Island can be distinctly divided into five major geological Belts in east-west direction which are Izumi Group (with Ryoke Belt), Sambagawa, Chichibu, Shimanto north , and Shimanto south (Figure 3.2) (Dahal 2008). Izumi Group and Sambagawa Belt, both lying on the northern part, are separated by Median Tectonic Line (MTL). Mikabu Tectonic Line (MiTL) separates Sambagawa and Chichibu Belt. Similarly, Butsuzo Tectonic Line (BTL) divides Chichibu and Shimanto-north groups whereas Shimanto-north and Shimanto-south lying on southern part are separated by Aki-Sukumo Tectonic Line (ATL). The northern part of Izumi Group is called Ryoke belt. Besides, there exists a narrow discontinuous strip between Sambagawa and Chichibu Belt known as Mikabu Belt. It has a width of 5 – 6 km. All of these Belts are recognized as being susceptible to landslide occurrence except Ryoke Belt. In the following, each belt is described in detail.

3.1.1 Ryoke Belt

It is a high temperature-low pressure paired-metamorphic Belt. It sharply differs from the high pressure-low temperature type Sambagawa metamorphic Belt. Altogether 20 % to

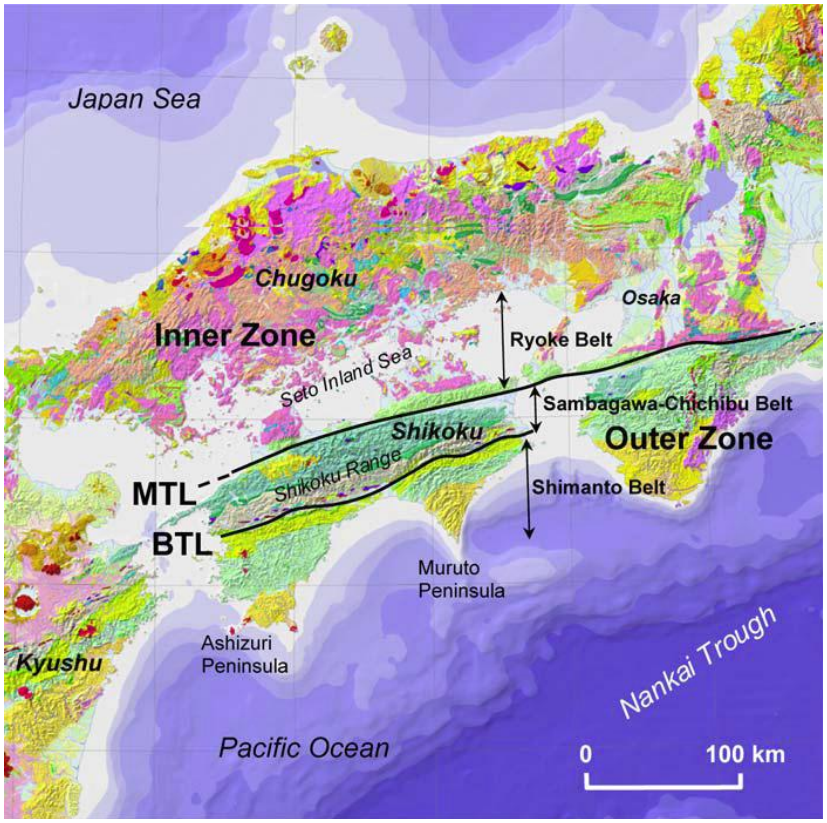

Figure 3.1 Regional geological map of Shikoku Island

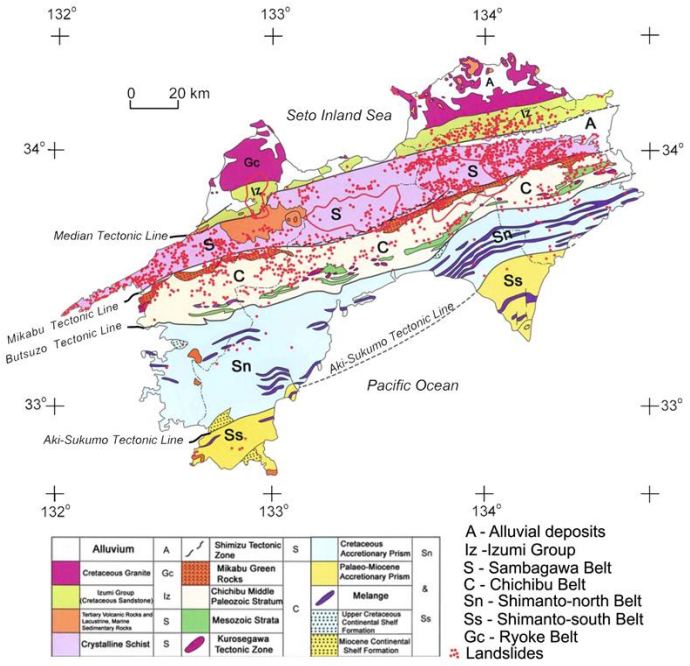

Figure 3.2 Geological map of Shikoku Island in detail (after Dahal 2008)

30 % of Ryoke Belt area consists of metamorphic rocks (e.g., Pelitic rocks, Psammitic rocks and granitic plutons known as the Ryoke granites). The innermost area on the outermost part of the inner zone of south west Japan (Figure 3.2) is furnished by rocks of Ryoke Belt. In Shikoku Island, Ryoke Belt is composed of three main rock units, namely late cretaceous granitic rocks, late Cretaceous sedimentary rocks (Izumi Group), and Miocene volcanic rocks. The Cretaceous granite rocks are dominant in the north of Seto Inland Sea.

On the southern part of Ryoke Belt or on the north of MTL, there is a narrow Belt running east-west called the Izumi Group. It consists of thick piles of intercalated sandstones and shales together with a few thin beds of acidic tuff which are of late Cretaceous age. The northern wing of Izumi group lies over the rocks of Ryoke Belt whereas southern wing is in fault contact with Sambagawa Belt. The major portion of Izumi group is marine and it yields fossils shells such as Inoceramus (Hashimoto 1991). The northern wing of Izumi Group is composed of basal conglomerates. It contains pebbles of granite, quartz, porphyry, and mica schist which are similar to the rocks of Ryoke Belt. The study area in this research lies in Ryoke Belt.

3.1.2 Sambagawa Belt

As mentioned earlier, Sambagawa Belt consists of high pressure-low temperature type metamorphic rocks. It lies nearly in the central part of Shikoku Island (Figure 3.2). It is mainly furnished by crystalline schist which can be categorized into four types: basic schist (metabasites or greenstone including amphibolite, pillow lava), quartz schist (metacherts of various composition), politic schist, and psammitic schists (metamorphosed greywacke sandstone). The Shikoku Mountains mainly comprise of these rocks. Due to low temperature-high pressure condition, laminated folded rock strata are common in this Belt.

3.1.3 Mikabu Belt

It is a short and narrow Belt (5 - 6 km width). It lies along the boundary between Sambagawa and Chichibu Belts (i.e., distributed along Mikabu Tectonic Line). It consists of metamorphic product of basalt and gabbro which have volcanic origin. But the dominant rock type is metabasites or greenstone. Besides, Mikabu greenstones are also found in significant proportion in this Belt. Greenstone comprises chief green-colored minerals e.g., quartz, feldspar, pyroxene, amphibole, and epidote. Because of these green-colored

minerals, the rock outcrop in this Belt appears green throughout the terrain. Mikabu greenstone is also known as one of the most weathering prone rock unit of Shikoku Island.

3.1.4 Chichibu Belt

It lies on the south of the Sambagawa Belt and Mikabu Belt. It mainly consists of Carboniferous to Jurassic sedimentary and low-grade metamorphic rocks which are distinguished all through the east-west length of arcs. Chert, greenstone, mudstone, and conglomerate are the major rock types of this Belt. Moreover, this Belt consists of late Triassic to middle Jurassic mudstone, sandstone and chert (Dahal 2008). The characteristics feature of Chichibu Belt is that it contains imbricate structure with a number of thrusted sheets and lenticular masses. Also, the masses of limestone and greenstone can be found embedded as olistoliths in sheared mudstones or are bordered by faults. Some limestone masses have algal fossils and yield fusalinids indicating Permian age. The bivalves, gastropods and ammonites present in traces indicate Triassic age (Hashimoto 1991).

3.1.5 Shimanto Belt

It is the southern most geological Belt of Shikoku Island. It occupies two southern peninsulas, Murote and Ashizuri. These protrude into the Pacific Ocean (Figure 3.2). The middle Miocene granitic and partially gabbroic rocks are sporadically distributed along the axes of these peninsulas. Based on distribution of lithologic and biostratigraphic assemblages, the Shimanto Belt has been subdivided into two distinct facies: Cretaceous (or northern) and Tertiary (or southern) Belts. The northern sub-Belt also consists of other two small Belts, a Lower to Middle Cretaceous unit in the south. The northern sub-Belt is composed of clastic sedimentary rocks which have characteristics feature of the absence of radiolarian chert. Abundant clastic sedimentary rocks and several regional-scale zones of intense deformation are found in upper cretaceous Shimanto Belt.

3.2 Geomorphology

Topographically, MTL divides Shikoku Island into a narrow northern sub-region (fronting on the Seto Inland Sea) and a wide southern region (facing Pacific Ocean). On the marginal area of Shikoku Island, plains, fans and delta deposits are found (Figure 3.3). The major towns of Shikoku i.e., Takamatsu, Matsuyama, Kochi, and Tokushima are situated on the main alluvial and deltaic plains. In the central and eastern part of Shikoku, Yoshino

River is major river system. The Tokushima plain consists of alluvial fan and alluvium as well as deltaic deposit of the Yoshino River. More than 80 % of the Shikoku Island is composed of steep upland terrain occupied by forest. The mountain areas are sparsely populated while the plain areas are densely populated. Mount Ishizuchi (1,982) is the highest peak of Shikoku. In addition to Mount Ishizuchi, Mount Tsurugi and Mount Kaifu are other famous mountain peaks. The colluvial deposits are found on most of the slopes of Shikoku Mountains. The steep mountains of tertiary sedimentary terrain have thin, loose and less cohesive residual colluviums.

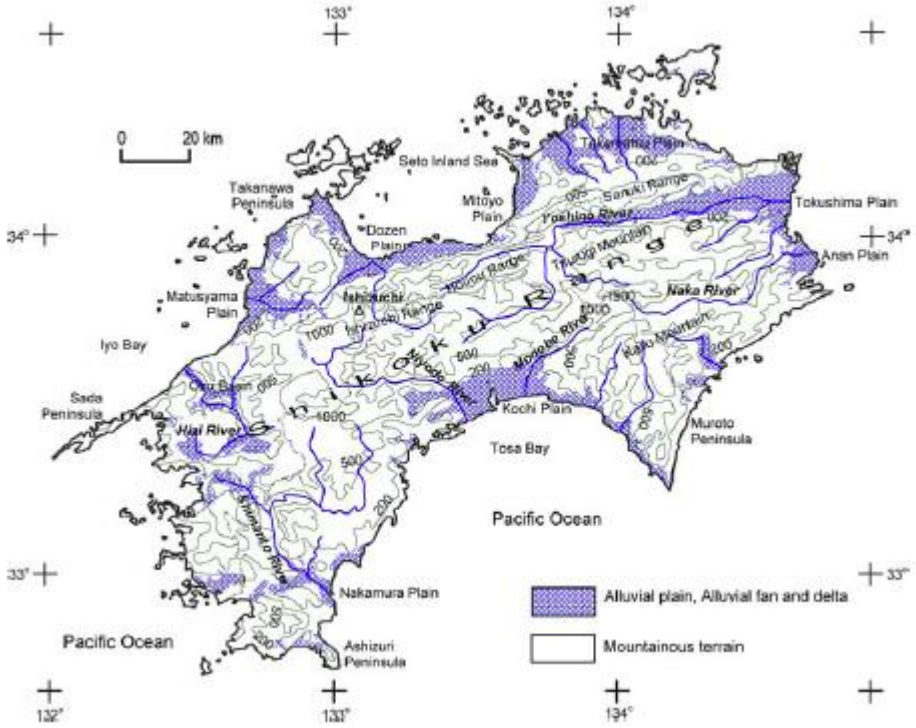

Figure 3.3 Regional geomorphological map of Shikoku Island (after Dahal 2008)

3.3 Climatic condition

Shikoku consists of humid subtropical climate. Such climate has warm summers and is constantly moist. Shikoku Island is characterized as a place of mild climate with heavy precipitation. The mean annual precipitation of Shikoku ranges between 1,000 m and 3,500 mm. This value is nearly 20 % higher than the mean annual precipitation in the whole Japan [according to Bhandary 2003, a maximum mean value around 1,950 mm in Hokuriku (northern) region and a minimum around 950 mm in Hokkaido region was recorded]. Northern part of Shikoku has comparatively lower value of annual rainfall. But,

an annual rainfall range of 3,500 mm hit the southern Shikoku Mountain Range which is significantly high in the whole country. The main cause of extreme rainfall in the southern part of the Shikoku Range is orographic effect of Shikoku Mountain Range. In fact, the winds of the moisture-rich vapor from Pacific Ocean get intercepted to mountains and extreme rainfall occurs in the southern part. Because of this, the northern part of Shikoku lies in the shadow zone and, hence it has Mediterranean type of climate when the winds of Pacific Ocean side is deemed for causing rainfall. June to October is heavy rainfall season in Shikoku even though 30 % of the days in a year experience rain. The main causes behind rainfall in an order of importance in Shikoku Island are typhoons, low atmospheric pressures, seasonal rain fronts, and thunderstorms (Bhandary 2003). The seasonal rain fronts cause extreme rainfall exceeding an hourly value of as high as 100 mm in June. Similarly, typhoons are responsible for extreme rainfall from July to October.

3.4 Chapter summary

In this chapter, geological, geomorphological and climatic settings of Shikoku Island were described. Shikoku is the smallest Island among the four principal Islands of Japan. More than 80% area of this Island is occupied by steep, upland terrain. The mountains are younger towards Pacific Ocean. The hillslopes are almost covered by thick forests of subtropical broadleaved trees, such as Japanese cedars and Japanese bamboos. As described in earlier paragraph, the four major tectonic lines (Median Tectonic Line, Mikabu Tectonic Line, Butsuzo Tectonic Line, and Aki-sukumo Tectonic Line) cut through the central part of Shikoku Island which separate the geology of Shikoku Island into five major geological Belts, namely Sambagawa, Chichibu, Shimanto-north, Shimanto-south, and Ryoke Belt. Each of the Belts includes various types of rocks different from each other. Landslides have been found commonly occurring in Sambagawa, Chichibu, and Mikabu Belt. Mid climate with comparatively heavy rainfall is found in Shikoku Island. Knowledge on geological, geomorphological, and climatic conditions of the area helps to understand the physical environments, under which landslide triggering occurs.

Chapter 4

Outline of rainfall-induced landslides in Shikoku Island

4.1 Typhoon events in Japan and Shikoku

Typhoons are one of the strongest meteorological events on earth. In Japan, June, September and October are a frequent typhoon season. A total of 1468 typhoon events originated from the North Pacific Ocean between 1951 and 2005. Among them, 163 typhoon events hit Japanese archipelago (Dahal 2008). Only in the year 2004, Japan was hit by ten typhoons. In fact, it was the maximum annual events of typhoon within last 55 years (Figure 4.1). Usually, June to October is known to be typhoon season in Japan. The data prepared by Japan Meterological Agency between 1951 and 2005 shows that only a few number of typhoons occur in February whereas August has higher numbers of typhoons. But there were no typhoon records in months of January, February, March, and December in Japan. From Figure 4.2, it is clear that typhoons are abundant in months of August and

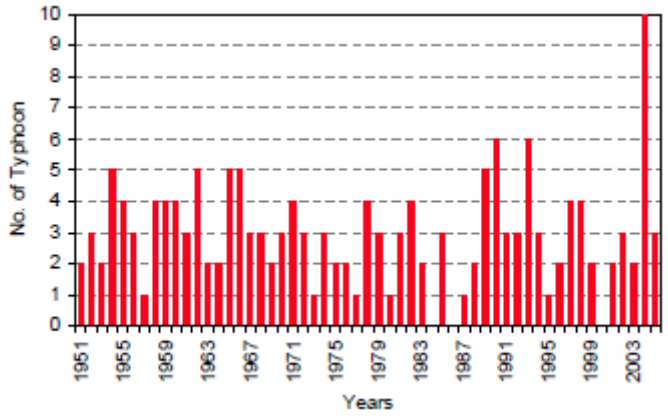

Figure 4.1 Number of typhoon events that occurred in last 55 years (source: Digital Typhoon, 2006 and JMA, 2005, Dahal et al. 2008d)

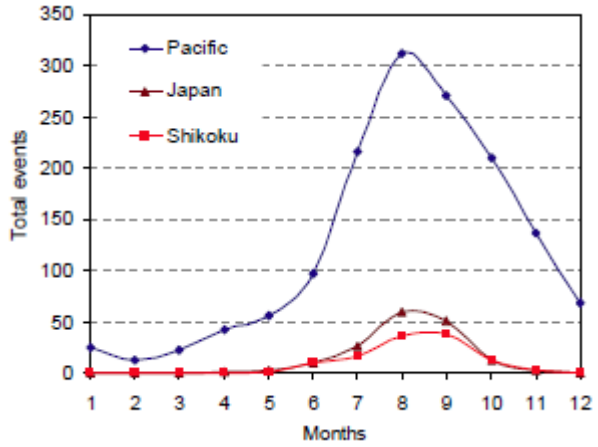

Figure 4.2 Typhoon events in Pacific Ocean, Japan and Shikoku in last 55 years (source: Digital Typhoon, 2006 and JMA, 2005, Dahal et al. 2008d)

September in Shikoku Island, Japan and Pacific Ocean. As mentioned in **Chapter 3**, there are various sources of rainfall in Japan and Shikoku, but typhoons are the major sources for triggering of shallow and deep-seated landslides.

4.2 Typhoon events of 2004

The storm and flood caused by 2004 typhoons led to 227 deaths and a large number of missing cases in whole Japan. It was the higher record since 1984 (JMA, 2005). The courses of nine typhoons which attacked Shikoku Island are shown in Figure 4.3. Figure 4.4 denotes isohyetal maps of most effective six typhoons in Shikoku. The storm eye position in the isohyetal maps of each typhoon events denotes the area of extreme rainfall. In such positions, there is maximum chance of triggering of slope failure. From the six isohyetal maps, it can be understood that the locations of the Shikoku Mountain Range were the most affected regions by extreme rainfalls. Typhoons 0423 and 0421 affected Ehime, Kochi, and Kagawa prefectures. Similarly, typhoons 0404, 0406, 0410, 0411, 0415, 0416, and 0418 caused extreme damage in Kochi, Tokushima, and Ehime prefectures. This led to several hundreds of slope failures in central and southern Shikoku. The slope failure damage was comparatively less in northern Shikoku. The rainfall intensity was abnormally higher in 2004 than in previous events. Figure 4.5 demonstrates that the events of hourly rainfall exceeding 50 mm were the greatest in 2004 than in other years. Such abnormally high hourly rainfall intensity and higher number of slope failures support huge slope failure disasters in Shikoku Island during various typhoons of 2004.

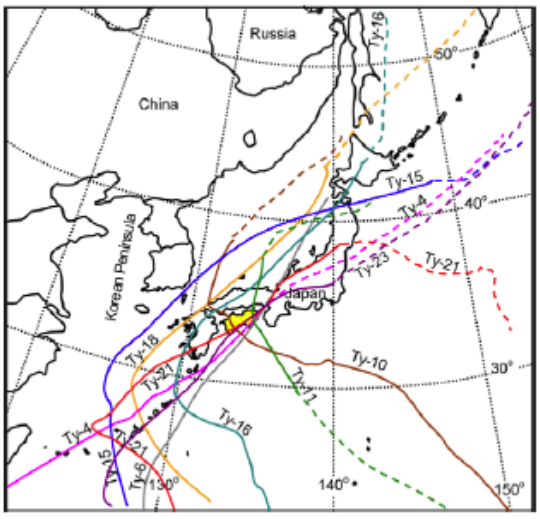

Figure 4.3 Paths of ten typhoons of the year 2004 passing through Japan (after Dahal 2008)

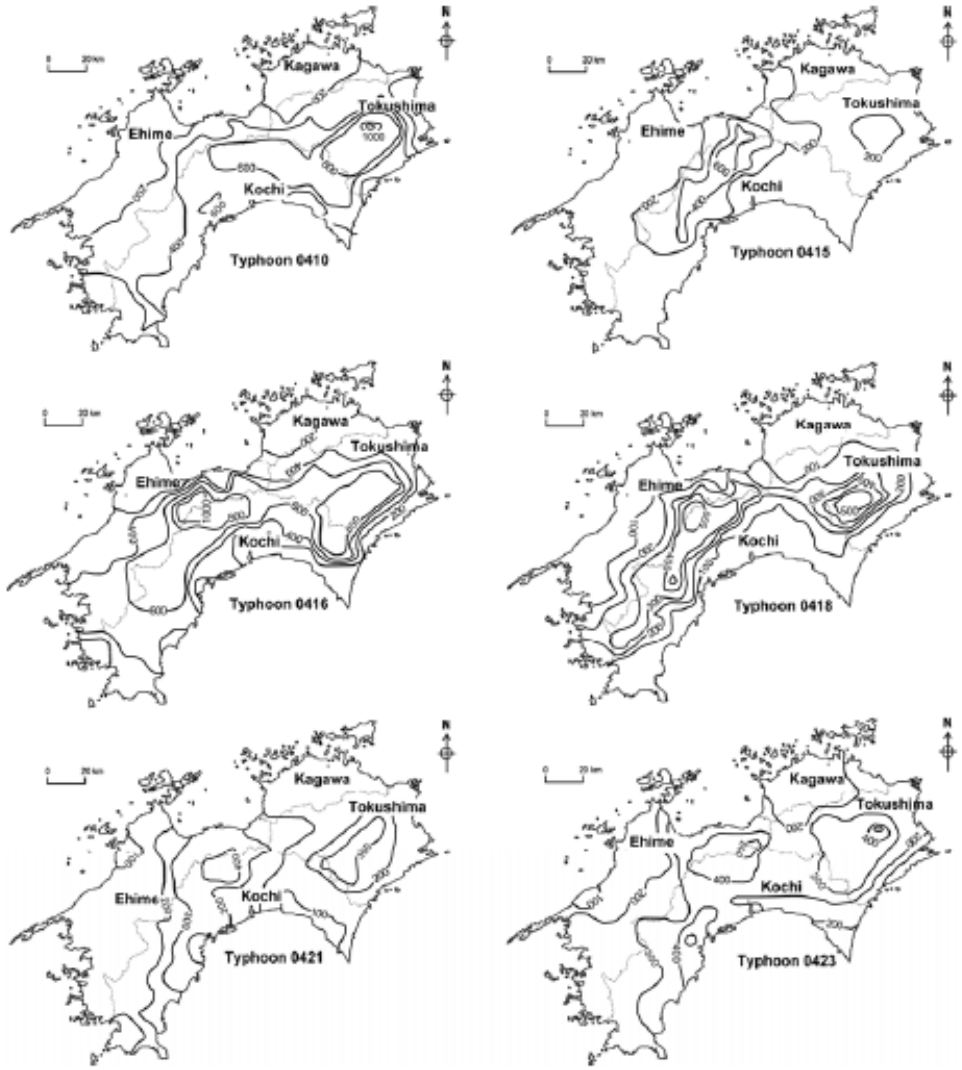

Figure 4.4 Showing Isohyetal map of most destructive six typhoons of the year 2004 (Source: AMeDAS data, Dahal 2008)

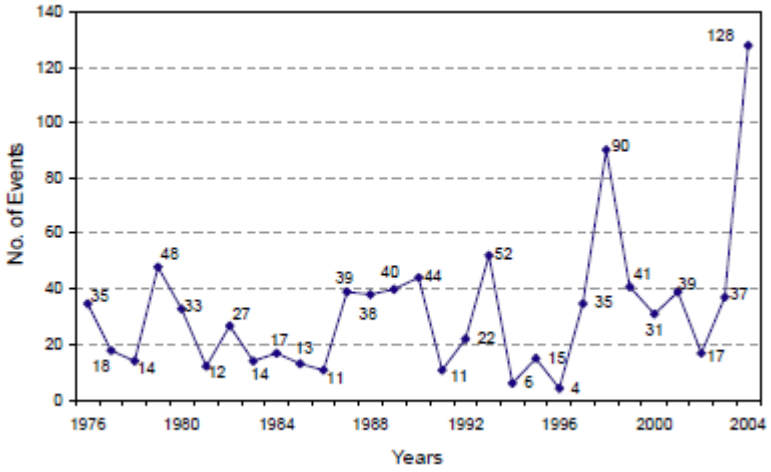

Figure 4.5 Showing maximum occurrences of typhoon-rainfall events of hourly rainfall intensity of more than 50 mm in Shikoku Island (after Dahal 2008)

4.3 Examples of typhoon rainfall-induced landslides in 2004

Although six typhoons severely impacted Shikoku Island (Figure 4.5), none of the single typhoon was able to cause heavy rainfall in the entire Shikoku. Typhoons 0410, 0411, 0415, 0416, and 0421 were aggressive in Tokushima, Kochi, and Ehime. Similarly, typhoons 0415, 0421, and 0423 were more damaging for Kagawa prefecture (Dahal 2008). The landslide occurrence scenario in Shikoku Island after the 2004 typhoon rainfall events is illustrated in Figure 4.6. This figure shows only the major or severely affected locations. Even a single location includes numerous failed spots as shown in Figure 4.7. In the following, some landslide events of 2004 which occurred near to human settlement and caused considerable economic loss are described.

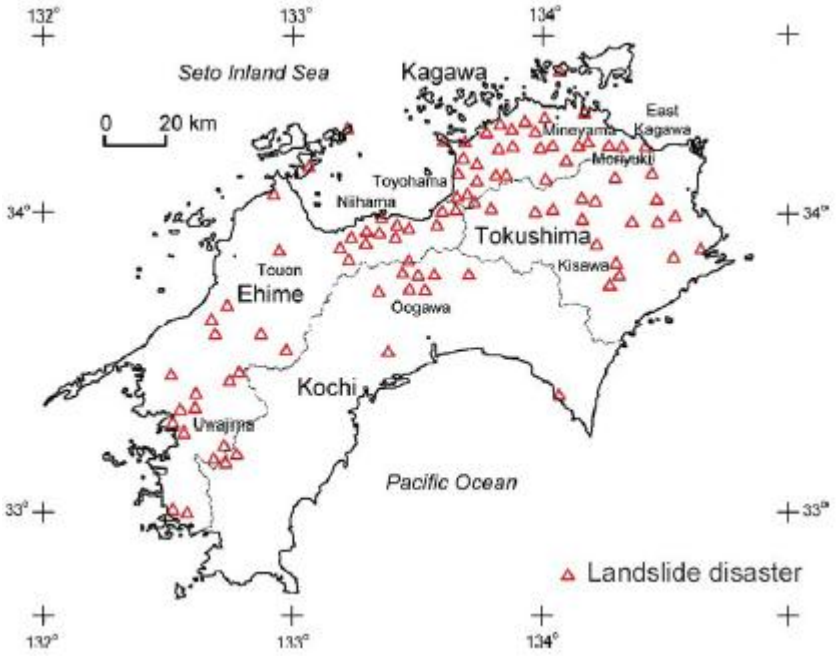

Figure 4.6 Showing landslide occurrences in Shikoku after 2004 (after Dahal 2008)

4.3.1 Landslides in Tokushima prefecture

The southern part of Shikoku received heavy rainfall (more than 2000 mm) due to typhoon 0410 (Namtheun) in the period from late July to early August whereby a total of four huge landslides were triggered in Ooyochi, Kashu, Azue, and Shiroishi area of Kisawa village in Naka district. An extensive damage was also found in Kaminaka Town, near Kisawa. The data recorded by the Shikoku Electric Power co., Inc., in Kaminaka Town showed that the maximum hourly rainfall and maximum one day accumulation exceeding 120 mm and

1,317 mm respectively were the main causes behind extensive damage in Kaminaka. Japan's previous record of highest daily precipitation was 1,114 mm which was obtained in Kito village (16 km southwest of Kisawa village) caused by Typhoon Fran on 11 September of 1976 (Wang et al., 2005a, Hiura et al., 2004). The maximum daily rainfall accumulation recorded in Kaminaka village (1,317 mm) in 2004 broke the previous record.

Figure 4.7 Showing small-scale slope failures in 2004 in forest area of northeast Shikoku

Furthermore, typhoons 046, 0411, 0416, 0418, and 0423 also impacted Tokushima prefecture whereby small- to medium-scale landslides were triggered along national and express highways and in the Naka River watershed. Typhoons 0411, 0416, 0418, and 0423 affected Kisawa and Kaminaka areas. A total of 550 mm rainfall was recorded in Kamikatsu during typhoon 0416. In the same way, 300 mm of daily rainfall was recorded in the southwestern part of Tokushima. Kisawa village is 17 km far in south of the Mt. Tsurugi (1,955 mm). It is furnished by various types of rocks such as Palaeozoic greenstone, Palaeozoic and Mesozoic pelite and greywacke, and serpentinite of the Mesozoic Kurosegawa terrain, as well as scarce limestone and chert. The upper sections of river valley situated in this village have steep slopes. Human settlements are found on the gentle slopes of old landslide mass. Cedar trees are the major green vegetations on recently failed areas. The exact time of failure for all of the landslides discussed above was not clear. The Ooyochi landslide was reported to occur between 20:00 hour and 23:00 hour of

1 August. But, the Azue landslide occurred nearly at the end of typhoon rainfall which was around 16:00 hour of 2 August.

4.3.2 Landslides in Kagawa prefecture

In 2004, the four typhoons i.e., typhoon 0415, 0416, 0421, and 0423 hit Kagawa prefecture. In fact, Kagawa prefecture is the most severely impacted prefecture of Shikoku Island. An hourly rainfall of 50 mm and one day rainfall accumulation of 200 mm caused numerous landslides and slope failures at various locations of Kagawa. Comparatively, a higher damage was found in highways and forest areas of Takamatsu city. Moriyuki and Monnyu were the most affected areas. Mineyama landslide at central Takamatsu and landslides that occurred at the base of the hills of Toyohama (Part of Kanonji City) are some examples of rainfall-triggered landslides in Kagawa.

The heavy typhoon rainfall in the afternoon of 17 August in Toyohama and Onohara areas (west Kagawa) caused five deaths in spite of a few landslides and debris flows. The rainfall was started at 11:00 hour of 17 August with no antecedent rainfall events in previous days. Typhoon 0415 with maximum accumulation of 246 mm and maximum hourly rainfall of 54 mm caused extensive damage in the whole area. In case of typhoon 0421, 249 mm of maximum daily rainfall and 65 mm of maximum hourly rainfall were recorded responsible for triggering of landslides. Aerial photographs were taken in this area after typhoons 0421 and 0423 in this area. From these photographs, it was understood that typhoon 0423 was less significant relative to typhoons 0415 and 0421 for triggering of landslides in west Kagawa. Alternating sandstones and shales of Izumi Group are found in the hillslopes in western Kagawa. This is why all the streams have a huge pile of debris beginning from the base of hillslopes.

Typhoon 0423 was effective in triggering landslides only in east Kagawa. During this typhoon event, an hourly rainfall of 125 mm was recorded in Maeyama whereas Yodayama received 107 mm/hr. As a result, many landslides and debris flows were created in the Shiratori, Moriyuki, Minamigawa, and Monnyu areas. Several landslides occurred also in the catchment of a small rivulet Tooritani at Moriyuki. A total of 674 mm of rainfall was recorded at Kusaka Pass during the same typhoon event. Likewise, Monnyu area experienced 495 mm of rain due to which many landslides were caused in Monnyu River and the reservoir area. At 15:00 hours of 20 October, a huge debirs flow occurred in the Monnyu River and this led to filling of the Monnyu reservoir by piles of sediments. Landslides occurred mainly in the weathering profile of Cretaceous granite and

granodiorite rocks in eastern Kagawa while in central Kagawa; landslides were found in the weathering profile of Cretaceous granite, meta-sandstone, and andesite.

4.3.3 Landslides in Ehime prefecture

Ehime prefecture suffered from typhoons 0415, 0416, 0418, 0421, and 0423. An hourly rainfall exceeding 50 mm and total rainfall of more than 400 mm were recorded in many rain gauge stations during these typhoon events. Particularly, rainfall due to typhoons 0415, 0421, and 0423 triggered many slope failures at different locations in northeast Ehime. The hardest hit area was Niihama City (about 140,000 residents), where many debris flows near the hill bases killed 25 people and destroyed 40 billion yen worth of property (Bhandary and Yatabe 2005). In addition, greater than 1500 slope failures and debris flows occurred only in the northeastern forests of Niihama during various typhoon events in that year. Niihama is separated from Shikoku Mountain Range by MTL. Green schist, sandstone and shale are the major rock types found in this area. Green schists of the Sambagawa Belt are found in the southern part whereas sandstone and shale of the Izumi Group are found in the northern part of Niihama. Izumi Group is composed of decomposed sandstone, either stiff clay resulting from weathering of shale or less disintegrated rock mass. These rocks are very weak. This is why most of the part of Izumi Group suffered extensive failure during the disaster. The slope failure events in Ibukimachi (Uwajima City), Kawauchi (Touon City), and Shingumachi (Shikoku Chuo City) are other examples of typhoon rainfall-induced slope failures in Ehime prefecture.

In the case of only typhoon 0415, a number of slope failures on the base of Shikoku Mountain at Niihama were triggered with 100 mm of continuous precipitation. Most of these failures were found on the sedimentary rocks of the Izumi Group. Similarly, during typhoon 0421, the failure started after forty hours of continuous rainfall (i.e., after time 16:00 hours of 29 September). During this time, one landslide at the Takamatsu, Matsuyama Express Highway killed four residents below the slope (Dahal et al. 2008d). In case of typhoon 0423, the maximum one day rainfall of 217 mm was recorded which is considered to be the cause of soil slips initiation after 34 hours of continuous rainfall.

4.3.4 Landslides in Kochi prefecture

Altogether seven typhoons (044, 046, 0410, 0411, 0415, 0418, and 0423) hit Kochi prefecture in 2004. Typhoon 0415 greatly affected Reihoku District. Okawa and Uwezugawa villages of this prefecture were also seriously impacted. Many landslides were

triggered in the Yoshino River basin on 17-18 August. A number of landslides occurred along the roadside slopes too. During heavy rainfall of various intensities during these typhoons, 100 mm of hourly precipitation at time 16:00-18:00 hours of 17 August and 205 mm of rainfall in 24 hours was recorded in the Komatsu rain gauge station. Similarly, a total of 518 mm rainfall was recorded during 01:00 to 18:00 hours with maximum rainfall intensity of 104 mm/hr. The total precipitation in three day continuous rainfall period was 1000 mm. Because of these reasons, many landslides and debris flows were also triggered at 17:00-18:00 hours of 17 August.

4.4 General features of landslides of 2004

Based on the landslide classification system proposed by Varnes (1978), the failed masses in Shikoku after 2004 typhoon events were classified as slope failures which have following characteristic features.

1. Various types of slope failures were identified such as transitional, rotational or a combination of both which is based on the shape of slip surface. But translational type was the most dominant type of failure (Dahal et al. 2006, Bhandary et al. 2013).
2. The volume of failure ranged generally between a few tens to a few hundreds of cubic meters.
3. Most of the failed masses had shallow depth of failure (less than 2 m).
4. Some slope failures were noticed along the colluviums and intact bedrock contact. Also the bedrocks were well exposed in some locations after the failure.
5. The failed masses in Ehime, Kochi, and Tokushima prefectures were chiefly composed of thick colluviums and intensely fractured green politic schist whereas in Kagawa prefecture, decomposed plutonic and volcanic rocks was the main composition.
6. A large number of failed masses in northeastern hills of Ehime were identified as translational slides. These were found on topographic hollows or zero-order basins and they start to flow in a first-order stream channel. The slip surface was found located between 0.3 m and 2 m between soil colluvium and decomposed bedrock. The initially failed mass in the upper section of some of the steep slopes was found completely utilized in transforming into the debris flows.
7. Most of the slope failures were found on gentle to steep mountain slopes with loose soil colluviums or residual deposits above the weathered sedimentary bedrock.

4.5 Chapter summary

In Chapter 4, brief information about typhoons in Japan and Shikoku, typhoon rainfall-induced landslides in various prefectures of Japan, and characteristics of landslides in 2004 was given. Japan is one of the most prominent typhoon regions of the world where many landslides triggered by heavy typhoon rainfalls occur ever year. In 2004, ten typhoons hit Japan and six of them caused significant impact in Shikoku Island. Due to extreme typhoon rainfalls of various intensities in that year, a large number of landslides and debris flows were triggered. The number of landslides was much higher in forest area compared to near human settlements. Along with heavy rainfalls, presence of unstable colluvium, weathered rocks, steep slopes etc. were major cause of landslide triggering in 2004. Most of the slope failures were shallow with a depth of <2 m. Simple circular to translational type of failures were the most common types. However, the failure processes in various prefectures were significantly different due to separate typhoon events, bedrock geology, thickness of colluvium, and soil permeability.

Chapter 5

Seepage and slope stability modeling of rainfall-induced slope failures in topographic hollows

Abstract

Topographic hollows contribute to the hillslope hydrology through collection of surface and subsurface groundwater flow into small area in the slope. This causes instability of the hillslopes in topographic hollows repeatedly. Despite extensive studies in the field of slope instability, hillslope hydrology in the topographic hollows has not been so exhaustively explored. In this regard, this study focuses on topographic hollows and their flow direction and flow accumulation characteristics, and highlights hillslope seepage so as to understand porewater pressure development phenomena in relation with slope failures in the topographic hollows. For this purpose, a small catchment in Niihama city of Shikoku Island in western Japan, with a record of seven slope failures triggered by a typhoon-caused heavy rainfall of 19-20 October 2004 was selected. After an extensive field work and computation of hydro-mechanical parameters in unsaturated and saturated conditions through a series of laboratory experiments, seepage and slope stability modelings were done in GeoStudio (2005) using the precipitation data of 19-20 October 2004. The results of seepage modeling showed that the porewater pressure was rapid transient in silty sand, and that the maximum porewater pressure was measured in an area close to the base of topographic hollows, was found to be higher with bigger topographic hollows and vice versa. Besides, a threshold relationship between topographic hollow area and maximum porewater pressure proposed in this study indicates that a topographic hollow of 1000 sq. m area can develop 1.253 kPa maximum porewater pressure necessary for instability.

Keywords: rainfall-induced slope failures, topographic hollows, seepage, slope instability

5.1 Introduction

Shallow landslides or slope failures are a typical geological and hydro-geotechnical problem of mountainous terrains of tropical and sub-tropical regions of the world. Problems related to shallow landslides are ubiquitous. There are three general types of extrinsic factors responsible for triggering the shallow landslides, namely i) geological factors (i.e., earthquakes, volcanic eruptions, etc.), ii) hydrological factors (such as intense rainfalls, a storm waves, rapid snow melting, etc.), and iii) human interventions due to development activities (such as improper slope excavation and loading, rapid reservoir drawdown, blasting vibration, etc).When rainfall is an extrinsic factor, the type of landslide depends on intensity-duration of the rainfall events and soil permeability (Pasuto and Silvano 1998, Guzzetti et al. 2004, Matsushi and Matsukura 2007, Dahal and Hasegawa 2008, Capparelli et al. 2009). For example, short and intense rainfall can trigger mostly shallow landslides and debris flows in relatively high permeability soils (such as granular soils) (Campbell 1975, Johnson and Sitar 1990), whereas moderate intensity rainfall distributed over a long period can initiate shallow as well as deep-seated landslides in relatively low permeability soils (such as clayey soils) (Cardinali et al. 2006).

Various studies show that rainfall threshold for landsliding varies from one region to another based on hydro-climatological and geophysical properties, such as regional and local rainfall characteristics and patterns, slope morphometry, soil characteristics, lithology, micro-climate and geological history (Crosta 1998, Van Asch et al. 1999). It may also vary with time (Crozier 1999), such as due to seasonal change in vegetation (Wieczorek and Glade 2005). Statistical models are frequently used to estimate rainfall threshold for landsliding such as in Caine (1980), Kim et al. (1991), Glade et al. (2000), Sidle and Dhakal (2002), Dahal et al. (2008c), in which statistical analyses between landslide events and rainfall characteristics are carried out. However, a statistical modeling is possible only when there is a good number of data available in relation with landslide events and rainfall conditions. For a limited number of data, hydrological models are pertinent to investigate rainfall-induced shallow landslide triggering mechanism (Terlien 1998).

Hydrological models have been widely applied to predict porewater pressure development due to rainfall infiltration (Brooks and Richards 1994, Ekanayake and Phillips 1999, Iverson 2000, Frattini et al. 2009). Generally, a coarse-grained soil slope fails in saturated condition because its high permeability leads to development of positive porewater pressure. In case of fine grained soils, however, there is no rapid development of positive porewater pressure owing to poor permeability. Failure of a fine-grained soil slope

in unsaturated state occurs rather because of decrease in shear strength of the soil due to loss of matric suction. Also, some studies suggest that shallow failures are due to increased positive porewater pressure, whereas reduction in matric suction leads to deep-seated failures (Corominas 2001, Guzzetti et al. 2004). To simulate both saturated and unsaturated failure mechanisms in the slope mass, hydrological models based on the topographical flow routing are in use. These yield simulated soil saturation above the impermeable bedrock which is usually used in slope stability modeling for accurate simulation of conceivable conditions. Few examples of hydrological slope stability models are TOPMODEL (Beven and Kirkby 1979), HYSWASOR (Van Genuchten 1980), CHASM (Anderson and Lioyd, 1991), HILLFLOW (Bronstert 1994) or GWFLUCT (Terlien 1996), SHALSTAB (Dietrich et al. 1998), SINMAP (Pack et al. 1998) and ASWSM (Crozier 1999). The GeoStudio (2005) is another coupled hydrological slope stability model, in which SEEP/W and SLOPE/W plugins are used to simulate instability mechanism of slopes during extreme rainfalls.

Shallow landslides are generally confined to steep slopes of topographic hollows (Hack and Goodlett 1960, Dietrich and Dunne 1978, Sidle et al. 1985, Reneau et al. 1990, Chen and Jan 2003, Miller and Burnett 2007), eventhough they may occur on planar slopes (May 2002). Topographic hollows consist of thick soil colluviums fed from immediate convex topography and have propensity to collect excess groundwater table during an extreme rainfall. However, they drain much slowly in comparison to ridges (Dunne 1978). This leads to rapid buildup of porewater pressure in the soil mantle of topographic hollow resulting in reduced shear strength (Montgomery and Dietrich 1994). Thus, topographic hollows are susceptible to slope mass movement as shallow rapid landslides. A hollow with high soil depth and wide area might experience repeated failures. Based on the way of development, topographic hollows are of two types namely type A and type B (Tsukamoto and Minematsu 1987). Type A is developed due to saturated interflow in the surface soil. A large number of spoon shaped hollows are formed with typical and distinct topography. Rapid weathering of bedrock materials and the short recurrence interval of surface soil slides are the characteristics features of this type of hollows. Topographic hollows in weathered granite areas and sedimentary areas are of this type in most parts of Japan (Tsukamoto and Minematsu 1987). Type B is developed due to saturated lateral flow or ground water outflow through highly fissured bedrocks. These are more common than type A. Between the A and B types, the dominant type is identified by the permeability of the weathered bedrock below soil colluviums. The possibility of failure during any given

period of hollow development depends on the soil depth, vegetation rooting strength, slope type, soil properties as well as stochastic processes triggering the slope failure (Sidle 1987).

Once a failure occurs in a topographic hollow, the materials tend to flow from adjacent hillslopes and accumulate into the hollow. The materials accumulate through various processes such as surface wash, soil creep, windthrow, surface ravel of soil and organic material, sloughing of material around the perimeter of the scar and detrital deposits from established vegetation (Dietrich and Dunne 1978, Swanson and Fredriksen 1982, Sidle et al. 1985). The process of accumulation continues till next slide occurs after certain interval. This is why topographic hollows are considered as fad and they soon fail (Dietrich et al. 1987). The liquefaction process on topographic hollows has been examined by Sassa (1986), who concludes that failure is enhanced by loading caused by sliding mass from the upper creeping and/or residual slope. Nevertheless, the slope failure mechanism with subsurface hydrology is still a topic of in-depth research. In this context, this research attempts to understand subsurface hydrology of topographic hollows in a tertiary sedimentary terrain, a part of Shikoku Island in western Japan.

The main objective of this study is to investigate hydrological and mechanical phenomena in topographic hollows for triggering slope failures during an extreme rainfall event. For this, a small catchment known as Higashifukubegawa catchment in Niihama city of Shikoku in western Japan, which was severely damaged by a typhoon rainfall event of 2004, was selected. Along with the main objective, the following are specific research objectives of this study.

(i) Understand the change in negative and positive porewater pressure distribution in the slopes of sedimentary terrain during extreme rainfall

(ii) Discover the role of hydrological parameters (i.e., soil permeability and porosity) within the topographic hollows for development of transient porewater pressure regime

(iii) Investigate the relationship between hillslope seepage and topographic hollow area

(iv) Understand the role of geotechnical properties of soil in slope failure

(v) Understand the contribution of topographic hollows in hillslope instability

5.2 Study area

5.2.1 Location and geological outline

The study area, as shown in Figure 5.1, is located in the northeastern part of Niihama City, in Ehime prefecture, Shikoku. Niihama city is one of the economically important cities in

the prefecture. It has many industries on the plain area. The selected catchment (Figure 5.2) opens in north and has tentative oval shape. Geographically, it extends from (33 ° 58' 12") N to (33 ° 58' 27'') N latitude, and (133 ° 22' 41'') E to (133 ° 22' 59'') E longitude. The spatial extent of the catchment is about 142,000 sq. m and the elevation ranges from 42 m to 213 m from the mean sea level. The north-, northeast-, east-, and northwest-facing slopes are dominant in the catchment.

Shikoku Island consists of three main geological units namely Ryoke, Sambagawa-Chichibu and Shimanto belts from north to south. The Higashifukuwegawa catchment falls in Ryoke belt and consists of tertiary shale and sandstone of the Izumi group. The sandstone is heavily fractured and intercalated with shale beds.

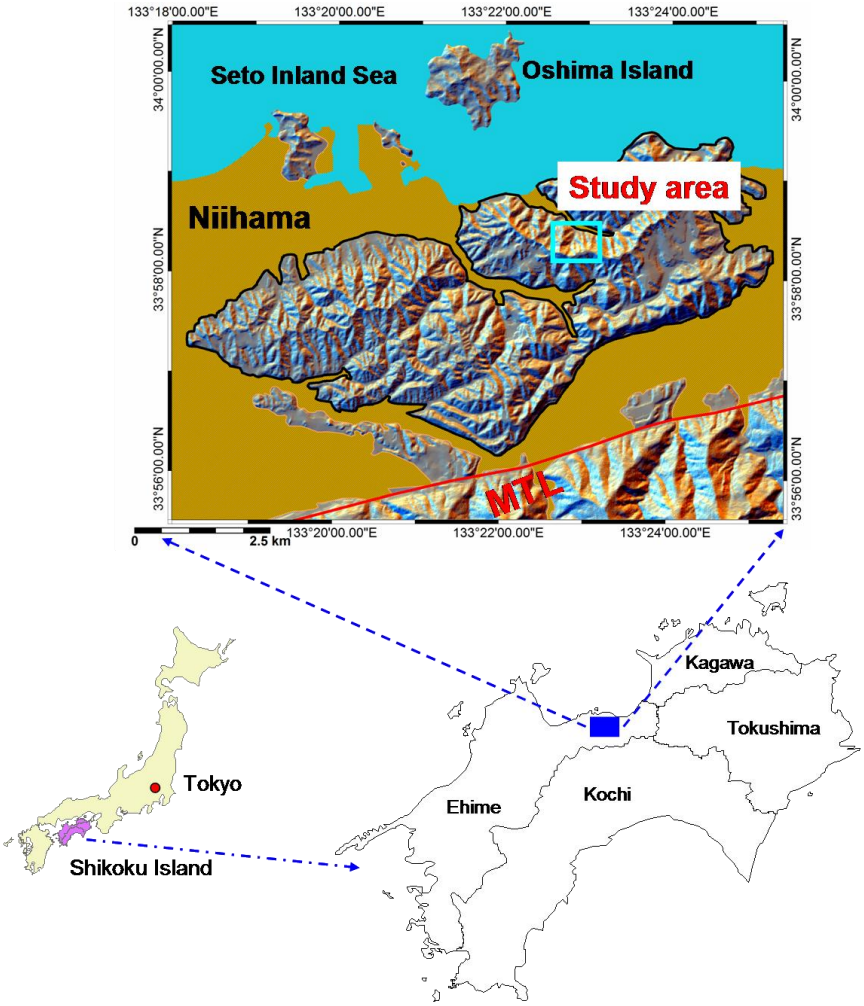

Figure 5.1 Location map of the study area

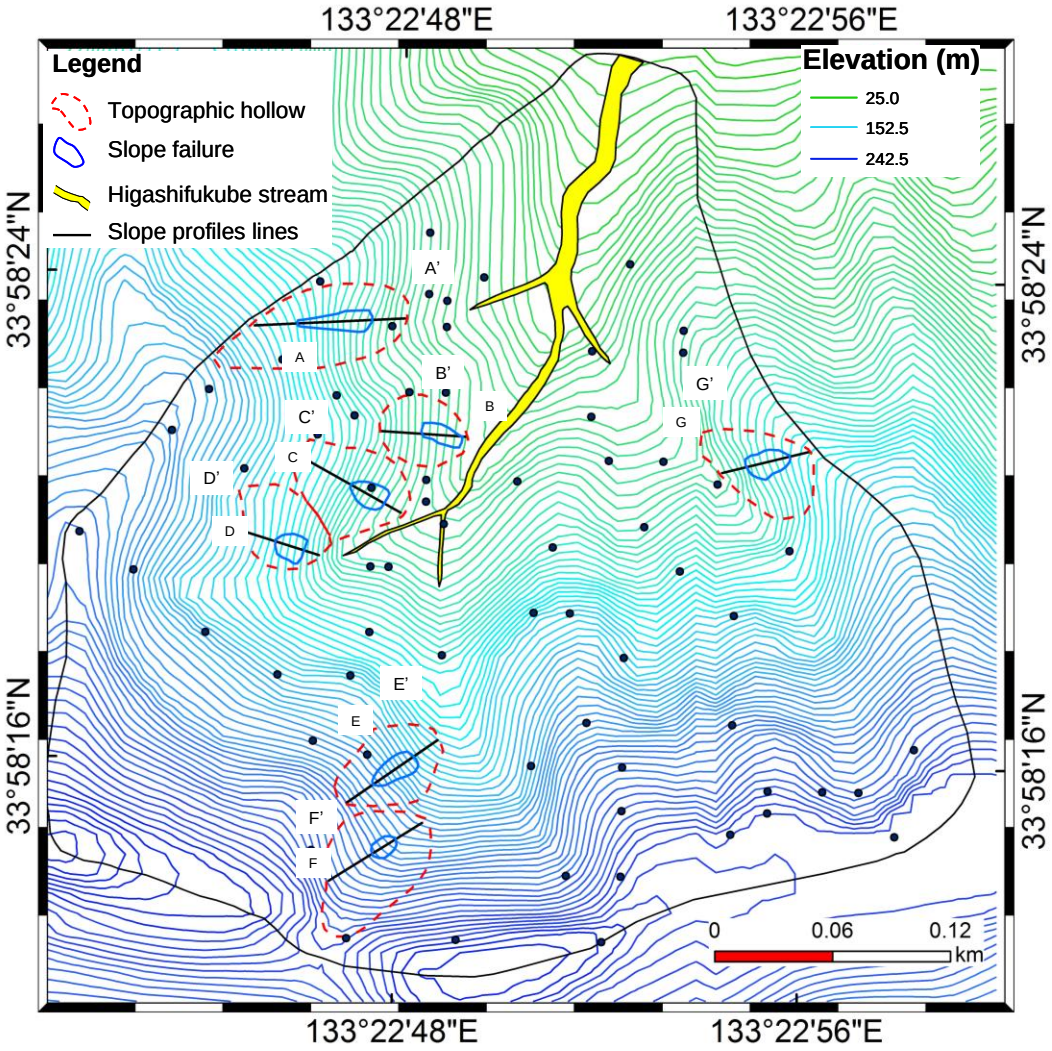

Figure 5.2 Higashifukubegawa catchment with topographic hollows, slope failures and slope profile lines (black points are the locations of measurement of soil thickness and soil thickness at each location is given in **Appendix A**)

5.2.2 Typhoon rainfall and slope failures in 2004

Typhoons are one of the strongest meteorological events on earth. These are formed as a result of strong interactions between high speed spinning clouds and Coriolis effect of the earth's rotation. They follow certain path (e.g., straight, parabolic, northward track, etc.) and can cause strong winds, heavy rainfalls, river floods, storm surges, and high ocean waves. Typhoon rainfalls are highly intense in comparison to any other types of rainfall. But they persist for a certain period only and are region specific. A particular area can receive relatively a greater amount of rainfall, so the impacts are localized and temporal. In Japan, August and September are a frequent typhoon season.

In 2004, Japan suffered a massive economic loss due to extreme typhoon rainfall events of various intensities. Nine out of ten typhoons that hit the Japanese archipelago in 2004 severely impacted Shikoku Island. Ehime prefecture suffered from typhoons 0415, 0416, 0418, 0421, and 0423. Particularly, rainfall due to typhoons 0415, 0421 and 0423 triggered many slope failures at different locations in northeast Ehime. The hardest hit area was Niihama City (about 140,000 residents), where many debris flows near the hill bases killed 25 people and destroyed 40 billion yen worth of property (Bhandary and Yatabe 2005). In addition, greater than 1500 slope failures and debris flows occurred only in the northeastern forests of Niihama during various typhoon events in that year. In the study area, a total of seven slope failures indicated as A, B, C, D, E, F and G in Figure 5.2 occurred during the heavy rainfall of 19-20 October 2004 caused by the typhoon 0423 (Tokage). Slope failures A, B and D were found in east-facing slopes, whereas C was in southeast, E and F were in northeast, and G was in west-facing slopes. The slope failures were found in seven different topographic hollows, namely A', B', C', D', E', F' and G' (Figure 5.2), recognized precisely in the topographical map based on flow direction and flow accumulation characteristics [Figure 5.3 (a, b)]. In this study, all these seven slope failures were considered for the seepage and instability analyses.

5.3 Parameter preparation

5.3.1 Field survey

Field investigation was conducted to observe changes in site conditions (geotechnical/hydrological conditions) and topographical features (geological/geomorphological characteristics). The study area was visited in October, November, December, and April of 2011 and November of 2012 to observe change in vegetation and response of the catchment slopes during various rainfalls in these months. A detailed field investigation was carried out to measure length/breadth of slope failures, soil thickness and soil permeability. The soil thickness above weathered bedrock was measured by dynamic cone penetration test near the failed slopes (Figure 5.2). The permeability within the unsaturated zone was measured by Hasegawa in-situ permeability tests (Daitou Techno Green, 2009). Furthermore, soil sampling was done for soil classification and measurement of shear strength parameters in the laboratory. It was done at the mid of each slope failure scarps. To determine the field density, 100 cubic centimeter steel tubes were used to collect undisturbed soil samples.

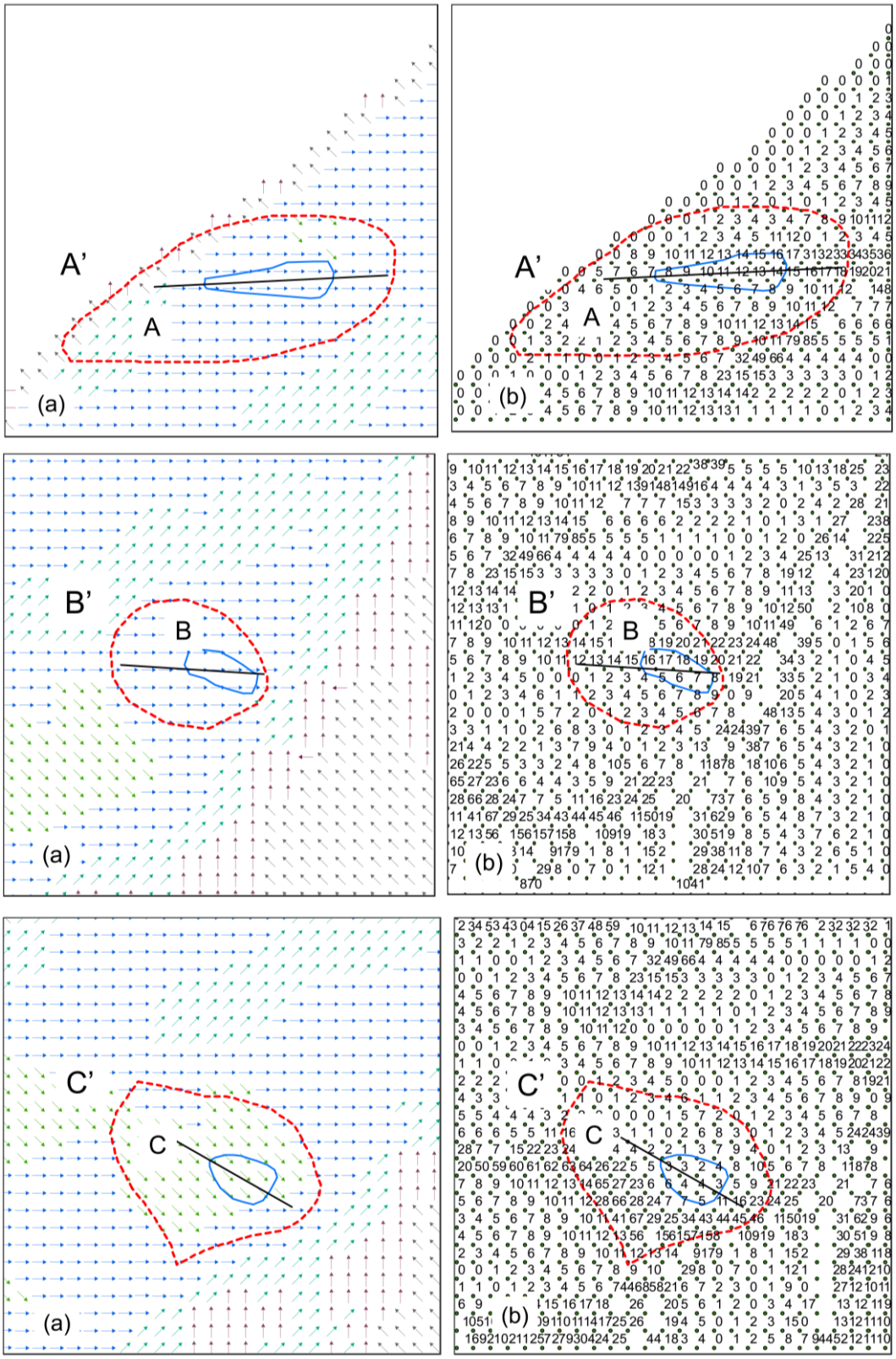

Figure 5.3 (a) Flow direction map and (b) Flow accumulation map (showing topographic hollows A', B', and C' recognized around slope failure A, B, and C based on flow direction and flow accumulation) **Continue**….

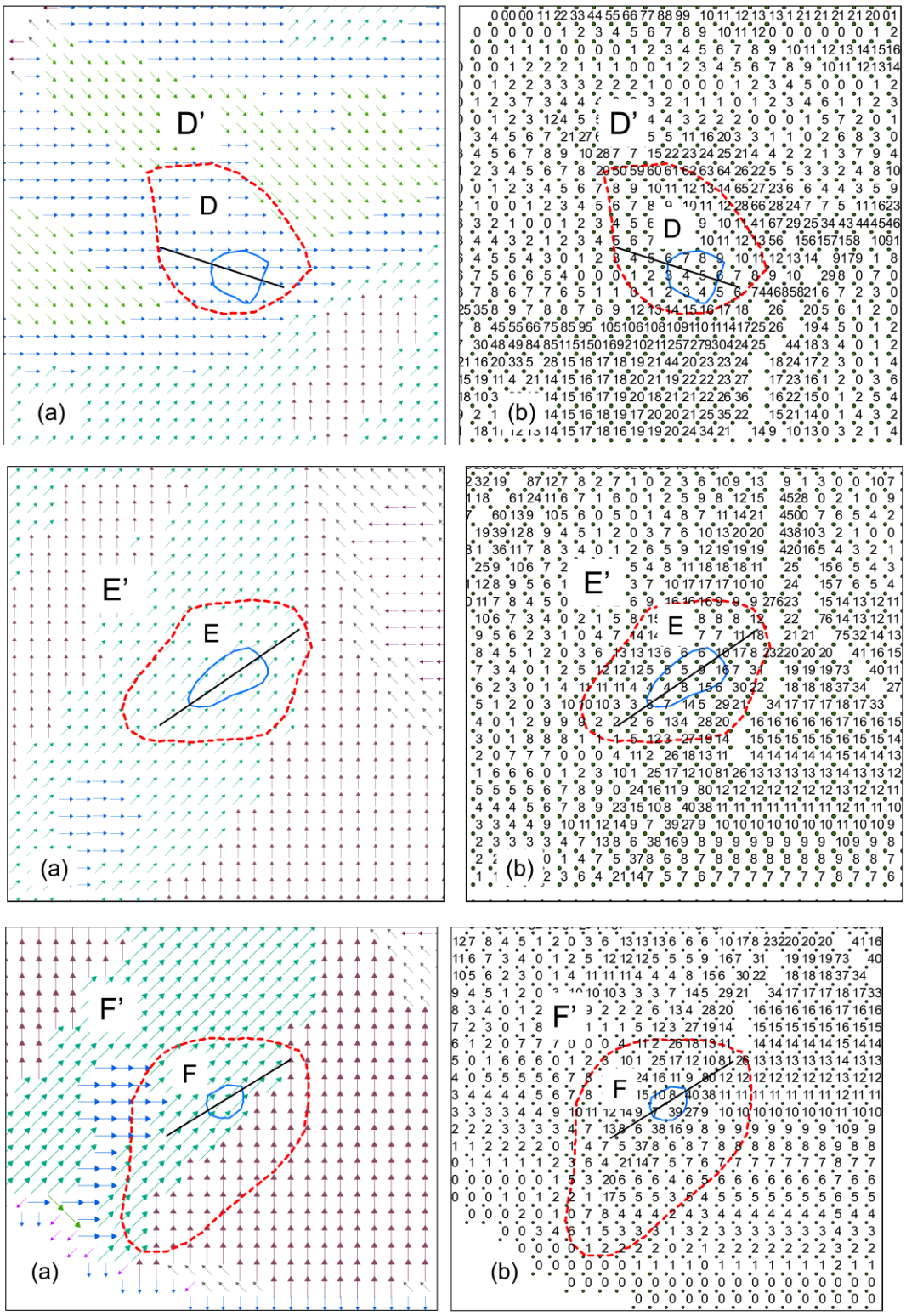

Figure 5.3 (a) Flow direction map and (b) Flow accumulation map (showing topographic hollows D', E', and F' delineated around slope failure D, E, and F based on flow direction and flow accumulation) **Continue**….

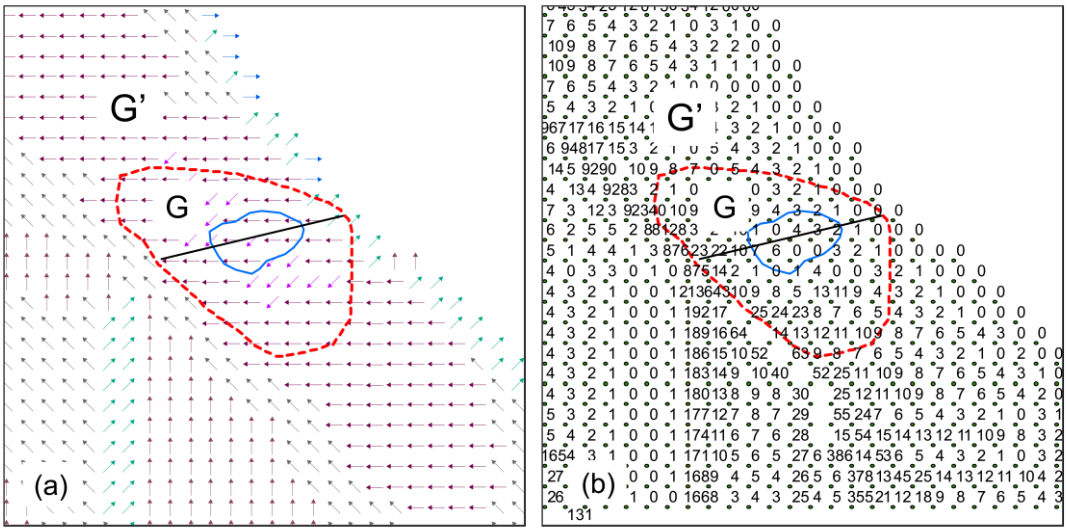

Figure 5.3 (a) Flow direction map and (b) Flow accumulation map (showing topographic hollow G' delineated around slope failure G based on flow direction and flow accumulation)

5.3.2 Laboratory tests

To obtain reliable information about the soil properties, a series of tests were performed. Firstly, basic laboratory tests were carried out (i.e., for unit weight, porosity, particle size distribution, etc.) and then the soils were classified based on Unified Soil Classification System (USCS). For this purpose, a wet sieve analysis was used for the coarser soil particles (>2 mm) and hydrometer test was used for the finer soil particles (<75µm). ASTM D422 and D4318 (ASTM, 1999a, b) standards were referred in the soil type classification. To determine frictional properties of the collected soil samples, direct shear tests were conducted. The specimens for direct shear test were prepared from the material finer than 2 mm. All the specimens were sheared in saturated drained conditions under 30 kPa, 80kPa, and 100 kPa of normal pressures.

5.3.3 Physical properties of slope materials

Based on the results of laboratory investigation and after referring to USCS, the soils found in the study area were classified into three types: silty sand (SM), silty gravel (GM) and silt (M). Among which, silty sand (SM) was dominant. The particle size distribution curves are more or less similar for all sites (Figure 5.4). Soil permeability value was found to range between 10^{-6} and 10^{-8} m/s, as obtained from in-situ permeability tests. The hydro-

mechanical parameters and geomorphological properties of seven failure sites are listed in Table 5.1. As stated above, soil cohesion and angle of internal friction were determined by direct shear tests while volumetric water content at saturation and unit weight were determined in the laboratory. All these parameters were used in the seepage and slope stability modeling as detailed out in sections 5.4.2 and 5.4.3.

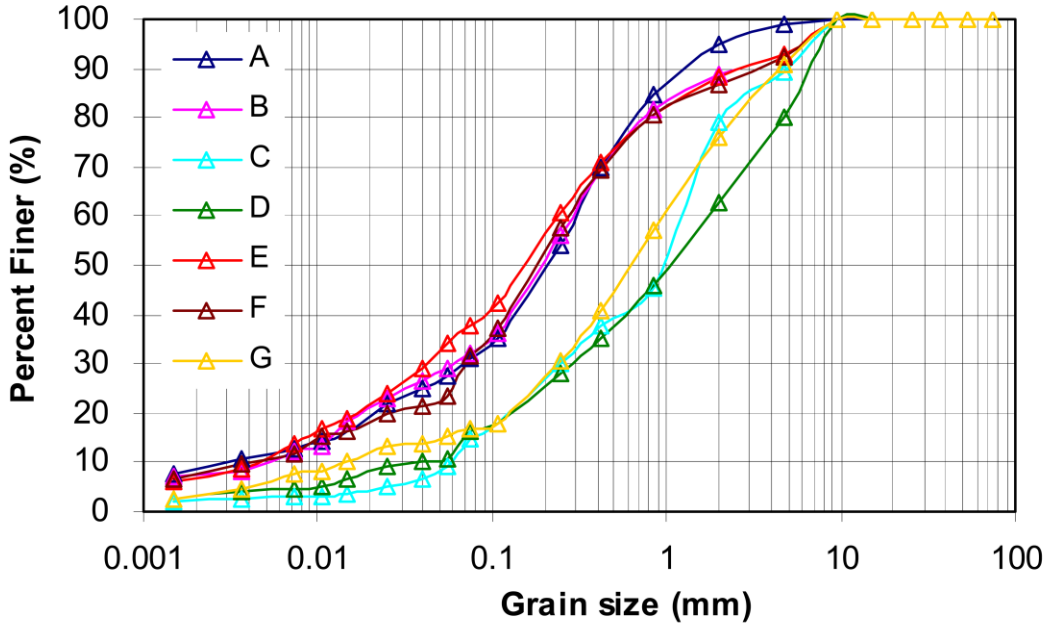

Figure 5.4 Grain size distributions of the soils from failed slopes

Table 5.1 Results of field and laboratory investigations

Slope failure spot	Slope failure length, L (m)	Slope failure breadth, B (m)	Average slope angle, Θ (°)	Soil thickness, D (m)	Effective cohesion*, c'(kN/m^2)	Unit weight*, γ (kN/m^3)	Effective angle of shearing resistance*, ϕ'(°)	Soil permeability, k (m/s)	Volumetric water content, n
A	38.02	10.45	33.38	0.60 - 1.10	0.49	16.92	34.86	1.20×10^{-6}	0.50
B	20.13	9.11	27.46	0.26 - 1.03	0.62	15.83	33.72	5.80×10^{-8}	0.45
C	19.33	12.92	33.00	0.11 - 1.42	1.44	16.92	34.14	6.80×10^{-8}	0.46
D	15.32	13.51	32.90	0.16 - 0.80	0.78	17.08	36.76	8.30×10^{-8}	0.48
E	25.02	12.26	38.86	0.12 - 1.18	0.86	17.22	33.01	1.70×10^{-8}	0.43
F	13.81	8.67	21.78	0.55 - 1.78	0.13	15.83	34.21	2.35×10^{-8}	0.50
G	22.32	13.41	29.70	0.33 - 0.99	1.33	16.79	33.85	3.10×10^{-7}	0.49

5.4 Numerical modeling

5.4.1 Program selection

To understand seepage in soil layers and to investigate potentiality of failure during rainfall, coupled SEEP/W-SLOPE/W models (Krahn 2004a, b) have been increasingly used (Anderson et al. 2000, Rahardjo et al. 2007, Dahal et al. 2009, Lee et al. 2009, Schnellmann et al. 2010, Muntohar et al. 2010, Rahimi et al. 2010). SEEP/W is a finite element-based program in GeoStudio (2005) which simulates porewater pressure distribution in natural slopes. It uses a numerical discretization technique to solve Darcy's equations for unsaturated and saturated flow conditions and runs the following water-flow governing equation in each time step to compute two-dimensional seepage.

$$\frac{\partial}{\partial x}\left(k_x \frac{\partial H}{\partial x}\right)+\frac{\partial}{\partial y}\left(k_y \frac{\partial H}{\partial y}\right)+q=m_w^2 \gamma_w \frac{\partial H}{\partial t} \qquad (5.1)$$

Where k_x is coefficient of permeability in x-direction; k_y is coefficient of permeability in y-direction; H is hydraulic head or total head; q is applied flux at the boundary; m_w is slope of soil-water characteristics curve; and γ_w is unit weight of water. A more detail about equation (5.1) can be seen in **Appendix B**.

On the other hand, SLOPE/W allows limit equilibrium analysis of soil slope. It uses various methods to compute factor of safety such as ordinary slice method, Bishop's method, Janbu's method, and Morgenstern-Price method. Also, within these methods, several soil strength models can be selected. Both deterministic and probabilistic parameters can be used to perform slope stability analysis. However, SLOPE/W lacks dynamic hydrological modeling of porewater pressure. Therefore, simulated seepage information is directly imported from SEEP/W. In this study, Morgenstern-Price method was used to compute factor of safety since it allows for various user-specified interslice force functions (such as constant, half-sine, clipped-sine, trapezoidal, and data-point specified) which the other methods do not provide. Modified Mohr-Coulomb soil strength model was used in the slope stability analysis to include variation in shear strength due to matric suction in unsaturated soil which is given below.

$$\tau = c'+(\sigma_n - u_w)\tan\phi'+(u_a - u_w)\tan\phi^b \qquad (5.2)$$

Where τ is the shear strength of unsaturated soil; c' is the effective cohesion; $(\sigma_n - u_w)$ is the net normal stress; σ_n is the total normal stress; (u_a-u_w) is the matric suction; u_w is the porewater pressure; ϕ' is the angle of shearing resistance; and ϕ^b is the angle expressing the rate of increase in shear strength relative to the matric suction.

5.4.2 Seepage modeling and results

For coupled seepage and slope stability modeling, longitudinal profiles of all seven failed slopes were prepared through the direction of maximum subsurface flow (Figure 5.2) using a Digital Elevation Model (DEM) of the study area and soil thickness data based on topographical break in the slopes (Figure 5.5). All profile continuums were discretized into a mesh of fine square elements with 4 nodes and 9 integration orders. The numbers of nodes were 4056, 2019, 2124, 1309, 1938, 3366, and 2300, whereas the numbers of mesh elements were 3375, 1616, 1590, 974, 1290, 2800, and 1722 for slope profiles A, B, C, D, E, F, and G respectively. The dimensions of all mesh elements were the same with a side length of <0.2 m and unit thickness. The homogenous soil colluvium above the bed rock was considered to be single layered for the modeling. Infinite element option to the toe of models was avoided since the slope sections directly lead to Higashifukubegawa stream in the downstream.

Soil water characteristics curves (SWCC) and soil permeability functions were portrayed as main input parameters. Soil water characteristics curve function was obtained from curves using similar grain size distribution function provided in GeoStudio (2005). Soil permeability function was estimated from SWCC using Fredlund and Xing (1994) criterion. This criterion removes the need to determine residual water content which is usually required for other predictive methods. The soil layers were considered isotropic (i.e., $k_x = k_y$). During the simulation, SWCC and soil permeability function were integrated with the field values of saturated water content and soil permeability. To avoid excessive high negative pore water pressure in the analysis, a limiting value of -20 kPa was applied as an initial condition. The initial water table was defined along the impervious bedrock. The day of failure in the study area was 20th October, but it is difficult to describe the initial seepage condition in the slope prior to the rainfall events since most of the days of October had considerable rainfall and no data were available for pore water variation. So, the simulation was performed considering extreme rainfall of 19-20 October 2004 caused by the typhoon event 0423.

The left vertical edge and the edge below the water table were assigned as a null flux boundary to prevent seepage contribution from upper slope sections and bedrock. The right vertical edge above water table was specified as null flux boundary with potential seepage face. The hourly rainfall record of 19-20 October of 2004, as the transient flux, was applied to the nodes on exposed sloping surface with potential seepage face as upper

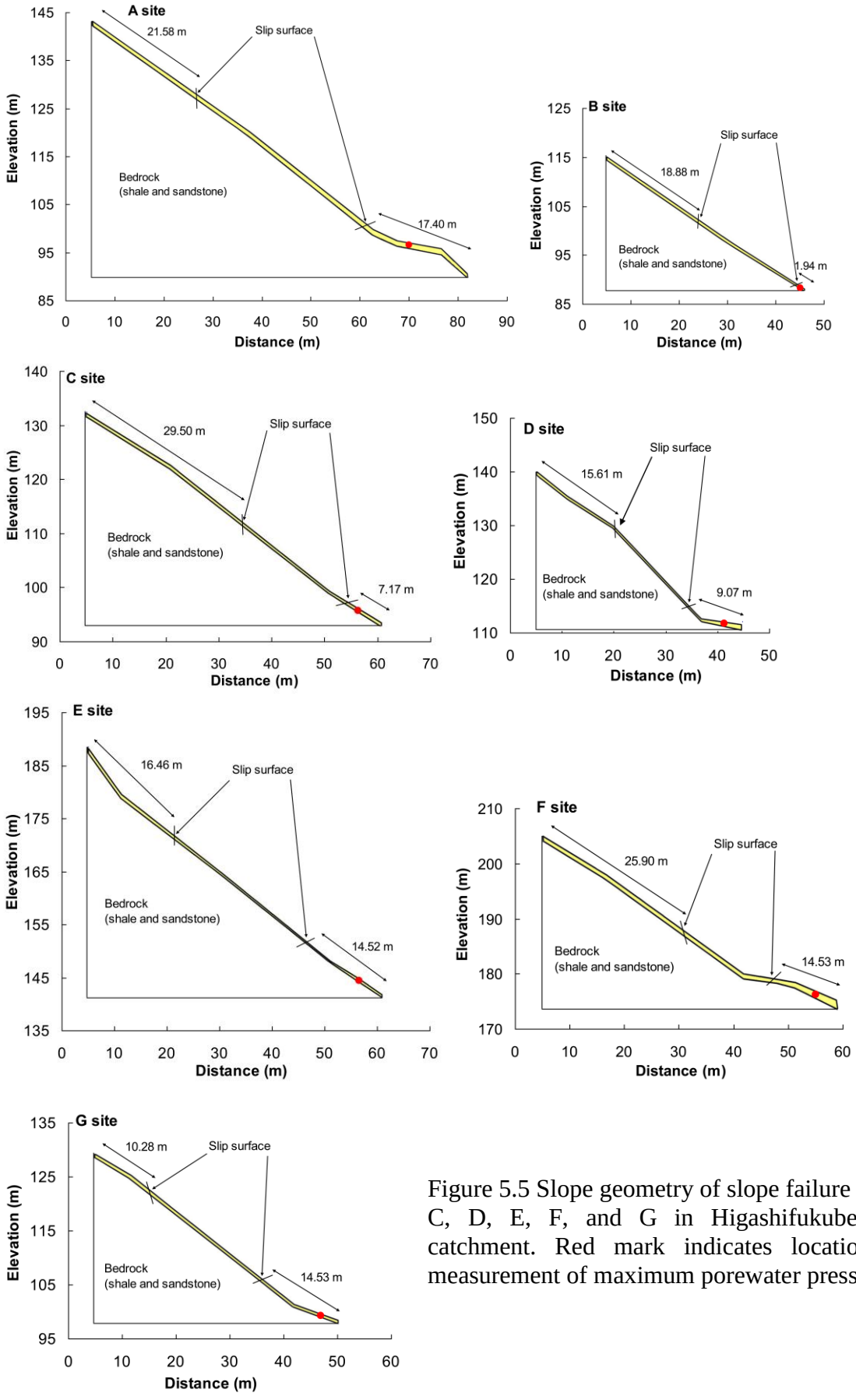

Figure 5.5 Slope geometry of slope failure A, B, C, D, E, F, and G in Higashifukubegawa catchment. Red mark indicates location of measurement of maximum porewater pressure.

boundary condition. Potential seepage face was considered to avoid ponding option to the slope. Figure 5.6 shows a complete layout of the finite element model. The rate of evaporation was not considered in this study because negligible evapotranspiration occurs during typhoon rainfall (Gasmo et al. 2000, Tsaparas et al. 2002). After all, simulations were performed with rainfall record of 19-20 October of 2004[see in **Appendix C**]. To reproduce the complexity of rainfall event, the hourly rainfall data were discretized into 283 time steps of 10 min length (total 47 hours 10 minutes). The maximum porewater pressure was also recorded in the lower elevation of topographic hollows along the slope profiles to investigate the relationship of hillslope hydrology with topographic hollow area.

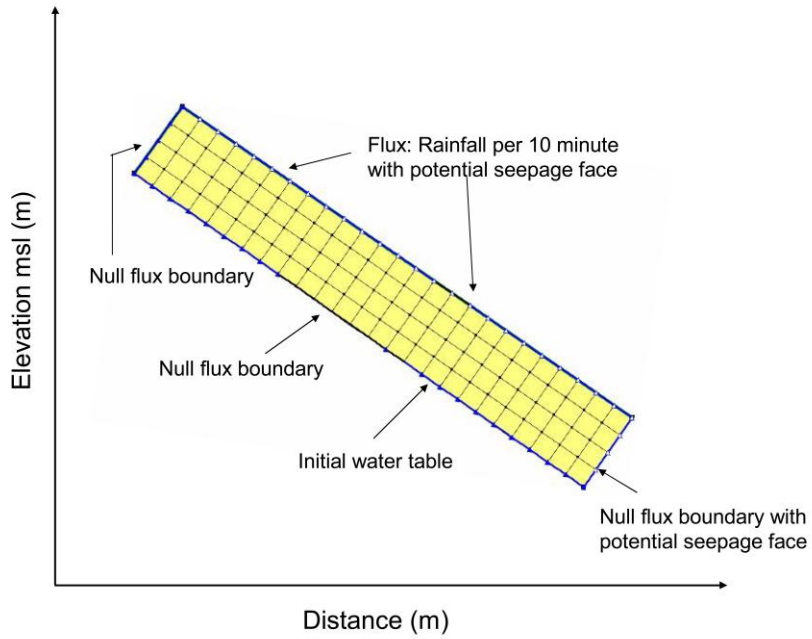

Figure 5.6 Finite element description of the model

Figure 5.7 shows the results of seepage modeling. In all slope failure sites, very rapid porewater pressure response was observed with beginning of precipitation infiltration through the soil by decreasing the matric suction. The porewater pressure regime was transient which was due to soil thickness, soil permeability, porosity and potential seepage face on the slope. Initially, the porewater pressure was negative. With continued rainfall for long enough, the porewater pressure increased gradually. The slope sections were partially saturated before 18:00 hour rainfall (time step 103) of 19th October and saturated condition was reached after 19:00 hour rainfall (time step 108). Between 20:00 hours of 19th October and 6:00 hours of 20 October, rainfall was insignificant. However, continuous

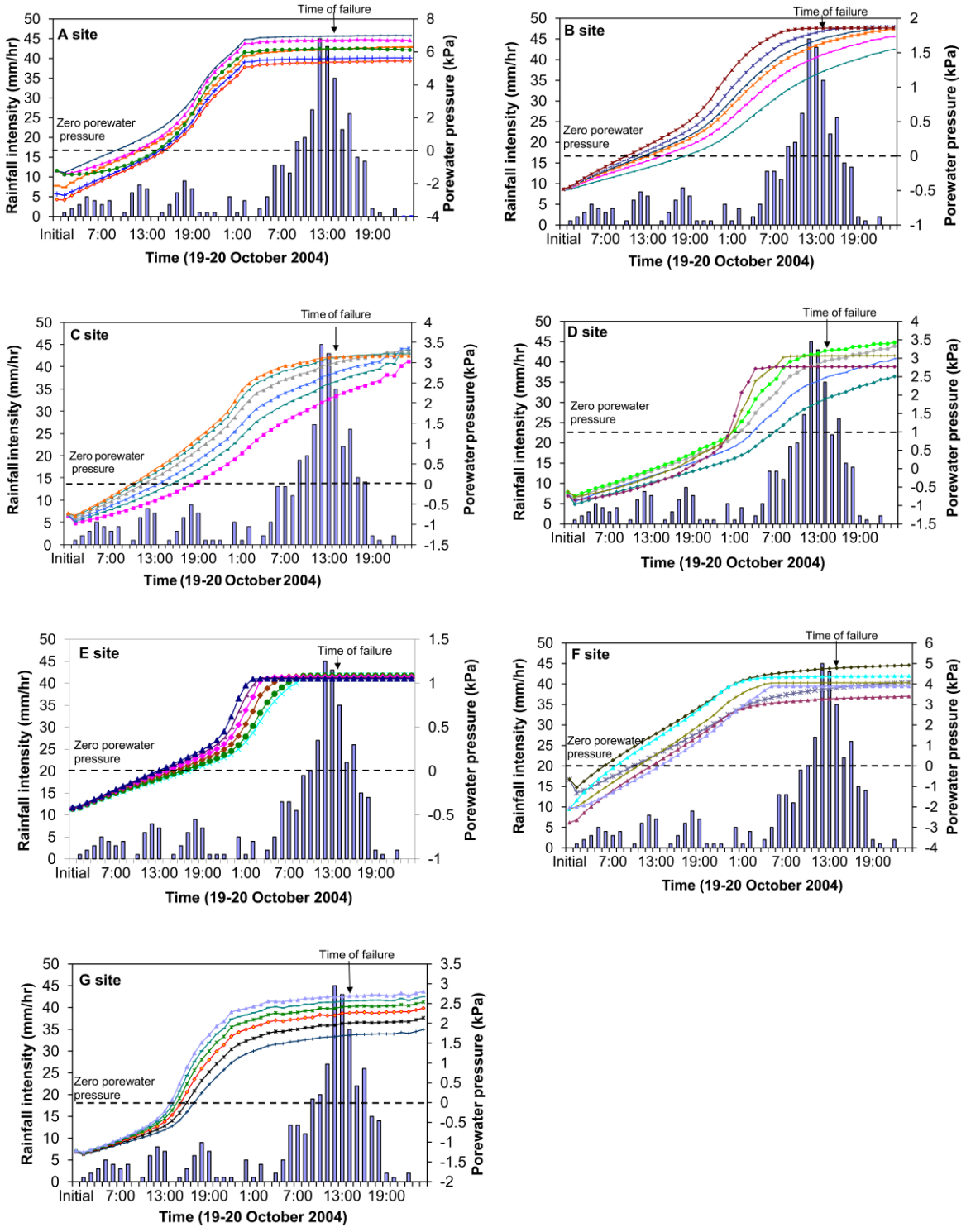

Figure 5.7 Porewater pressure variation in slip surface of seven slope failure sites A, B, C, D, E, F, and G. The low porewater pressure curves represent porewater pressure at nodes of higher elevation along slip surfaces as shown in H-Illustration. The optimized slip surfaces are shown in Figure 5.11

and very rapid rise in porewater pressure was observed at all nodes along slip surface during this period. The rainfall again increased from 8:00 hrs of 20th October and the peak positive porewater pressure reached at 14:00 hour (time step 223) of the same day at majority of nodes.

Figure 5.8 illustrates variation of topographic hollow area with its hydrological characteristics. From this figure, it is evident that bigger the area of topographic hollow, higher is the porewater pressure generation and vice versa. Using maximum porewater pressure data recorded in the area close to the base of topographic hollows, a threshold relationship between maximum porewater pressure and topographic hollow area was established (Figure 5.9). The threshold, exhibited by lower the boundary of the points representing maximum porewater pressure, can be expressed as follows.

$$u = 5.2 \times 10^{-6} \times a^{1.794} \quad (5.3)$$

Where u is maximum porewater pressure in kPa and a is topographic hollow area in sq. m. Equation (5.3) has a coefficient of determination of 0.994. According to this threshold relation, for topographic hollows of area such as 1000 sq. m, the maximum porewater pressure of 1.253 kPa is necessary to cause instability.

5.4.3 Slope stability modeling and results

The two-dimensional seepage simulated in SEEP/W is directly linked to SLOPE/W for slope stability analysis. The exposed slip surface of slope failures defined by field visit and Google Earth Image interpretation was maintained constant throughout the entire typhoon event of 19-20 October 2004. The hydro-mechanical parameters to be used in SLOPE/W are already determined [Table 5.1]. The shear strength due to role of suction (ϕ^b) was not determined in the laboratory. Instead, it was assumed to be 2/3 of ϕ'. Still the geo-mechanical parameters are average which may vary from the actual field values. For example, the effective cohesion, effective angle of shearing resistance, and unit weight are relatively low due to presence of organic matter (dead and decaying plant roots) (Dahal *et al.* 2011). As mentioned above, the value of ϕ^b was assumed. As mentioned above, the value of ϕ^b was assumed. To compensate such uncertainties, it is necessary to perform sensitivity analysis in stability analysis. Sensitivity analysis examines the interrelationship of various parameters used in analysis and then calculates factor of safety based on changes in given parameters such as cohesion, friction angle, unit weight and shear strength contribution due to matric suction (ϕ^b). Owing to this, the factor of

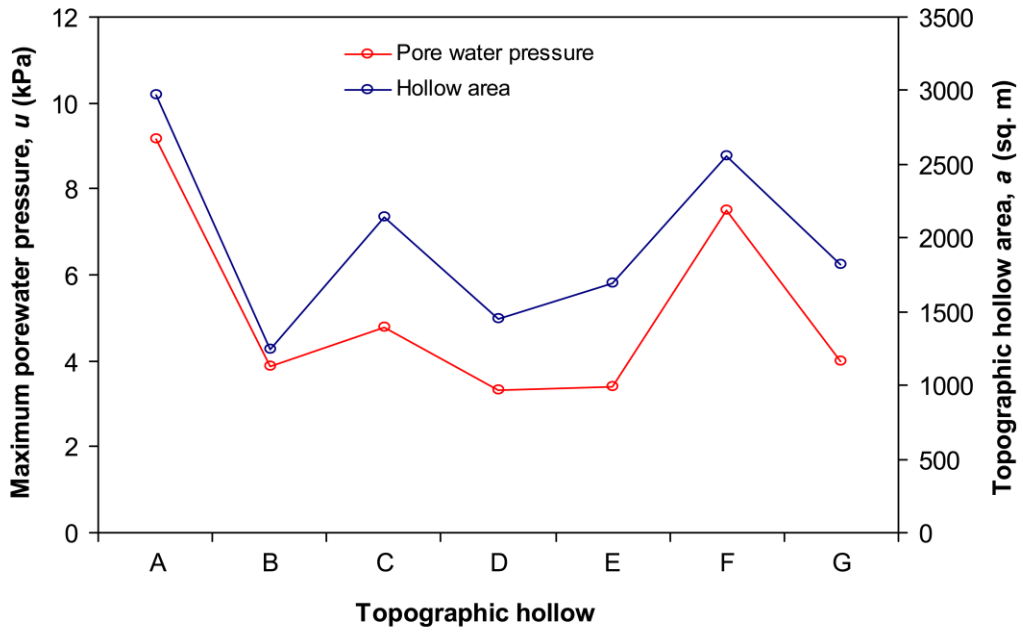

Figure 5.8 Variation of maximum porewater pressure with topographic hollow area

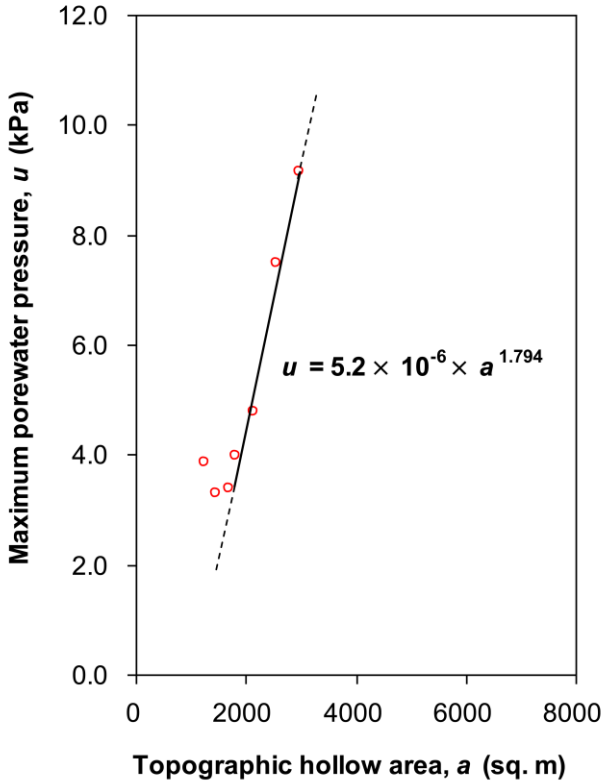

Figure 5.9 Maximum porewater pressure – topographic hollow area threshold curve for slope failure in Higashifukubegawa of Niihama in western Japan

safety distribution via sensitivity analysis has been deemed in this study to compute the factor of safety distribution. For this, minimum and maximum values of cohesion, friction angle, unit weight were assigned as material properties in SLOPE/W environment. Morgenstern-Price (1965) method which satisfies both force and moment equilibrium was adopted with half-sine user specified interslice force function available in SLOPE/W to compute factor of safety. The entry and exit function was used to find the slip centre and the potential failure surface. A total of 2000 iterations were specified in each time step in limit equilibrium analysis. To reduce the basic equation of limit equilibrium method, the sliding mass was divided into 30 vertical slices. In the simulations, the fully specified slip surfaces were also optimized to obtain the most critical value.

Results of slope stability modeling are shown in Figure 5.10. The results illustrate that factor of safety decreases with increase in precipitation under constant soil permeability and volumetric water content values. A sudden decrease in factor of safety was observed at some significant rainfall hours accordingly 8:00, 13:00, 19:00 hours of 19th October and 8:00, 11:00, 14:00, 18:00 hours of 20th October. The corresponding time steps are 43, 73, 109 on 19th October and 187, 205, 223, 247 on 20th October. Immediately after each of these particular hours, the factor of safety began to recover till next significant rainfall hour was reached. At 14:00 hour of 20th October (or time step 223), the factor of safety reduced to <1 in all seven sites (i.e., 0.994, 0.997, 0.998, 0.987, 0.996, 0.998 and 0.993 for A, B, C, D, E, F, and G respectively) which was congruent and it is due to rise in groundwater table up to the crest of the slope. The optimized critical slip surfaces and respective factor of safety on the date of failure are exhibited in Figure 5.11.

5.5 Discussion

The problem of seepage and slope instability in topographic hollow is not a new but ambiguous topic. Although a number of studies have described seepage role in triggering rainfall-induced landslides (Casagli et al. 2006, Tofani et al. 2006, and Harris et al. 2012), they have not considered contribution of topographic hollow in slope instability mechanism. In this regard, this is the first study which has focused topographic hollows and explicitly presented the hydrological and mechanical phenomena in topographic hollows responsible for triggering of slope failure during heavy typhoon rainfall event.

Topographic hollows enhance slope failure through both convergence of subsurface flow into small area in the slope and effect of slope gradient on slope stability

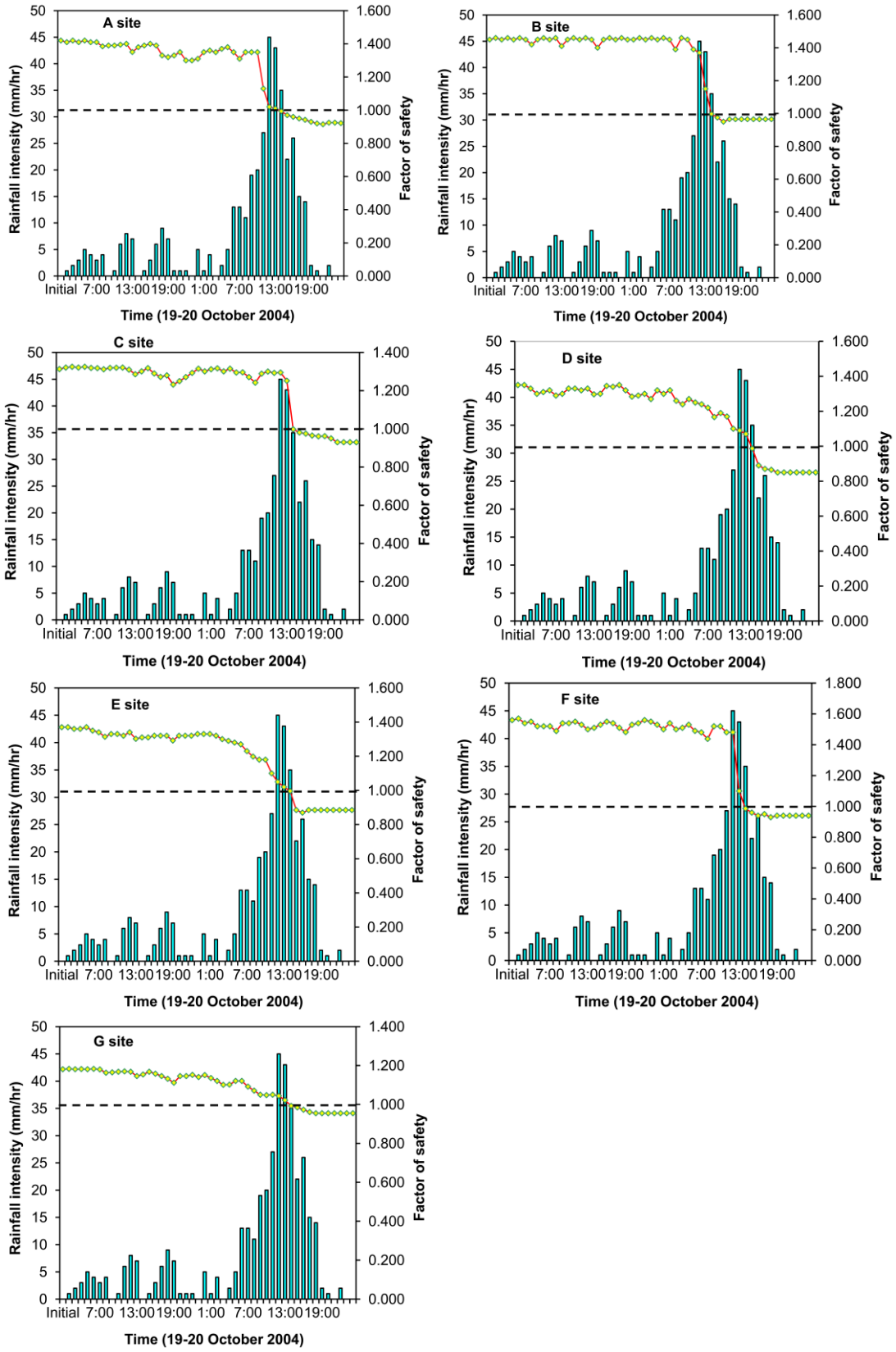

Figure 5.10 Factor of safety distribution in slope failure A, B, C, D, E, F, and G with rainfall of 19-20 October 2004.

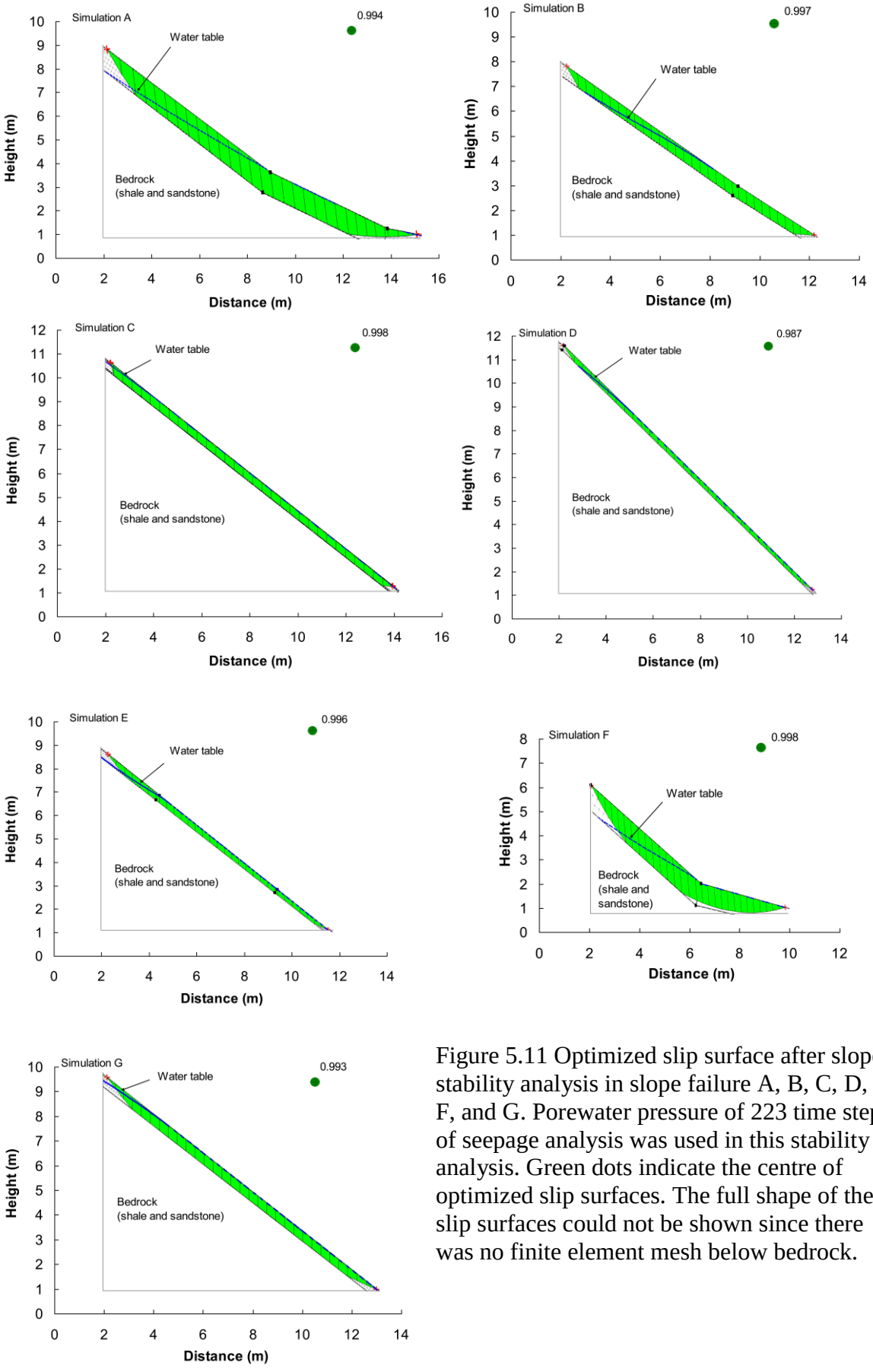

Figure 5.11 Optimized slip surface after slope stability analysis in slope failure A, B, C, D, E, F, and G. Porewater pressure of 223 time step of seepage analysis was used in this stability analysis. Green dots indicate the centre of optimized slip surfaces. The full shape of the slip surfaces could not be shown since there was no finite element mesh below bedrock.

(Talebi et al. 2008a, Montgomery et al. 1997). A number of studies, similar to this study, have linked slope hydrology to instability mechanism in the topographic hollows (Sidle et al. 1987, Montgomery and Dietrich 1994, D`Odorico and Fagherazzi 2003, Talebi et al. 2007). Some monitoring studies have discussed the response of soil in topographic hollow such as variation in subsurface runoff, porewater pressure and temperature during heavy rainstorm (Fannin and Jaakkola 1999, Uchida et al. 2003). Any hydrological and slope stability model without incorporating hollow or basin topography could not represent complexity of topography within the basin (Thorne et al. 1987). Furthermore, the contribution of topographic hollows on hillslope hydrology and slope instability can only be understood when hollows are recognized accurately. Considering this fact, in this study, seven topographic hollows (A', B', C', D', E', F', and G') were identified in topographic map in Higashifukubegawa watershed based on flow direction and flow accumulation characteristics [Figure 5.2 and 5.3 (a, b)]. Hollow A' is oval, B' and D' are rounded whereas C', E', F' and G' are nearly elliptical shaped. The maximum porewater pressures developed in the area closer to the base of topographic hollows were 9.15 kPa, 3.48 kPa, 4.77 kPa, 3.30 kPa, 3.38 kPa, 7.49 kPa, 3.98 kPa for A', B', C', D', E', F', and G' respectively. The bigger hollows produced higher porewater pressure since higher amount of subsurface flow is usually concentrated in bigger hollows and vice versa. A tentative equation of threshold relationship between maximum porewater pressure and topographic hollow area was established. Slope failure A, B, C, D, E, F, and G were identified on respective topographic hollows. All of these slope failures were triggered by extreme rainfall caused by typhoon 0423 in 19-20 October 2004. Therefore, the seepage and slope stability simulations were performed in seven slope failures employing Geostudio (2005) to understand hydrological and instability mechanism in triggering slope failure in topographic hollows.

In seepage simulations, transient porewater pressure was noted at all nodes along potential slip surface during rainfall. Parched water table was started to develop after 10:00 am of rainfall on 19th October. The rainfall prior to major rainfall on 20th October which started at 2:00 am on 19th October continuously increased the transient porewater pressure and enhanced the failure phenomenon. The half-sine interslice force function was used in Morgenstern-Price method to compute factor of safety since it tends to concentrate the interslice shear forces towards the middle of the sliding mass and also diminishes the interslice shear in the crest and toe areas. The results of the slope stability analysis showed that factor of safety was minimum (FS <1) at all sites only after 14:00 pm (time step 223)

on 20th October 2004 (i.e., after 38 hours of continuous rainfall). This implies that failure must have occurred between 14:00 pm and 16:00 pm on the same day. One landslide at Takamatsu-Matsuyama Express Highway in Niihama nearby the study area, which was triggered by the same typhoon event (typhoon 0423), was reported to occur after 10:00 am of 20th October (i.e., after 34 hours of continuous rainfall) (Dahal 2009). It was 4 hours earlier than the failure time in Higashifukubegawa. The failure time in the study area estimated from the seepage and slope stability simulation revealed peak time of failure. The slope failure might have begun in earlier hour of rainfall as higher porewater pressure accumulation (Figure 5.7) also supports this assumption. Moreover, the maximum hourly rainfall and maximum accumulation were 50 mm and 320 mm respectively on the day of failure. The rainfall event with such maximum hourly rainfall intensity and maximum one day rainfall accumulation can cause slope failure in the hilly regions, is well understood (Caine1980, Larsen and Simon 1993, Guzzetti et a. 2004, Aleotti 2004, Dahal et al. 2006, Brunetti et al. 2010). In the simulations, the optimized slip surfaces were comparatively shorter than the actual field value which means that failure problem was started in the upper reach of scarp and the sliding mass also pushed down the slope materials of lower reach. From this research, it is well understood that the topographic hollows collect excess subsurface flow during extreme rainfall and are responsible for instability of hillslopes of sedimentary terrain.

5.6 Conclusions

Topographic hollows are responsible for slope failure during extreme rainfall which is also evident in the present study. The aim of this study was to investigate hydro-mechanical phenomena in topographic hollow for rainfall-induced slope failures during extreme typhoon rainfall event. For this, a typical small catchment in Niihama city of Shikoku in western Japan was selected. The study was preceded with accurate recognition of topographic hollows and identification of slope failures within them. Various field/laboratory experiments were conducted to obtain hydrological and mechanical properties of soil in the topographic hollows. With input of hydrological properties, slope geometry and slope profile of failed slopes, numerical simulations of seepage were performed in SEEP/W program using rainfall record of 19-20 October 2004. The finite element seepage model with simulated seepage is directly linked to SLOPE/W program. Slope stability simulations were carried out using seepage and geotechnical properties of soil. From this study, following conclusions were drawn.

1. Slope failure in topographic hollows occurs due to transient positive and negative porewater pressure development and it is observed in Higashifukubegawa catchment of Niihama.
2. If silty sand is the predominant soil type in topographic hollow, the increment in porewater pressure is always rapid transient which results slope failure.
3. From the numerical modeling, it is understood that slope gradient, rainfall, saturated permeability of soil, porosity, and initial porewater pressure as the main controlling factors for instability in topographic hollows.
4. Maximum porewater pressure recorded in the lower elevation of topographic hollows indicates that bigger the size of topographic hollow, higher is the porewater pressure rise.
5. In this study, a tentative threshold equation relating maximum porewater pressure generated in topographic hollows with topographic hollow area is proposed using only seven topographic hollows and slope failures. This is preliminary attempt and in next research, this kind of work will be replicated and checked in other area of similar geomorphological settings.

Chapter 6

Deterministic slope failure hazard assessment in a model catchment and its replication in neighborhood terrain

Abstract

In this work, we prepare and replicate a deterministic slope failure hazard model in small-scale catchments of tertiary sedimentary terrain of Niihama city in western Japan. It is generally difficult to replicate a deterministic model from one catchment to another due to lack of exactly similar geo-mechanical and hydrological parameters. To overcome this problem, discriminant function modeling was done amongst the deterministic slope failure hazard model and the DEM-based causal factors of slope failure, which yielded an empirical parametric relationship or a discriminant function equation. This parametric relationship was used to predict the slope failure hazard index in a total of forty target catchments in the study area. From ROC plots, the prediction rate between 0.719 – 0.814 and 0.704 – 0.805 was obtained with inventories of September and October slope failures respectively. This means September slope failures were better predicted than October slope failures by approximately 1%. The results exhibit that prediction of slope failure hazard index is possible even in a small catchment scale in similar geophysical settings. Moreover, the replication of the deterministic model through discriminant function modeling was found to be successful with moderate to good accuracy without any use of geo-mechanical and hydrological parameters.

Keywords: rainfall-induced slope failure, deterministic modeling, discriminant function modeling, small catchments of Niihama

6.1 Introduction

Rainfall-induced shallow landslides or simply slope failures in topographic hollows generally occur due to rapid increase in porewater pressure during heavy rainfalls. The process of porewater pressure increase depends on a number of factors, e.g., topographic hollow area, soil type, soil depth, slope morphology, slope gradient, vegetation pattern, microclimate, lithology, geological history, rainfall pattern, etc. (Crosta 1998, Crozier 1999, Van Asch et al. 1999, D'Odorico and Fagherazzi 2003, Wieczorek and Glade 2005). Rainfall events are temporal and their impacts are localized, so they make slope failure process a stochastic phenomenon (Talebi et al. 2008a). It is often hard to remark when and where hillslopes fail and how widespread a potential slope failure event could be during a rainfall event (Godt et al. 2008). Moreover, rainfall-triggered slope failure is a recurring problem in the hillslopes of loose colluvium. So, the slope failure hazard analysis and its management in catchment scales has been a primary concern to geoscientists and geoengineers (Montgomery and Dietrich 1994, Guzzetti et al. 2005, Zolfaghari and Health 2008, Hadmoko et al. 2010, Ching et al. 2011, Arnone et al. 2011, Ghimire 2011, Dahal et al. 2012, Segoni et al. 2012). Slope failure hazard maps in catchment scales can be used as a cost-effective tool for slope failure hazard mitigation planning and risk analysis. With the availability of advanced mapping tools, such as ILWIS, GIS, Remote sensing, etc., and high resolution digital topographical data, a number of methods have been developed mainly for spatial prediction of potential slope failures, which include heuristic methods, statistical methods, and deterministic methods (Soeters and van Westen 1996, Guzzetti et al. 2006).

Heuristic methods (such as in Barredo et al. 2000, Dai et al. 2002, Saha et al. 2002, Pavel et al. 2008, Bijukchhen et al. 2012) are based on expert opinion. Therefore, these methods can not be easily replicated in other areas. In addition, these methods do not include the influence of geo-mechanics and porewater pressure, which are deemed necessary in deterministic methods (Jia et al. 2012).

In statistical methods, a relationship between slope failure location and independent causal factors of the slope failure is established in the form of an empirical parametric function, which is then used to obtain a slope failure hazard map of the target catchment area (Carrara et al. 1999, Cannon et al. 2004, Bell 2007, Dahal et al. 2008a, Pradhan et al. 2010) and also to replicate the hazard index of one catchment to another with the similar set of parameters (Ghimire et al. 2011, Dahal et al. 2012, etc.). However,

like in heuristic methods, the statistical methods also do not incorporate the influence of geo-mechanical processes and hillslope hydrology.

In the deterministic methods, on the other hand, the causal factors are expressed in algebraic terms to determine the factor of safety (Wu and Sidle 1995, Borga et al. 1998, Terlien et al. 1995, D'Odorico and Fagherazzi 2003, Salciarini et al. 2008, Godt et al. 2008, Harp et al. 2009). These approaches utilize a large amount of detailed geo-mechanical and hydrological parameters derived from field and/or laboratory experiments, and computer tool-based modeling. In most occasions, however, the geo-mechanical and hydrological parameters are not available for a large extent of target area (Aleotti and Chowdhury 1999, Wang et al. 2013). Therefore, application of a deterministic method in a larger area or its replication from one catchment to another through the same set of geo-mechanical and hydrological parameters is difficult due to limitations in the availability of these parameters. In this study, we employ deterministic hazard modeling technique to prepare a slope failure hazard map in a tertiary sedimentary terrain of Shikoku Region in west Japan that suffered a large number of slope failures and debris flows leading to heavy loss of life and property in 2004. The study area is relatively small, so the spatial variations in the causal factors, such as amount of precipitation, geology, vegetation, aspect, etc., are negligible, which leads to a situation that a less number of causal factors considered in the hazard analysis results in extremely low prediction rate. It is inevitable that such an area needs deterministic approach for the hazard analysis. So, the prime objective of this study is to prepare a deterministic slope failure hazard model for a catchment and replicate that to other catchments of the study area so as to generate slope failure hazard maps. For this, we selected a small catchment in the study area as the model site, which was severely damaged during the extreme typhoon rainfall events of 2004, and forty other catchments in the same terrain for replicating the hazard model.

6.2 Study area

The study area is situated on the northeastern hills of Niihama city in Ehime prefecture of Japan (Figure 6.1). In 2004, this area suffered an extensive slope failure damage due to extreme typhoon rainfalls of September and October. The total study area covers 30.5 sq. km with ground elevation ranging from 2.5 m to 285 m. It is surrounded by river flood plains in all directions except for the northeast corner where it faces the Seto Inland Sea. Two rivers in Niihama, Kawahigashi and Kawanishi, divide the study area hills into two main regions; Kita-yama and Nishi-no-yama. The study area is well-forested with short-

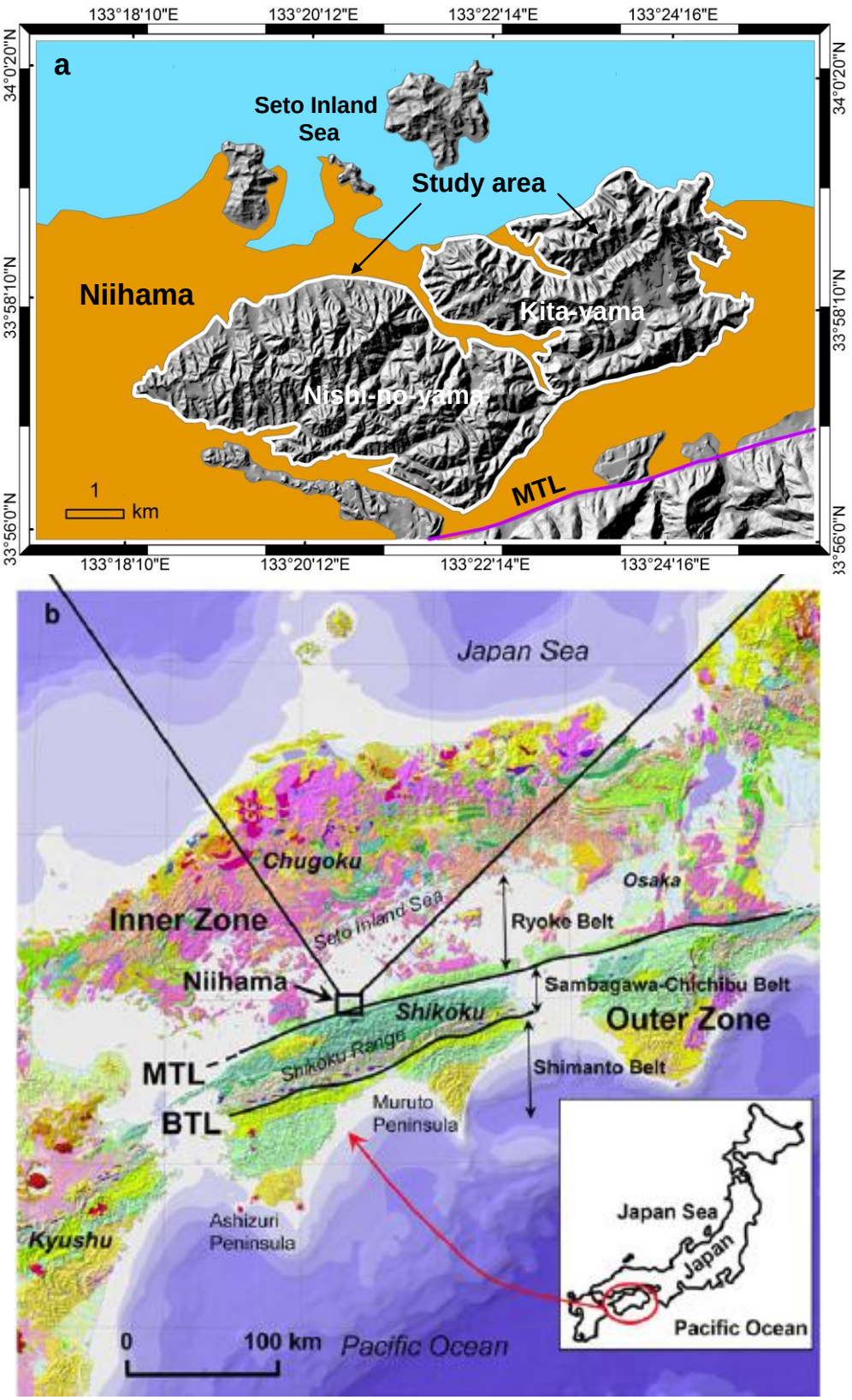

Figure 6.1 **a** Location map of the study area and **b** geological outline of Shikoku Island (modified after Bhandary et al. 2013)

height evergreen and deciduous plants such as Japanese red pine (Pinus deniflora), camphor (Cinanamomum camphora), and Japanese oak (Quercus serrata and Quercus variabilis), Baby rosa (Rosa multiflora), and China root (Smilax china). The upper section of the hillslopes consists of loose, and thin, colluvial soil over impervious bedrock, which is subjected to frequent slope failures. The bases of slopes have debris flow deposits. Also, densely populated residence areas are found close to the hill bases.

The geology of Shikoku region is characterized by three distinct units, namely Ryoke Belt, Sambagawa-Chichibu Belt, and Shimanto Belt. Two northerly dipping major faults, the Median Tectonic Line (MTL) on north and the Butsuzo Tectonic Line (BTL) on south, separate the three geological units (Hashimoto 1991, Dahal et al. 2011). The selected study area falls in the Ryoke Belt and it consists of tertiary shales and sandstones of the late Cretaceous age often known as Izumi group. Typical feature of this geological formation is that piles of intercalated sandstone and shale run in east-west direction.

Japan often experiences heavy rainfalls during periods of extreme climate such as typhoon. Usually, June to October is known to be typhoon season in Japan. In 2004, a series of nine typhoons hit Shikoku Island causing extreme typhoon rainfalls of various intensities, which resulted in a massive loss of life and property. Typhoon 0423 and 0421 severely impacted Ehime, Kochi, and Kagawa prefectures in the region. Niihama city (about 140,000 residents) in Ehime prefecture was the hardest hit area where many debris flows near the hill bases caused 25 deaths and 40 billion yen worth property damage (Bhandary and Yatabe 2005). A total of 424 slope failures in September and 1396 slope failures in October were identified to have occurred in the selected area (Figure 6.2). A higher number of slope failures was found in the Kita-yama area than the Nishi-no-yama area. It was later understood that the maximum hourly rainfall exceeding 50 mm and maximum one day rainfall exceeding 300 mm were the main causes of slope failures (Dahal et al. 2006, Bhandary et al. 2013). Altogether 41 catchments were delineated in the topographical map (Figure 6.2) in the study area. The catchments were selected on the basis of abundance of both September and October slope failures. Figure 6.3 shows the selected catchments in detail (indicated by MC and W1-W40; here, MC is the model catchment and others are the test catchments). In this study, both September and October slope failures were utilized separately to assess the prediction accuracy of slope failure hazard maps in the selected test catchments.

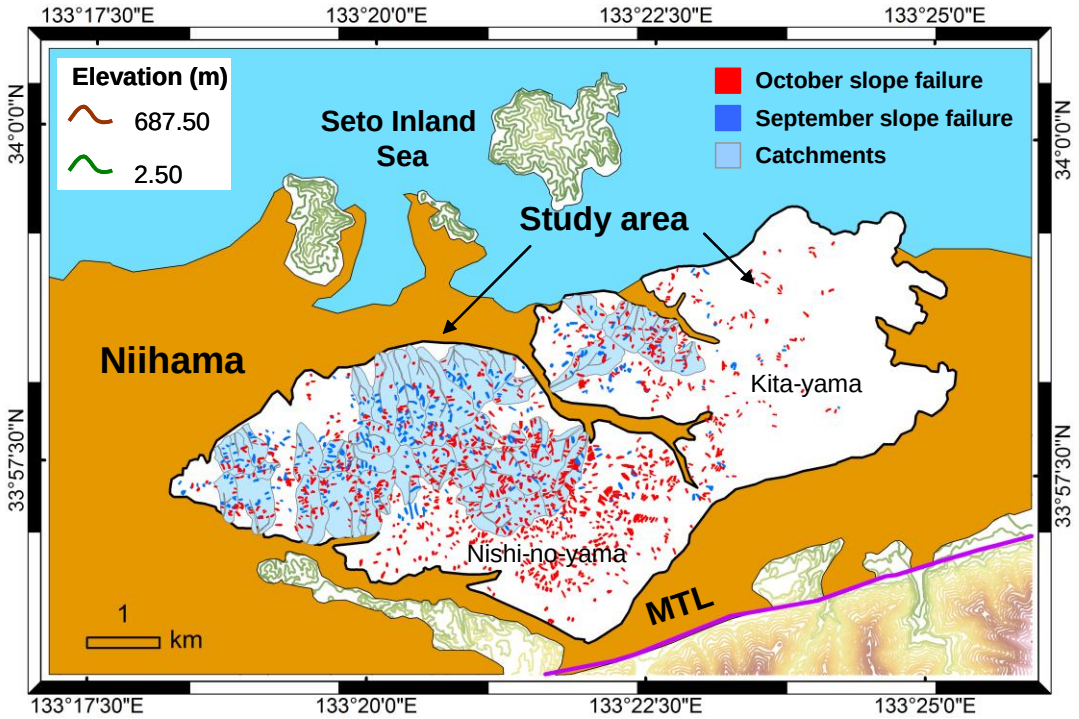

Figure 6.2 Showing distribution of September and October slope failures of 2004 in selected catchments of Niihama

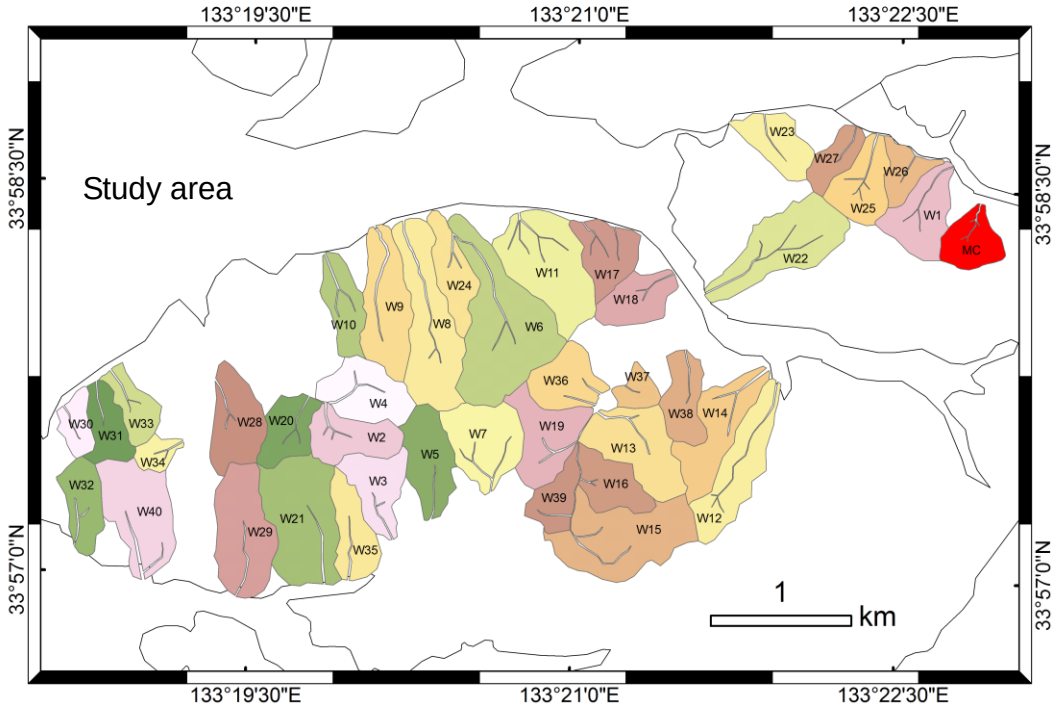

Figure 6.3 The selected model and test catchments in detail

6.3 Methodology

The research framework of this study is illustrated in Figure 6.4. Higashifukubegawa catchment indicated by MC in Figure 6.3 was used for the deterministic slope failure hazard assessment. For this, basic geo-mechanical and hydrological properties of soil, obtained from various sources, were utilized. Both hydrological and stability models were considered in hazard assessment. Hydrological modeling was done at a hillslope scale. From the sub-surface hydrology of individual hillslope profiles, the catchment scale hydrology was derived. The result obtained from the hydrological modeling was then used in stability modeling in pixel basis for the entire model catchment so as to obtain a deterministic slope failure hazard model. The deterministic model thus obtained was then replicated to the test catchments through statistical regression modeling using DEM-derived parameters. The following subsections describe the details of the methods and materials used in the analysis.

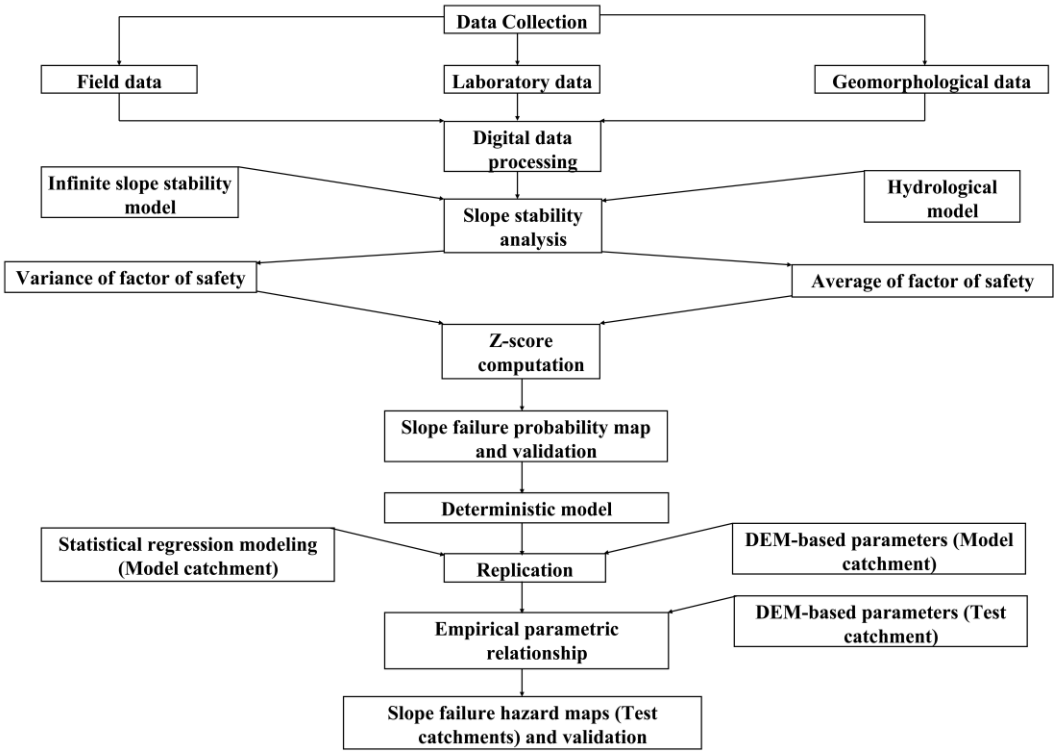

Figure 6.4 Research flow in this study

6.3.1 Model catchment

Higashifukubegawa catchment has tentative oval shape (Figure 6.5). It has spatial extension of 142,000 sq.m and the elevation varies from 42 m to 213 m from mean sea level. The catchment is characterized by steep slopes with shallow colluvium. The slope varies between 0 and 60.57° with mean value of 32.37°. Almost 2/3 of the catchment has slope between 20°and 40°. A detailed slope failure inventory of the catchment was prepared through field checks, Google Earth Image interpretation and inventories of September and October slope failures of 2004. After this, there are no inventories of September and October slope failures for model catchment. The detailed slope failure inventory contains seven slope failures (Figure 6.5) each lying on separate topographic hollows or zero order basins.

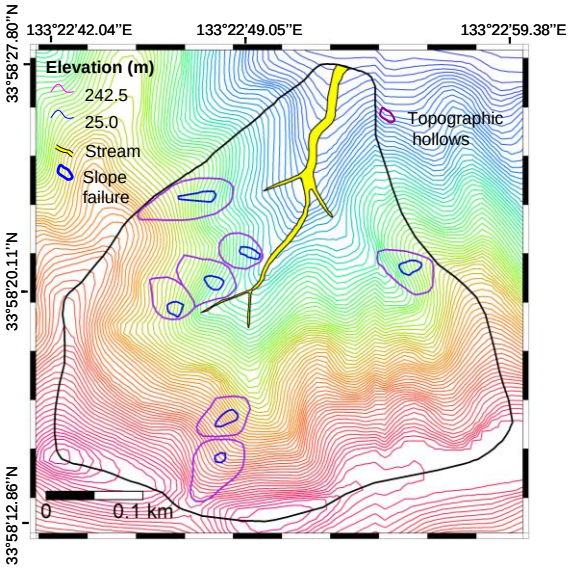

Figure 6.5 Higashifukubegawa catchment with detailed slope failure inventory (showing slope failures within topographic hollows)

6.3.2 Geo-mechanical and hydrological data collection

Field visits were made in October, November, December, and April of 2011 and November of 2012 in the model catchment to observe the response of catchment slopes during various rainfall events in these months. To obtain detailed in-situ/laboratory data, the model catchment was divided into 25 sq. m blocks. The total number of blocks is 261 (Figure 6.6). The in-situ tests such as dynamic cone penetration test to measure the soil thickness above weathered bedrock and Hasegawa in-situ permeability test (Daitou Techno Green, 2009) to measure soil permeability within the unsaturated zone were conducted in

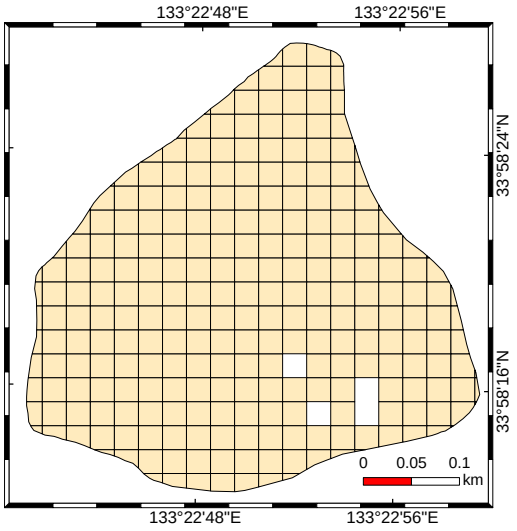

Figure 6.6 Division of model catchment into 25 sq. m blocks (the hollow boxes represent bedrock which were excluded from the study)

each square block. These tests revealed that soil thickness varied from 0.1 m to 1.91 m and soil permeability from 10^{-5} m/s to 10^{-8} m/s in the model catchment. At least one soil sampling was done at each block to determine the basic geo-mechanical properties of soil and to classify the soil type. Mohr-Coulomb parameters of soil strength (C', ϕ') were determined from direct shear test results. Root cohesion (C'_r) was estimated from the findings of Neupane (2005) and information provided by Sidle (1991) for similar types of plants in this study. Also the laboratory tests for saturated unit weight (γ_{sat}), bulk unit weight (γ_t), porosity or volumetric water content (n), and particle size distribution of soil were conducted following the specifications of ASTM. Based on the results of particle size distribution (after referring to USCS and ASTM standards), the soils were classified into five major soil domains namely SM (fine), SM (coarse), SM (medium), GM, and M [SM is silty sand, GM is silty gravel, and M is silt]. The determined geo-mechanical/hydrological data and soil type for each square block is presented **Appendix D**. The extreme values of geo-mechanical and hydrological properties in five major soil domains are given in Table 6.1. Based on soil domains, the model area was partitioned into five zones (Figure 6.7) for deterministic slope failure hazard modeling (see in section **6.3.5**).

6.3.3 Model selection

The reliability of a hazard map depends not only on quality/amount of the incorporated data and working scale but also on appropriate methodology (Baeza and Corominas 2001).

Table 6.1 Geo-mechanical and hydrological properties of soil domains

Soil properties	Major soil domains									
	SM (fine)		SM (medium		SM (coarse)		GM (medium)		M	
	MIN	*MAX*	*MIN*	*MAX*	*MIN*	*MAX*	*MIN*	*MAX*	*MIN*	*MAX*
C' (kN/m^2)	0.31	10.76	1.62	14.11	0.31	12.50	4.49	10.85	9.48	12.50
ϕ' (°)	23.91	43.59	20.92	40.59	22.15	44.59	21.91	33.14	24.33	34.64
C'_r (kN/m^2)	1.92	4.79	0.00	4.79	1.50	4.48	1.92	4.31	1.40	3.35
γ_t (kN/m^3)	10.58	15.04	11.74	16.74	9.58	14.07	14.44	15.07	11.59	13.94
γ_{sat} (kN/m^3)	15.43	18.90	16.33	19.90	15.33	17.39	16.79	17.19	17.43	18.29
n	0.48	0.51	0.45	0.55	0.45	0.52	0.42	0.47	0.41	0.51
k (m/s)	6.12×10^{-8}	2.66×10^{-5}	7.18×10^{-8}	4.67×10^{-5}	8.01×10^{-8}	3.69×10^{-5}	7.78×10^{-8}	1.48×10^{-5}	6.16×10^{-8}	2.17×10^{-5}

Note: The saturation depth (h) and soil depth (z) data are not included in this table. The spatial distribution of these two properties will be prepared in raster format for the whole model area (see in section **6.3.5**)

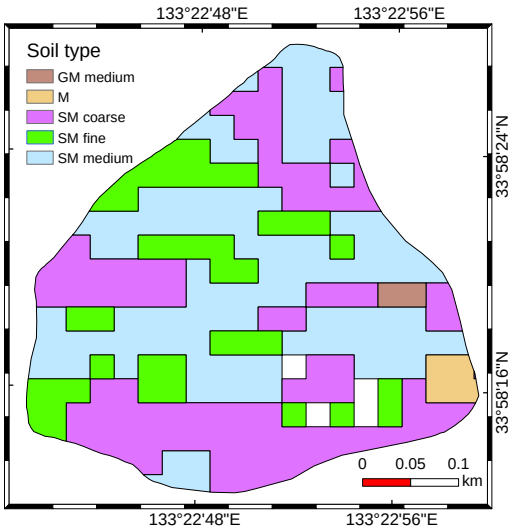

Figure 6.7 Major soil domains in model catchment after soil classification

The models should be chosen also with climatic realization. For this study, we chose SEEP/W (GeoStudio 2005) as a hydrological modeling tool and considered infinite slopes for the stability modeling. Likewise, we used a discriminant function model (multivariate regression model) for the replication purpose. These models have been acknowledged worldwide in recent landslide research such as Gasmo et al. 2000, Acharya et al. 2006, Godt et al. 2008, Lee et al. 2008, Trandafir et al. 2008, Eeckhaut et al. 2009, Cascini et al. 2010, Tarolli et al. 2011, Ghosh et al. 2012, Harris et al. 2012, Jagielko et al. 2012, etc. SEEP/W (GeoStudio 2005) hydrological model is firstly used in slope failure hazard assessment in this study. The following sub-sections briefly describe the models.

6.3.3.1 Hydrological model

As also stated earlier, rainfall is temporal stochastic phenomenon. Amount of rainfall varies with time (Ng and Shi 1998), and with time varying infiltration, the porewater pressure rises/falls above impervious bedrock. This rise/fall (transient behavior) of porewater pressure often controls hillslope instability (Reid and Iverson 1992). But, it is difficult to estimate transient porewater pressure information required to stability analysis of hillslopes (Harp et al. 2009). SEEP/W (GeoStudio 2005) solves this problem. It is a finite element mesh model of non-linearized Richard's equation. Richard's equation explains both saturated and unsaturated Darcian flows through soil layers. Richards's equation to compute 2-dimensional seepage in SEEP/W has the following form.

$$\frac{\partial}{\partial x}\left(k_x \frac{\partial H}{\partial x}\right)+\frac{\partial}{\partial y}\left(k_y \frac{\partial H}{\partial y}\right)+q=m_w^2 \gamma_w \frac{\partial H}{\partial t} \qquad (6.1)$$

Where k_x is coefficient of permeability in x-direction; k_y is coefficient of permeability in y-direction; H is hydraulic head or total head; q is applied flux at the boundary; $m^2{}_w$ is slope of soil-water characteristics curve; and γ_w is unit weight of water. With these inputs, this study uses SEEP/W to compute transient porewater pressure distribution in hillslopes. The computed seepage is then used in infinite slope stability model.

6.3.3.2 Infinite slope stability model

The hillslopes with loose soil colluviums can be recognized as infinite slopes when the soil thickness is limited compared to slope length and width, slope gradient is constant throughout the length, and underlying ground water flow is parallel to the ground surface (Taylor 1948). In such slopes, the failure mass is analyzed as a movement of single block of soil neglecting head and toe portions (Arnone et al. 2011). Infinite slopes are easily destabilized due to rapid rise in positive porewater pressure or loss of soil suction during rainfall (Iverson et al. 1997).The slope mass fails typically at or near the contact between the soil colluvium and impervious bedrock. Generally, the nature of failure is translational. The shear strength acting along the slip surface is given by Mohr-Coulomb criterion (Terzaghi and peck 1967).

$$\tau = C' + (\sigma_n - u_w)\tan\phi' \qquad (6.2)$$

Where τ is shear strength of unsaturated soil; C' is effective cohesion (kN/m^2); (σ_n - u_w) is net normal stress; σ_n is total normal stress (kN/m^2); u_w is porewater pressure (kN/m^2); and ϕ' is angle of shearing resistance (°). During failure, shear stress (T) exceeds shear strength (τ). The ratio F =τ/T is called factor of safety. For an infinite slope, factor of safety can be expressed as below (Hammond et al. 1992).

$$FS = \frac{C' + C'_r + \cos^2\beta[h(\gamma_{sat} - \gamma_w) + \gamma_t(D-h)]\tan\phi'}{\sin\beta\cos\beta[h\gamma_{sat} + \gamma_t(D-h)]} \qquad (6.3)$$

Where C'_r is effective root strength; β is slope inclination (°); γ_{sat} (kN/m^3) is saturated unit weight of soil; γ_t (kN/m^3) is bulk unit weight of soil; h is vertical saturation depth (m); and D is vertical soil depth (m) (as expressed in section **6.3.3.1**; h is estimated from hydrological modeling). The effect of surcharge is neglected in the study. The derivation of equation (6.3) is presented in **Appendix E**. When factor of safety is greater than 1, the hillslope is stable and when it is equal to 1, the slope mass is in verge of failure (limit equilibrium state). An infinitesimally perturbation can result sliding. Equation (6.3) can be expressed in simplified form as follows:

$$FS = \frac{C' + C'_r + A\cos^2\beta\tan\phi'}{B\sin\beta\cos\beta} \qquad (6.4)$$

In which

$$A = h(\gamma_{sat} - \gamma_w) + \gamma_t(D-h) \qquad B = h\gamma_{sat} + \gamma_t(D-h)$$
;

The Mohr-coulomb strength parameters (i.e., C', ϕ') computed in laboratory and root strength (C'_r) may vary from the actual field values. So, these include some degree of uncertainty. The erroneous strength parameters either should not be used (van Westen and Terlien 1996) or the factor of safety computed by using such parameters should be checked for error. Various methods exist in the literature about analyzing propagation of error (Ward et al. 1981, Hammond et al. 1992, Terlien 1996, Burrough and McDonnell 1998).

Calculating expected value and variance of factor of safety and incorporating these into stability analysis to compute z-score is one of the reliable methods (Dahal et al. 2008b). Based on these, equation 6.4 is converted in following linear form.

$$FS = \alpha_1 C' + \alpha_1 C'_r + \alpha_2 \tan\phi' \qquad (6.5)$$

Where

$$\alpha_1 = \frac{1}{B\sin\beta\cos\beta} \quad ; \qquad \alpha_2 = \frac{A\cos B}{B\sin B}$$

In this study, the expected value and variance of factor of safety, and z-score are ascertained by using following equations (Ward et al. 1981, Ross 2004).

$$E[FS] = \alpha_1 E[C'] + \alpha_1 E[C'_r] + \alpha_2 E[\tan\phi'] \qquad (6.6)$$

$$V[FS] = \alpha_1^{\,2} V[C'] + \alpha_1^{\,2} V[C'_r] + \alpha_2^{\,2} V[\tan\phi'] \qquad (6.7)$$

$$Z = \frac{1 - E(FS)}{\sqrt{V(FS)}} \qquad (6.8)$$

Where, E[.] is expected value; V[.] is variance, Z is z-score. The expected values and variance of Mohr-Coulomb strength parameters are computed based on their nature of distribution (see in section **6.3.5**). E[FS] is average value of factor of safety. V[FS] gives total propagation of error due to variation of C', C'_r, and $tan\phi'$. z-score is equivalent to corrected factor of safety score or factor of safety score after adjusting error. It is considered as susceptibility/hazard score (Guzzetti et al. 2005, Dahal et al. 2008b). In this study, failure probability score is computed from z-score which is then implemented into ILWIS **3.8.1** to prepare slope failure probability map. Thus, with availability of geo-mechanical (C', C'_r, ϕ', γ_{sat}, γ_t), hydrological (h), and geometric properties (β), the

evaluation of hillslope instability or slope failure hazard is possible which is carried out in this study.

6.3.3.3 Discriminant function model

Discriminant function model is used to determine the relationship between outcome or dependent variable (e.g., slope failure) and independent or predictor variables (causal factors of slope failure) (Nagarajan et al. 2002, Carrara et al. 2003, Ghosh et al. 2012, Jagielko et al. 2012). This model is required when there are multiple (i.e., >2) categories of dependent variables (e.g., types of failures). The model determines multiple combinations of employed independent variables (which are the discriminant functions) and selects the most significant combination (it is the combination that best discriminates categories of dependent variables) (Baeza et al. 2010, Dong et al. 2009). For example, if there are *m* categories of dependent variables, the possible combination of independent variables or discriminant functions will be *m*-1. Finally, the selected combination of variables is included in the discriminant function equation. Discriminant function equation is a linear combination of weighted independent variables as given below.

$$DFs = b_o + b_1 \times X_1 + b_2 \times X_2 + b_3 \times X_3 + \ldots . b_n \times X_n \qquad (6.9)$$

Where DFs is discriminant function score; b_o is coefficient that maximizes the variability between categories of dependent variables; b_n is discriminant weight value or discriminant coefficient. The negative/positive sign of discriminant weight values determine the contribution of employed independent variables to discriminante categories of dependent variables (or these determine significance of independent variables to cause instability); X_n is the most significant combination of independent variables (slope failure causal factors). The goodness of fit of discriminant function model is tested with Wilk's lambda test (Jamaludin et al. 2006, He et al. 2012, Baeza et al. 2010, Ghosh et al. 2012). Wilk's Lambda score measures the discriminating potential of a combination of parameters. Smaller the value of Wilk's Lambda, higher is the discriminating capability. Hence, small value of Wilk's Lambda (<1) is always preferred in discriminant function analysis. In Wilk's Lambda test, if the significance of chi-square value is less than 0.05, the combination of parameters is significant and the discriminant function model can be accepted (Baeza et al. 2001, Ghosh 2012). In this study, different low and high hazard

classes of deterministic slope failure hazard model were used as categories of dependent variables and slope failure causal factors (DEM-based parameters) as independent variables in discriminant function modeling.

6.3.4 Seepage modeling

Seepage modeling was performed in SEEP/W (GeoStudio 2005) to obtain porewater pressure information required to slope stability analysis in model catchment. For this, 55 slope profiles were drawn in the model area parallel to the direction of maximum subsurface flow. Their locations are represented by slope profile lines in Figure 6.8. The profile geometry of these lines was prepared using DEM (5 m resolution) of the study area and soil thickness data considering topographical break in slope (Figure 6.9). All the profile continuums were discretized into a mesh of fine squares with 4 nodes and 9 integration order. The dimension of all the elements were same with a side length of <0.2 m and unit thickness. Soil water characteristics curve (SWCC) and soil permeability were two major input parameters required to seepage simulation of each profile unit. For this, mean values of volumetric water content (porosity) and soil permeability of all the square blocks lying below slope profile were computed for each slope profile. The computed mean values were integrated with SWCC and soil permeability functions available in SEEP/W library. SEEP/W is highly sensitive to initial ground water table condition. To

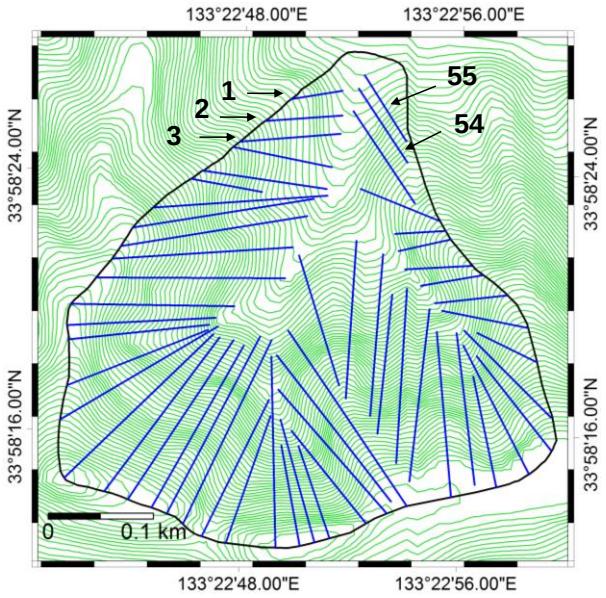

Figure 6.8 Showing 55 slope profile lines constructed in entire model catchment

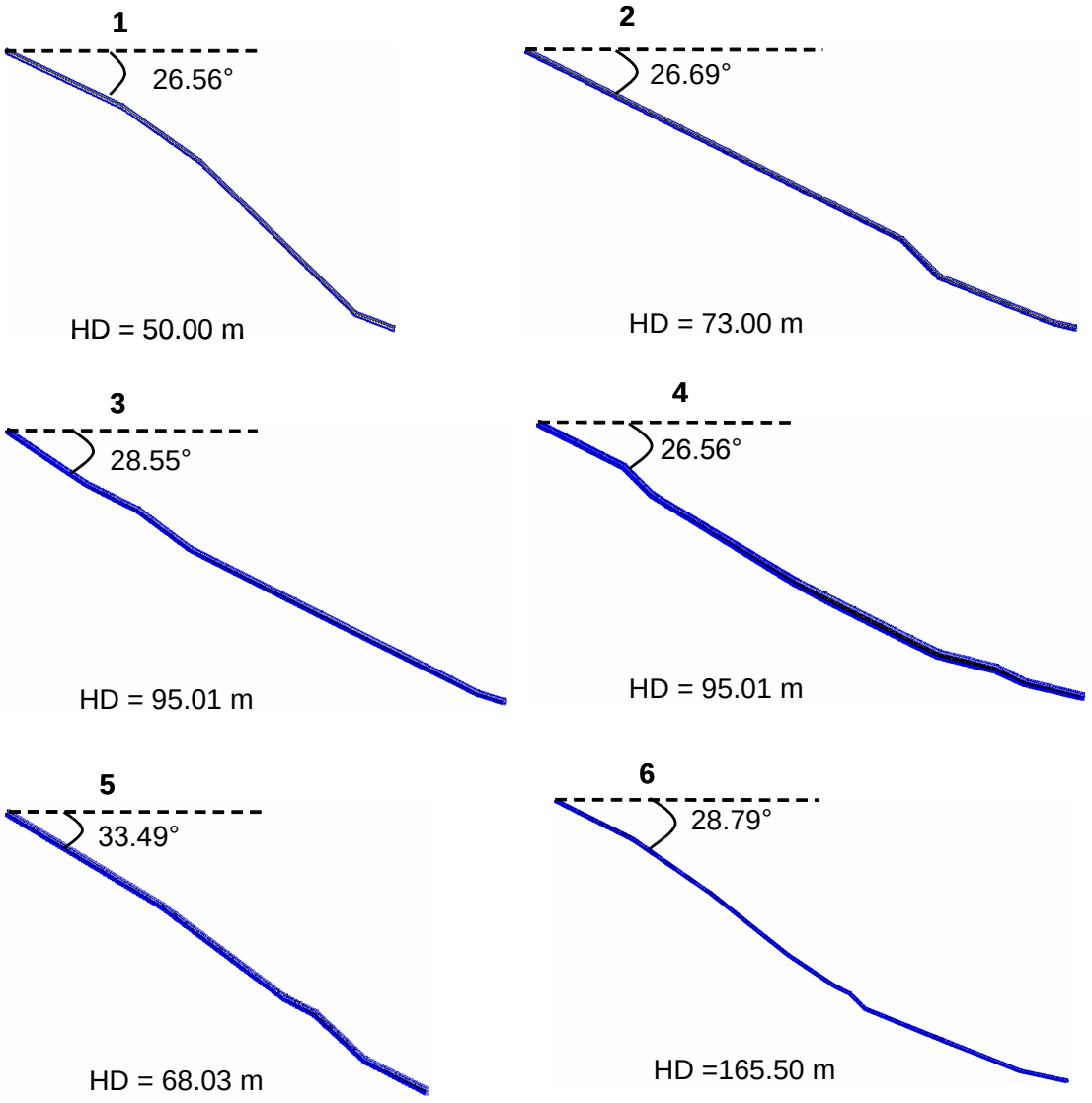

Figure 6.9 Examples of geometrical configurations of slope profiles from Figure 6.8 (showing profile 1, 2, 3, 4, 5, and 6)

prevent unnecessary negative porewater pressure regime, a limiting value of -20 kPa suction was applied as initial condition. The initial ground water table was defined along the boundary between soil colluvium and bedrock. Boundary conditions control porewater pressure distribution along profile length. A null flux boundary condition was applied on the left vertical edge, right vertical edge, and along bedrock (Figure 6.10). The phreatic line itself acts as upper boundary along exposed sloping face. Potential seepage face was considered on right vertical edge and along exposed sloping face so as to avoid ponding to the slope.

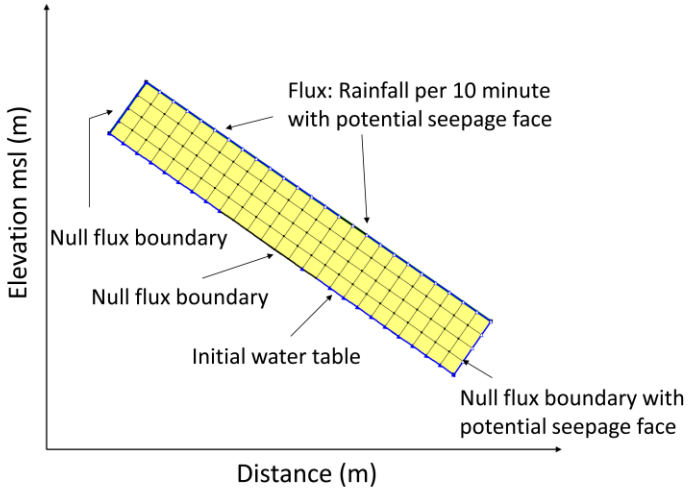

Figure 6.10 Boundary conditions applied to finite element mesh model

Almost all the days of October had considerable rainfall and slope failure occurred on 20th October. But no data were available for porewater pressure variation which could describe the initial seepage condition in the slopes prior to the rainfall events. So, the initial seepage conditions were neglected and the simulation was preceded with precipitation data of 19-20 October of 2004. The two day hourly rainfall data were discretized into 283 time steps of 10 min length and applied onto the exposed face of profiles from upward at equal pressure head and elevation condition. Transient pore water pressure lines (transient pore water pressure distributions) were developed at each time step. The ground water tables at succeeding time steps had higher depths compared to preceding ones along each profile length due to accumulation of rainfall above the bedrock. The peak hourly rainfall intensity was at 12:00 hour of 20th October 2004. The eyewitness for exact time of failure was lacking on 20th October. But, peak porewater pressure reached two hours after peak rainfall hour (i.e., at 14:00 rainfall hour) on 20th October in all simulations. This implies that the slope failure in model catchment might have begun at 14:00 hours of rainfall on 20th October (i.e., 38 hours of continuous rainfall of 19-20 October). Owing to this, the ground water table developed at 14:00 hours of rainfall on 20th October 2004 was decided to implement in limit equilibrium analysis. The vertical depth of saturation was recorded at various points along each slope profile in the selected ground water table. With these data, a point map of saturation depths was prepared.

6.3.5 Deterministic slope failure hazard modeling

The geo-mechanical and hydrological properties (Table 6.1) of hillslope materials were parameterized in ILWIS **3.8.1** platform. The point map of soil depth (prepared in field) and saturation depth (prepared from seepage modeling) covering entire model area were digitized. The spatial correlation of both data was investigated. Spatial correlation provides semivariogram model about the spatial behavior of soil properties (Jorge 2009). Rotational Quadratic semivariogram model was best fitted by both digital soil depth and saturation depth data [Figure 6.11 (a, b, c)], and this model yielded values of nugget, sill and range for each data type. These three parameters were inputs to Kriging interpolation along with

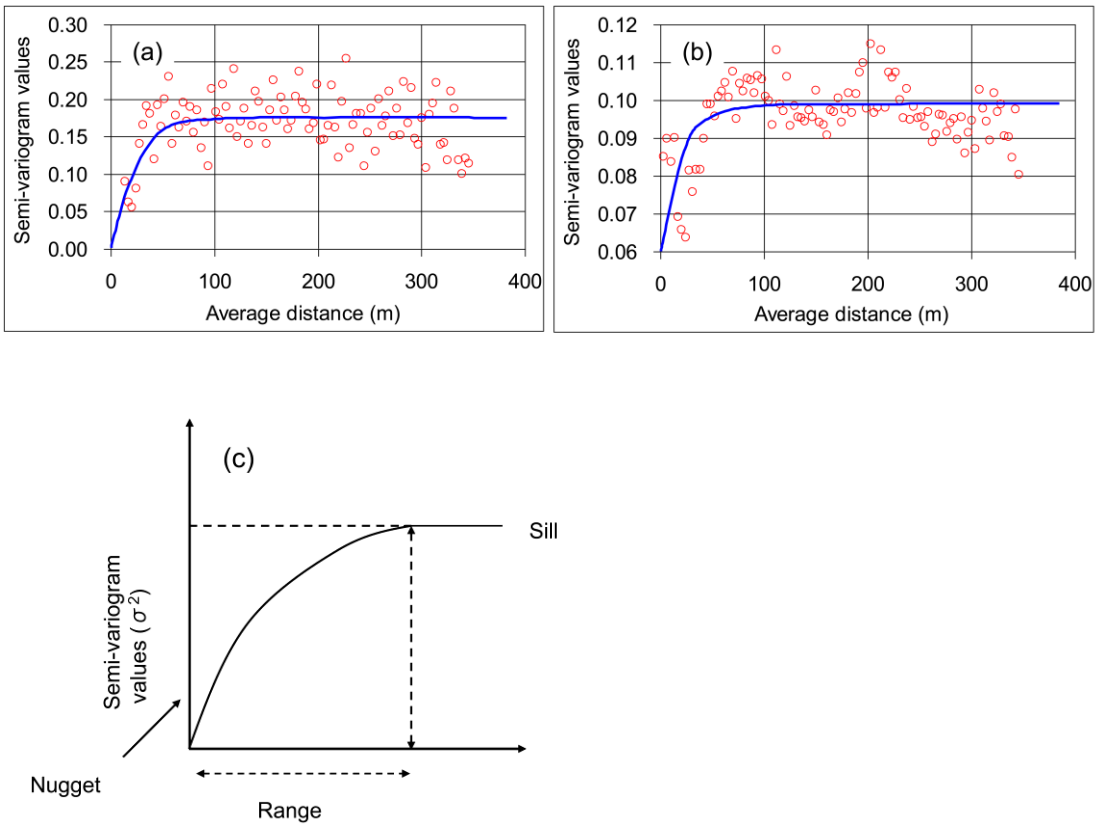

Figure 6.11 Rotational quadratic semi-variogram models to estimate spatial distribution of (a) soil depth, and (b) saturation depth in model catchment. Nugget, sill and range were the fit parameters for both models which is illustrated in (c)

respective soil spatial properties. With ordinary Kriging interpolation method, the randomly distributed point values of soil depth and saturation depth are converted into regularly distributed grid values. To prepare saturated unit weight and bulk unit weight map, firstly the average value of these properties (Table 6.1) were computed for each zone of model area, and then converted into raster image using ILWIS functions. To prepare

expected and variance maps of strength parameters (C', C'_r, ϕ'), the uniform distribution of these properties was assumed in the entire model area. For uniformly distributed data, the expected values and variance are computed using following relationships.

$$E[X] = \frac{(a+b)}{2} \qquad (6.10)$$

$$V[X] = \frac{(b-a)^2}{12} \qquad (6.11)$$

Where a and b are minimum and maximum values of strength parameters. These values were employed to compute expected values and variances of strength parameters for each zone outside ILWIS. The computed expected values and variances were then imported into ILWIS and converted into generalized continuous raster form. Slope gradient map was obtained from DEM of the model catchment. All these maps were used for deterministic slope failure hazard modeling.

To obtain a robust deterministic slope failure hazard model, a complete parametric analysis was performed by varying shear strength parameters (C', C'_r, ϕ'). Expected map and variance map of factor of safety were prepared on a cell-by-cell basis (5 m resolution) using equation 6.6 and 6.7. These maps were directly implemented in z-score computation (equation 6.8). z-score herein is slope failure hazard score. The area under standardized normal weights of z-score between F=1 and $Z = -\infty$ gives failure probability. If it is the case with large voluminous data, as in present study, the commercially available spreadsheet software can be utilized to calculate probability from z-score (Dahal et al. 2008b). In this study, z-score was exported to Microsoft Excel and NORMSDIST function was employed to compute probability. This process of calculation of failure probability is in accordance with Terlien (1996) and van Westen and Terlien (1996). The probability value computed in excel was imported into ILWIS and rasterized to prepare slope failure probability map. This map was validated with the detailed slope failure inventory of the model catchment. The hazard classes were determined by visual inspection of distribution of pixels with higher values of probability from ROC prediction rate. Generally, high hazard classes consists of pixels with high probability values (greatest number of pixels where slope failures occurred) and the low hazard classes cover the regions of low probability values (fewest number of slope failure pixels). Finally, the zonation map was once again crosschecked with the detailed slope failure inventory for spatial agreement.

6.3.6 Replication of deterministic model and accuracy check

After confirming a good predictive success rate from validation, the results of deterministic slope failure hazard model were applied to forty selected test catchments of the study area. For this, firstly discriminant function modeling was carried out amongst the deterministic model and causal factors of slope failure and discriminant function equation was obtained for the model catchment. Using this equation and using the same set of seven DEM-based slope failure causal parameters, the slope failure hazard index maps were obtained in test catchments. These maps were compared separately with prevailing slope failure inventories of 2004 September and October to check their prediction accuracy.

6.4 Results

6.4.1 Deterministic modeling

Figure 6.12 shows the slope failure probability map obtained after performing full parametric modeling of shear strength parameters. To validate this map against detailed slope failure inventory, ROC curve (AUROC) method (Zweig and Campbell 1993) was used. It determines predictive capability of a model (Yesilnacar and Topal 2005, Van Den Eeckhaut et al. 2006). ROC makes a diagnosis for spatial agreement of prevailing slope failures with failure probability score. The variables to ROC curve analysis in SPSS are binary (0-1) map of slope failure inventory and failure probability score. Based on degree

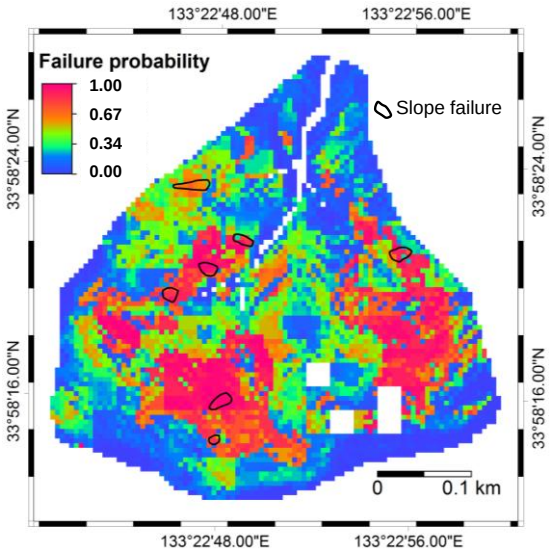

Figure 6.12 Slope failure probability map

of spatial matching between these two variables, ROC curve method determines area under the ROC curve (AUROC). This area is the measure of robustness of model to predict future slope failures. The AUROC value of the model catchment based on its detailed slope failure inventory was 0.82 (Figure 6.13). The ROC curve also suggests that about 68% of the slope failure numbers were concentrated in areas showing upper 20% of the failure probability index. These reasonably verify a good ability of model to predict future slope failures.

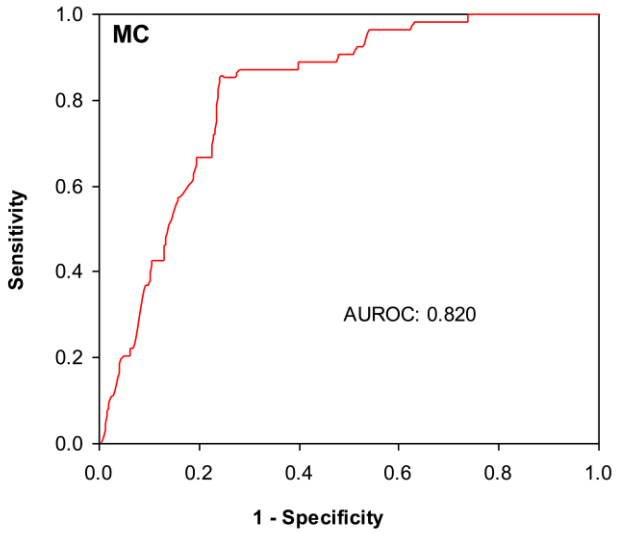

Figure 6.13 Area under ROC curve estimated from Higashifukubegawa catchment after deterministic slope failure hazard modeling

Based on ROC prediction rate and coverage of higher percentage of slope failure in higher value of probability, the slope failure probability map was classified into four hazard classes: Stable (S, <30 % probability value), Metastable (MS, 30 % – 50 % probability value), Quasistable (QS, 50 % – 70 % probability value), and Unstable (U, 70 % - 100 % probability value) (Figure 6.14) which is from low to high hazard level. The classes were assigned the colors green, yellow, blue, and red respectively. This is deterministic slope failure hazard model in Higashifukubegawa catchment. Finally, the zonation map was crossed with raster map of detailed slope failure inventory. The result (Figure 6.15) shows that a total of 92.6 % of the slope failures were found to occur in U class which is very promising. Also, only a few pixels of slope failures were located in QS

and MS classes (which are 1.90 % and 5.60 % of the total slope failures respectively). There was no slope failure pixel in S class.

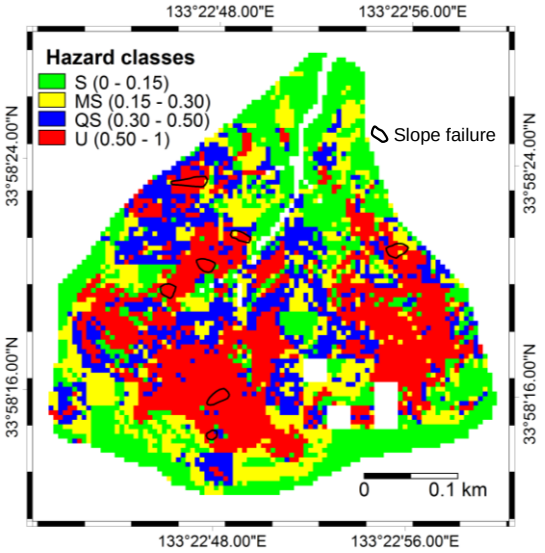

Figure 6.14 Slope failure hazard zonation map of Higashifukubegawa catchment

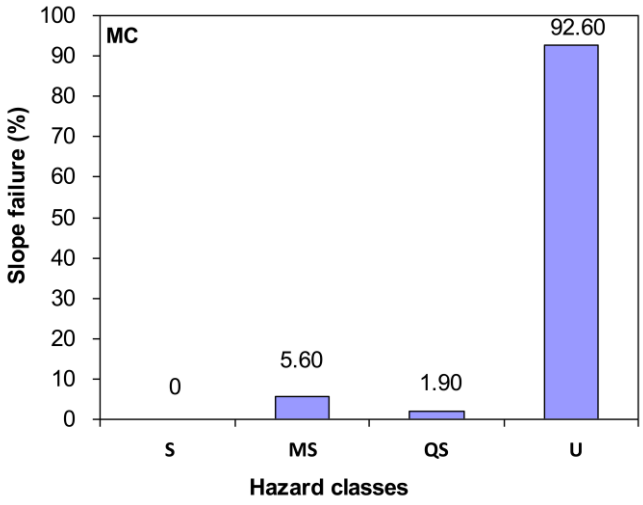

Figure 6.15 Slope failure distribution in hazard classes of deterministic model

6.4.2 Discriminant function modeling

As mentioned earlier, the categories of dependent variables and independent variables are required to obtain discriminant function equation. Here, the four hazard classes of deterministic model: S, MS, QS, and U were used as categories of dependent variables. A failure probability number: 1, 2, 3, and 4 was assigned to the classes from low to high

hazard class. Similarly, a set of seven significant and easily available topographical and hydro-geological parameters, namely slope, relief, plan curvature, profile curvature, wetness index, flow accumulation, and drainage density were selected as independent variables in model catchment. All of these parameters were derived from DEM (5 m resolution). With inputs of abovementioned dependent and independent variables, discriminant function modeling was performed in SPSS platform employing ENTER method. The results of discriminant function modeling are presented in Table 6.2, 6.3 and 6.4.

Table 6.2 Unstandardized
Canonocal Discriminant Function Coefficients

Parameters	Functions		
	1	2	3
Slope	0.101	0.003	0.012
Relief	-0.0000178	0.017	0.009
Plan curvature	-0.014	-0.047	0.362
Profile curvature	-0.755	0.321	0.328
Wetness index	0.067	-0.118	0.314
Flow accumulation	-0.0003190	-0.001	0.0000708
Drainage density	7.565	-8.124	36.413
Constant	-3.711	-1.454	-3.651

Table 6.3 Wilk's Lambda test

Function (s)	Wilk's Lambda	Chi-square	df	Sig.
1 through 3	0.705	1932.105	21	0.000
2 throguh 3	0.987	74.947	12	3.76E-11
3	0.996	23.394	5	2.84E-04

Table 6.4 Standardized
Canonical Discriminant Function Coefficients

Parameters	Functions		
	1	2	3
Slope	0.988	0.027	0.114
Relief	-0.00100	0.874	0.459
Plan curvature	-0.016	-0.052	0.400
Profile curvature	-0.207	0.088	0.090
Wetness index	0.112	-0.198	0.524
Flow accumulation	-0.10500	0.229	0.023
Drainage density	0.174	-0.187	0.837

The discriminant function model produced three combinations of casual parameters of slope failure or discriminant functions (Table 6.2) which was 1 less than number of hazard classes of deterministic model. All the three combinations of parameters were found significant since significance of chi-square value was less than 0.05 in all combinations (Table 6.3). However, the lowest Wilk's Lambda score (0.734) and significance level (0.00) of the first combination enable us to confirm that first

combination is the most significant among the three (i.e., it most discriminates the hazard classes of deterministic model or the group means are significantly different for this combination). Based on these results, the first combination of parameters or discriminant function is included in the discriminant function equation which is given below.

$$DFs = -3.711 + 0.101 \times Slope - 0.0000178 \times Relief - 0.014 \times Plan\ curvature - 0.755 \times Profile\ curvature + 0.067 \times Wetness\ index - 0.0003190 \times Flow\ accumulation + 7.565 \times Drainage\ density \quad (6.12)$$

Where DFs is discriminant function score. The factors in this equation are discriminant weight values of parameters or magnitude of parametric contribution to slope instability. The discriminant function represents magnitude of parametric contribution to slope instability.The discriminating potential of the employed independent slope failure causal parameters to the hazard classes can be understood from Standardized Canonical Discriminant Function Coefficients listed in Table 6.4.

6.4.3 Replication and validation

To apply the results from discriminant function modeling, the same set of seven DEM-derived slope failure causal parameter maps were prepared in all the test catchments. The discriminant weight values of parameters of the model catchment were applied to corresponding parameters of the test catchments and discriminant function equation was portrayed to compute discriminant function score or slope failure hazard index. Figure 6.16 shows resulting slope failure hazard index maps of two typical test catchments W20 and W30. The slope failure hazard score was more or less similar in all forty catchments. To check prediction accuracy, the resulting hazard maps were crossed with existing inventories of September and October slope failures of 2004 and ROC curves were plotted. The area under ROC curve gives prediction rate. Figure 6.17 exhibits prediction rate obtained with hazard index maps of catchments W20 and W30. The prediction rate with respect to September and October slope failures in forty test catchments is summarized in Table 6.5. From this table, it is understood that the prediction rate was higher with the inventory of September slope failure in twenty-two test catchments (W1, W3, W4, W5, W9, W10, W12, W16, W17, W18, W19, W20, W21, W22, W25, W26, W28, W29, W32, W36, W37, and W38) whereas in remaining test catchments, the prediction rate was higher

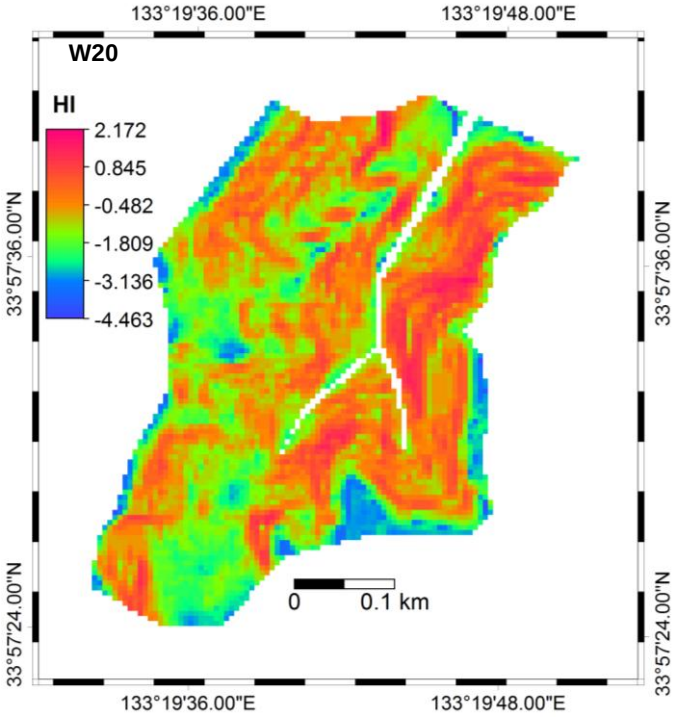

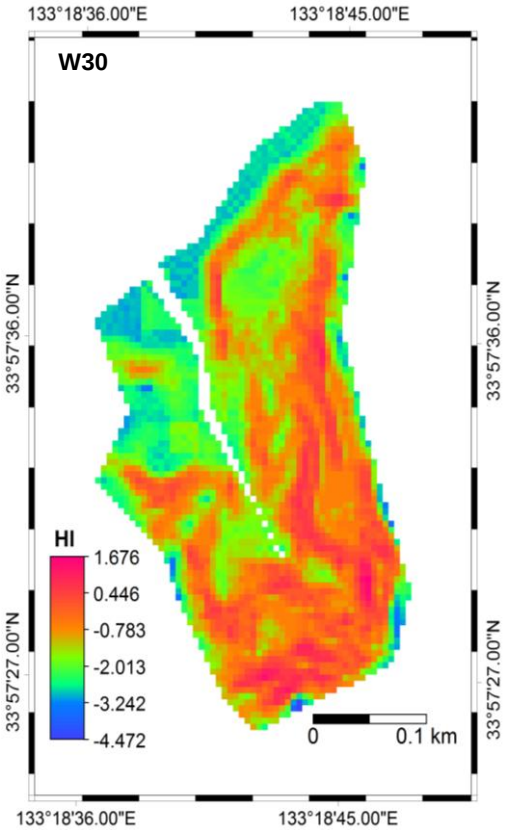

Figure 6.16 Slope failure hazard index maps of catchments W20 and W30 after applying discriminant function weight values of each parameters from Higashifukubegawa catchment (HI: Hazard Index)

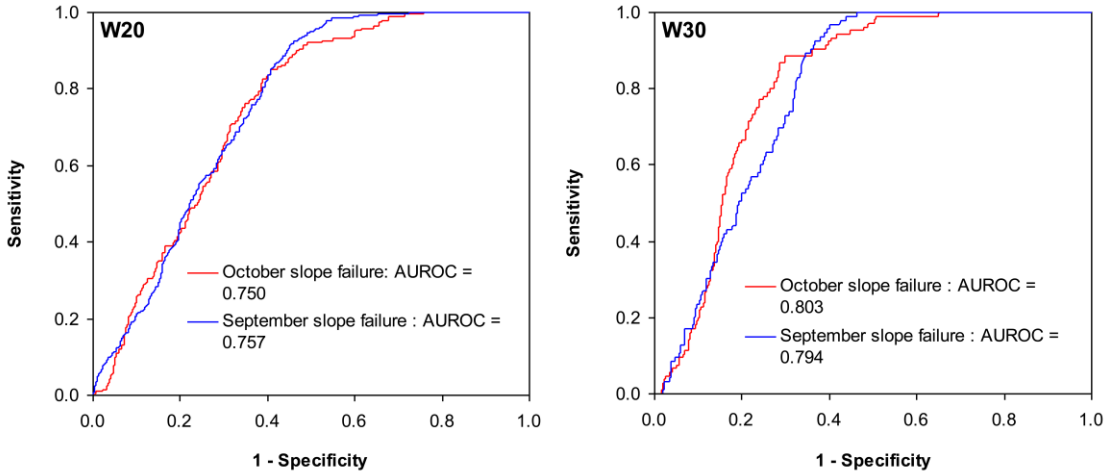

Figure 6.17 Area under ROC curve estimated for slope failure hazard index of catchments W20 and W30 after replication of deterministic model

Table 6.5 ROC prediction rates for test catchments

Catchment ID	Prediction rate		Catchment ID	Prediction rate	
	October slope failure	September slope failure		October slope failure	September slope failure
W1	0.704	0.743	W21	0.805	0.802
W2	0.732	0.726	W22	0.798	0.784
W3	0.731	0.752	W23	0.733	0.746
W4	0.727	0.740	W24	0.763	0.807
W5	0.762	0.789	W25	0.743	0.730
W6	0.751	0.734	W26	0.763	0.784
W7	0.754	0.736	W27	0.734	0.743
W8	0.794	0.759	W28	0.741	0.789
W9	0.790	0.814	W29	0.790	0.752
W10	0.760	0.814	W30	0.803	0.794
W11	0.788	0.741	W31	0.800	0.796
W12	0.761	0.768	W32	0.783	0.799
W13	0.755	0.719	W33	0.727	0.765
W14	0.788	0.760	W34	0.738	0.773
W15	0.773	0.783	W35	0.744	0.763
W16	0.772	0.788	W36	0.735	0.721
W17	0.791	0.772	W37	0.743	0.735
W18	0.741	0.753	W38	0.725	0.747
W19	0.776	0.780	W39	0.783	0.735
W20	0.750	0.757	W40	0.805	0.770

with the inventory of October slope failure. In overall, the prediction rates from 0.719 to 0.814 and 0.704 to 0.805 were noted with the inventories of September and October slope failures respectively from Table 6.5. This implies that the prediction of September slope failure was better than October slope failure by approximately 1%. However, a moderate to good prediction accuracy was obtained with both inventories for spatial agreement.

6.5 Discussion

In this study, deterministic slope failure hazard analysis was carried out in Higashifukubegawa catchment. But this kind of analysis can not be conducted in all other test catchments since it is very difficult to obtain detailed geo-mechanical and hydrological properties of soils required to the analysis. Therefore, it is necessary to explore for replication methodology which incorporates deterministic model and can predict slope failure hazard in catchments of similar geological and geomorphological settings. In this study, we have presented and examined replication process of deterministic slope failure hazard model in numerous catchments of the selected study area. The deterministic model prepared in Higashifukubegawa catchment included area under ROC as 0.82 which is a good success rate. The results of deterministic model from Higashifukubegawa were then replicated through discriminant function modeling using DEM-based parameters. In this research, it is assumed that the underlying physical processes associated with hillslope failures would be same in similar geological/geomorphological settings and index properties of soil do not vary significantly. Under such conditions, hillslopes fail in a similar way or under the same combination of parameters.

The discriminant function modeling performed between deterministic model and a set of seven DEM-based parameters (i.e., slope, relief, plan curvature, profile curvature, wetness index, flow accumulation, and drainage density) in the model catchment resulted in a significant combination of parameters or discriminant function with Wilk's lambda (0.705), Chi-square value (1932.105), and significance level of Chi-square value (0.000). As a result, the model characteristics were transferred into an empirical parametric relationship known as discriminant function equation. This relationship was applied to forty test catchments of the study area with the same set of DEM-based parameters and slope failure hazard index maps were obtained. In results, the prediction accuracies were found varying over a wide range, from moderate to good with both inventories. In few catchments, the accuracy was in the same range of model accuracy rate (0.82). From this, it is well understood that if replication of deterministic model was carried out employing parameters-based multivariate regression modeling, the prediction accuracy can be significantly increased. Replication of slope failure hazard, as in present study, can be reviewed in a very few catchment-scale studies like Ghimire 2011 and Dahal et al. 2012 with similar reasonable performance. However, this study has firstly indicated the possibility of replication of deterministic slope failure hazard model although research on deterministic shallow landslide hazard assessment or physically based modeling of shallow

landslides has been practiced worldwide since last few decades (Montgomery and Dietrich 1994, Borga et al. 1998, Moon et al. 2004, Rosso et al. 2006, Meisina and Scarabelli 2007, Dahal et al. 2008b, Salciarini et al. 2008, Godt et al. 2008, Sorbino et al. 2010). The parametric relation obtained in Higashifukubegawa catchment can be used to predict slope failure hazard conditions in any other areas with similar geological/geomorphological characteristics if DEM-based parameters were available. Further, the replication of deterministic model could be performed with higher accuracy if enough considerations were given to the quality of geo-mechanical and hydrological parameters in model catchments as well as quality of DEM-based parameters.

6.6 Conclusions

From this work, we conclude with the following statements.

i) We are successful in connecting hillslope-scale (local-scale) sub-surface hydrology to catchment-scale (landscape-scale) sub-surface hydrology.
ii) We understood that geo-mechanical and hydrological properties of the hillslope materials are the key controlling factors of slope failure hazard in tertiary sedimentary terrain in Shikoku Region of Japan.
iii) We have obtained 0.719 – 0.814 and 0.704 – 0.805 prediction accuracy rate for the spatial prediction of slope failures compared to the 2004 September and October slope failure inventories respectively. This reasonably validates the model and replication process.
iv) We have been successful in replicating the model through parameters-based multivariate modeling for the purpose of predicting slope failure hazard index without using geo-mechanical and hydrological parameters.
v) Finally, the work in this study indicates that the replication process used here to predict slope failure hazard condition in small catchment scale has a wide applicability in any other areas of the similar geological and geomorphological characteristics.

Chapter 7

Numerical analyses on influence of basic parameters of topography on hillslope instability in a small catchment

Abstract

This study was attempted to identify the influence of three basic parameters constituting topography (slope inclination, soil depth, and slope length) on hillslope instability in a small catchment, known as Higashifukubegawa of Shikoku Island, Japan. The typhoon rainfall of 19-20 October, 2004 was significant in causing a total seven slope failures in the catchment since other rainfall events of various intensities in the same year did not cause failure. To understand the influence of three basic parameters, numerical modeling of seepage and slope stability was performed in slope profiles prepared from slope failure data of the catchment in GeoStudio (2005). The change in porewater pressure distribution and slope mass weight due to variation in values of basic parameters across their reasonable range was used to interpret the change in factors of safety. This study demonstrates how hillslope instability changes with basic parameters of topography under the same simulating conditions of hydrological and geo-mechanical parameters.

Keywords: unsaturated hillslopes, instability, numerical modeling, subsurface hydrological response to rainfall, factor of safety

7.1 Introduction

Hillslopes are fundamental units of a catchment. They have complex subsurface hydrology. Shallow landslide or slope failure is common form of hillslope instability (Talebi et al. 2007). The problems resulting from hillslope instability are worldwide (van Schalkwyk and Thomas 1991, Claessens et al. 2007, Dahal et al. 2008c, Godt et al. 2008, Giannecchini et al. 2012). Medium to steep hillslopes of catchments, particularly in tropical and subtropical regions experiencing heavy rainfall, fail time and again. It has been generally understood that failure occurs due to increase in positive porewater pressure. But, catchment slopes with well drained soil types can become unstable even under partially saturated soil conditions. Hillslope instability may present a considerable constraint on downslope engineering structures, such as roads, drainage systems etc. In larger areas, it may result in major ecological and environmental problems (Sidle and Ochiai 2006, Talebi et al. 2008b, Hsu et al. 2010). Therefore, it is necessary to fully understand the phenomena associated with hillslope instability for slope land management in mountainous area.

The major phenomena that affect hillslope instability are the phenomena related to complex subsurface hydrological change. The hillslope subsurface hydrology depends on rainfall infiltration through soil. There are two types of parameters that affect rainfall infiltration: internal parameters and external parameters. Hydrological properties of soils, such as moisture retention characteristics and soil permeability are internal parameters whereas climatic conditions, like rainfall intensity and duration, rainfall pattern, and evapotranspiration rate are external parameters. Both internal and external parameters affecting rainfall infiltration are controlled by topography. Therefore, topography is major controlling factor of all kinds of hillslope instability problems. A topographical unit constitutes slope inclination, slope shape, slope length, slope width, and soil depth (Dietrich et al.1987, Iida 1999, Dietrich et al. 2008a, Talebi et al. 2008, Cha and Kim 2011), and therefore these can be considered as topographic parameters.

Influence of topography on hillslope instability through subsurface hydrology has been widely acknowledged in a large number of earlier to recent slope failure studies, such as Montgomery and Dietrich 1994, Wu and Sidle 1995, Burton and Bathurst 1998, Pack et al. 1998, Borga et al. 2002, Dahal et al. 2008, Salciarini et al. 2008, Harp et al. 2009 etc. However, in these studies, only slope inclination has been reported as important parameter from view point of slope stability. Some theoretical studies (e.g., Griffiths et al. 2011, Cha and Kim 2011) have investigated the influence of slope inclination and soil depth on stability analysis of infinite slopes. The deficits in these studies are: (i) infinite slope

analysis is not sufficient to completely represent the real conditions of hillslopes, and (ii) slope transient porewater pressure behavior in response to rainfall and its influence on hillslope instability can not be understood from these studies. Many other researches (Troch et al. 2002, Dhakal and Sidle 2003, Hilbert et al. 2004, 2007; Talebi et al. 2007, 2008) have shown that despite slope inclination and soil depth, the geometric parameters of hillslopes (plan shapes and profile curvatures) also have significant impact on subsurface flow response and instability of complex hillslopes. For example, Talebi et al. 2008b used Hillslope Storage Bossinesq hydrological model (Boussinesq1877, Troch et al. 2003) coupling one-dimensional Richard's equation and infinite slope stability model to evaluate the influence of nine characteristic hillslope types with three different profile curvatures (concave, straight, convex) and three different plan shapes (convergent, parallel, divergent) on slope instability. Three-dimensional modeling program of dynamic hydrology and stability, like Integrated Hydrological Stability Model (InH-SM) (VanderKwaak 1999) and GEOtop-FS (Rigon et al. 2006) have also been used to simulate hillslope hydrologic response and stability in some studies (Loague et al. 2005, Simoni et al. 2008). But, high degree of simplification and preciseness in parameters is required for such sophisticated models which is difficult to manage in most occasions. To account slope instability due to parameters of topography in simple types of slopes (generally planar), either the assumptions of these models should be reduced or simplified two-dimensional modeling on seepage and slope stability can be performed. Influence of slope length on slope instability has not been clearly presented in any previous study.

Only three parameters: slope inclination, soil depth and slope length can be considered as basic parameters of topography as these determine the initial soil subsurface zone moisture storage and instability prior to rainfall. The other parameters, like plan shapes, profile curvatures, and slope width lie entirely within the three parameters along slope profile and display their role on instability depending on local conditions of the three parameters. Unless and until the influence of basic parameters is well explored, the mechanism of hillslope instability can not be fully understood. The main problem in abovementioned studies is that they are case studies reported either from different geographical locations or based on field/laboratory investigation or performed in various modeling programs. They have treated underlying mechanisms differently and suggested different conclusions on triggering of slope failure. In this context, this study attempts to evaluate the influence of three basic parameters on hillslope instability. The main objective of this study is to fully demonstrate influence of the three basic parameters of topography

on unsaturated zone moisture storage change and sliding tendency of slope mass during rainfall. For this, a small catchment known as Higashifukubegawa in tertiary sedimentary terrain of Shikoku Island of Japan was selected.

7.2 Study area

Higashifukubegawa catchment, as shown in Figure 7.1, is located in the northeastern part of Niihama City, in Ehime prefecture of Shikoku Island, western Japan. Geographically, it extends from (33 ° 58' 12") N to (33 ° 58' 27'') N latitude, and (133 ° 22' 41'') E to (133 ° 22' 59'') E longitude. There are many reasons behind selection of this catchment for this study. For example, the catchment is very small (142,000 sq. m) and elevation ranges from 42 m to 213 m from the mean sea level. Same types of green vegetations (short-height evergreen and deciduous plants) are found in the catchment. Geology is uniform.

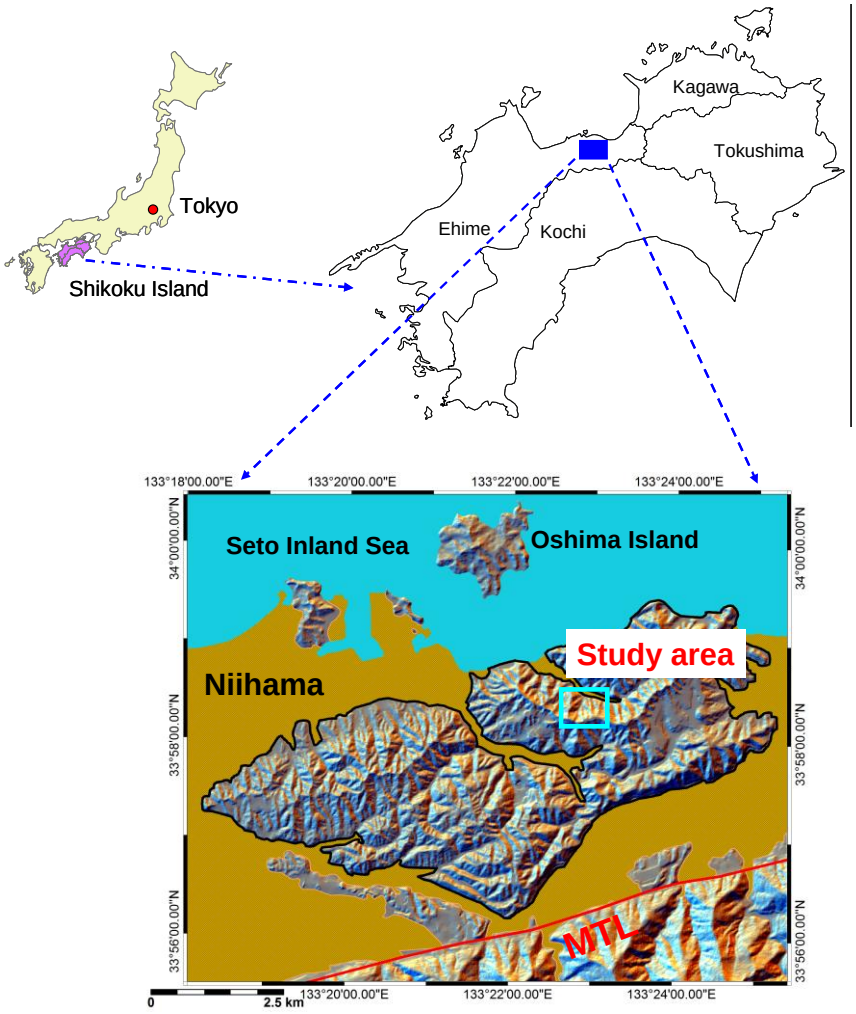

Figure 7.1 Location map of study area

Tertiary shale and sandstone of the Izumi group entirely cover the catchment. The main reason of selection is that moderate to steep slopes of this catchment consist of coarse-grained, less cohesive and loose shallow soil colluviums where subsurface storm flow is dominant flow mechanism. Hillslopes with such soils exhibit unsaturated percolation and rapid response of porewater pressure increase during heavy rainfall. Higashifukubegawa catchment experienced extreme typhoon rainfalls of various intensities in 2004 which caused a total of seven slope failures (Figure 7.2). Based on field checks and Google Earth Image interpretation, the boundaries of slope failures were delineated. All the slope failures were affirmed in topographic hollows; between 120.60 m and 196.00 m elevations. In this study, various parameters of seven slope failures of Higashifukubegawa were considered in slope instability evaluation.

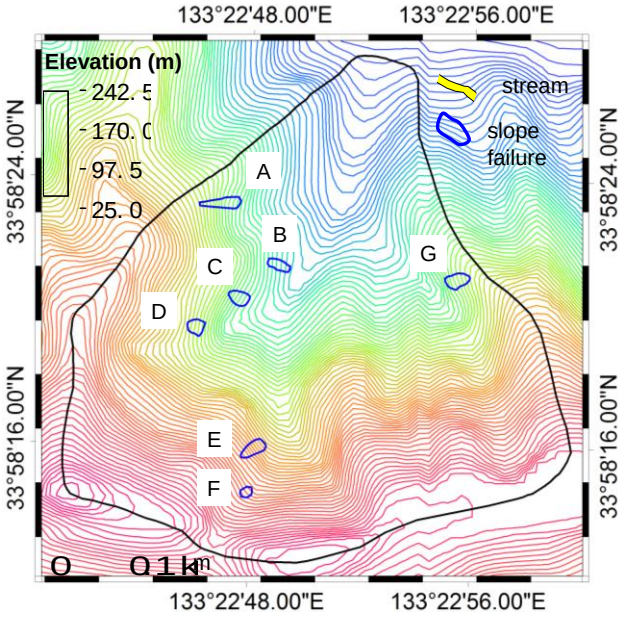

Figure 7.2 Higashifukubegawa catchment with 2004 typhoon rainfall-induced slope failures A, B, C, D, E, F and G

7.3 Parameter exploration

Field visits were made to Higashifukubegawa catchment in October, November, December, and April of 2011 and November of 2012. A detailed field investigation was carried out to measure length/breadth of slope failures, soil thickness and soil permeability. The soil thickness above weathered bedrock was measured by dynamic cone penetration test near the failed slopes. The permeability within the unsaturated zone was measured by Hasegawa in-situ permeability tests (Daitou Techno Green, 2009). Soil samples were

collected at the mid of each slope failure spots and examined in laboratory for Mohr-Coulomb parameters of shear strength as well as physical properties of soil. Direct shear tests were conducted to determine Mohr-Coulomb parameters of strength (C', ϕ'). The laboratory tests for unit weight (γ), porosity or volumetric water content (n), and particle size distribution of soil were conducted following specifications of ASTM (ASTM 1999 a, b). Based on the results of laboratory investigation and after referring to USCS, three groups of soils were identified: silty sand (SM), silty gravel (GM) and silt (M). But, silty sand (SM) was prevalent. These soils were derived from weathering of underlying bedrock composed of tertiary sandstone and shale. Various hydrological, geo-mechanical and topographic parameters of the seven slope failures obtained as a result of field visits, field/laboratory investigations are summarized in Table 7.1. From this table, the variability in values of parameters among seven slope failures was well recognized. Including this variability, the value range of parameters was prepared which is presented in Table 7.2. Employing the recognized values range of parameters, hillslope profiles were constructed (see in section 7.4.2), and then hydrological and slope stability modeling were performed in these slope profiles (see in section 7.4.3 and 7.4.4).

Table 7.1 Hydro-mechanical properties of soil and characteristics of slope failure

Slope failure spot	Slope failure length, L (m)	Slope failure breadth, B (m)	Average slope angle, Θ (°)	Soil thickness, D (m)	Effective cohesion*, C (kN/m^2)	Unit weight*, γ (kN/m^3)	Effective friction, angle*, ϕ (°)	Soil permeability, k (m/s)	Volumetric water content, n
A	38.02	10.45	33.38	0.60 - 1.10	0.49	16.92	34.86	1.20×10^{-6}	0.50
B	20.13	9.11	27.46	0.26 - 1.03	0.62	15.83	33.72	5.80×10^{-8}	0.45
C	19.33	12.92	33.00	0.11 - 1.42	1.44	16.92	34.14	6.80×10^{-8}	0.46
D	15.32	13.51	32.90	0.16 - 0.80	0.78	17.08	36.76	8.30×10^{-8}	0.48
E	25.02	12.26	38.86	0.12 - 1.18	0.86	17.22	33.01	1.70×10^{-8}	0.43
F	13.81	8.67	21.78	0.55 - 1.78	0.13	15.83	34.21	2.35×10^{-8}	0.50
G	22.32	13.41	29.70	0.33 - 0.99	1.33	16.79	33.85	3.10×10^{-7}	0.49

Table 7.2 Parameters exploration within the range over which they were varied in Higashifukubegawa catchment

Parameters	Value range
Slope failure length, L (m)	12.00 - 40.00
Slope failure breadth, B (m)	7.00 - 14.00
Average slope angle, Θ (°)	20 - 40
Soil thickness, D (m)	0.10 - 1.80
Effective cohesion*, C (kN/m^2)	0.10 - 1.50
Unit weight*, γ (kN/m^3)	14.00 - 18.00
Effective friction angle*, ϕ (°)	32.00 - 37.00
Soil permeability, k (m/s)	1.6×10^{-8} - 1.3×10^{-6}
Volumetric water content, n	0.42 - 0.50

Note: *These values are mean values and, therefore factor of safety via sensitivity computation was performed during slope stability modeling (after this, slope failure length (L) is referred as slope length)

7.4 Numerical modeling

7.4.1 Program selection

In this study, SEEP/W and SLOPE/W plug-ins of GeoStudio (2005) were employed to examine hillslope instability. SEEP/W is commonly used program to explore subsurface hydrologic response of hillslopes to rainfall (Tofani et al. 2005, Rahardjo et al. 2007, Dahal et al. 2009, Zhan et al. 2013). The 2-dimentional Richard's equation is coded in this program to predict porewater pressure which is given below.

$$\frac{\partial}{\partial x}\left(k_x \frac{\partial H}{\partial x}\right) + \frac{\partial}{\partial y}\left(k_y \frac{\partial H}{\partial y}\right) + q = m_w^2 \gamma_w \frac{\partial H}{\partial t}$$

Where k_x is coefficient of permeability in x-direction; k_y is coefficient of permeability in y-direction; H is hydraulic head or total head; q is applied flux at the boundary; m_w is slope of soil-water characteristics curve; and γ_w is unit weight of water. Richards's equation considers vertical redistribution of infiltrated rainfall (Iverson 2000). To solve Richards's equation, SEEP/W accepts soil water characteristics curve (SWCC) function and soil permeability curve (SPC) function of exponential form, and then realistically models to predict porewater pressure distribution both in saturated and unsaturated state of soil in finite element method framework.

SLOPE/W computes factor of safety using limit equilibrium approach. It allows use of geo-mechanical parameters and porewater pressure profiles from SEEP/W and realistically models to predict instability condition of hillslopes. For this, Morgenstern-Price method was selected within SLOPE/W in this study. In the Morgenstern-Price method, Modified-Coulomb shear strength criterion was employed to include both saturated and unsaturated shear strength variation in soil.

7.4.2 Hillslope profile construction

The model should be simple so that the influence of parameters on slope instability can be easily recognized. Also it should be field representative so that the conclusions can be applied to the natural slopes (Milledge et al. 2012). Understanding these, a hillslope profile with slope length, L; slope inclination, Θ; and soil depth, D; was defined as presented in Figure 7.3. The upslope and downslope topography have significant effect on stability of natural slopes. To capture the contribution of upslope and downslope topography, 10 m slope length was provided on upslope and downslope of the slope profile. Then, slope length, slope inclination, and soil depth were varied (Figure 7.3) across the range over

which they were varied in Higashifukubegawa catchment (Table 7.2) and a total of 240 slope profiles were constructed. A homogenous, isotropic and single layer of sandy silt colluvium was considered in all the slope profiles.

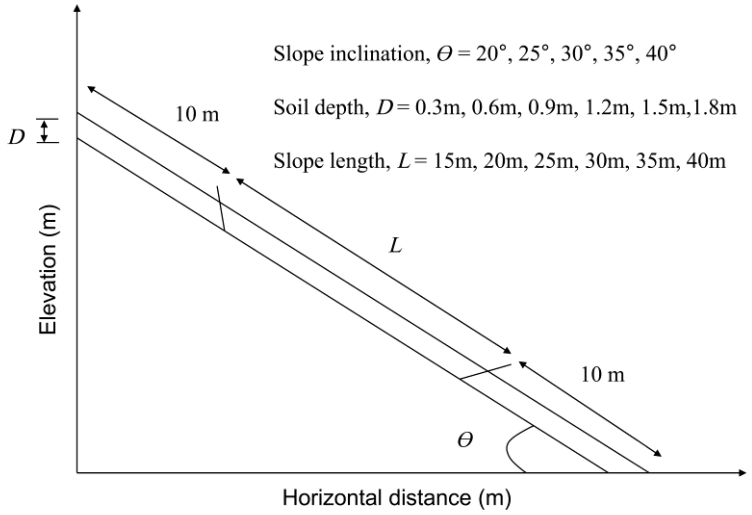

Figure 7.3 Typical hillslope profile (a total of 240 models were constructed from this profile by varying slope inclination, soil depth, and slope length)

7.4.3 Seepage modeling

As mentioned in earlier section, SEEP/W requires finite element mesh model to perform seepage modeling. So, all the slope profiles were discritized into finite element mesh of fine parallelogram elements with 4 nodes and 9 integration orders. The sides of all mesh elements have the same length of 0.1 m and unit thickness. Boundary conditions are very important in seepage modeling since they control development of porewater pressure. Boundary conditions were defined as depicted in Figure 7.4. The left and right vertical faces of the model have null flux boundary. The bottom inclined face also has null flux boundary. But, the top exposed sloping face has rainfall intensity as a flux boundary. Potential seepage face was provided on the top exposed sloping face and right vertical face so that the excess water could drain away from the slope. Considering potential seepage face does not allow building up porewater pressure greater than 0 kPa when rainfall flux is greater than soil permeability. This simulates real field condition where excess rainwater at the ground surface is removed from the slope as runoff (Gasmo et al. 2000).

Seepage modeling was performed under same hydrological conditions in all the slope profiles. Two soil properties, namely volumetric water content or SWCC function and SPC function of silty sand were assigned as the major input to the finite element model.

SWCC function was used from GeoStudio library whereas SPC function was predicted from SWCC using Fredlund and Xing (1994) criterion. This criterion eliminates the necessity to determine residual water content which is usually required for other predictive methods. The following representative values of hydrological parameters were selected from Table 7.2: porosity as n = 0.46 and soil permeability as k = 9.0×10^{-8} m/s. During simulation, the SWCC function and SPC function were integrated with the selected values of porosity and soil permeability.

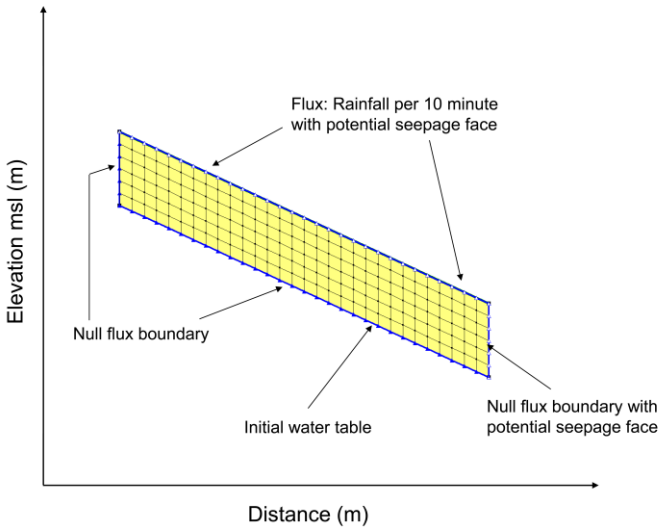

Figure 7.4 A complete layout of two dimensional finite element mesh model after applying boundary conditions

Hillslopes with highly permeable soils (e.g., sand, silty sand, sandy silt, silty clay etc.) develop high matric suction during dry season or when there is no rainfall. Such slopes rather fail in unsaturated condition due to loss of matric suction during heavy rainfall (Lu et al. 2008). In such soil slopes, the stability evaluation incorporating saturated flow or positive porewater pressure is meaningless (Lu and Godt 2008, de Compass et al. 1991). Only transient analysis can explore unsaturated moisture content in such soil slopes (Lu et al. 2008) required to stability analysis. For this reason, seepage modeling was decided to perform in transient condition in this study. After setting up all necessary conditions, seepage modeling was started applying hourly rainfall record of 19-20 October of 2004 (Figure 7.5) as a flux boundary in upper exposed sloping face of the finite element model. To reproduce the complexity of rainfall event, the hourly rainfall data were discretized into 283 time steps of 10 min length (total 47 hours 10 minutes). Transient seepage modeling predicts water tables equal to the number of time steps of rainfall flux. After seepage modeling, the porewater pressure profiles were recorded at the middle of

each slope (Figure 7.6) to interpret the role of porewater pressure on instability (see in section **7.5**).

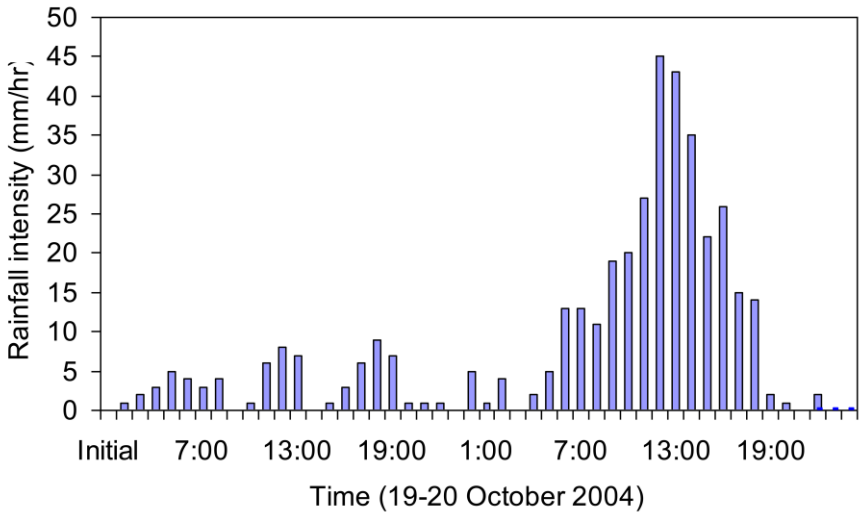

Figure 7.5 Hourly typhoon rainfall data of 19-20 October 2004 in the study area catchment

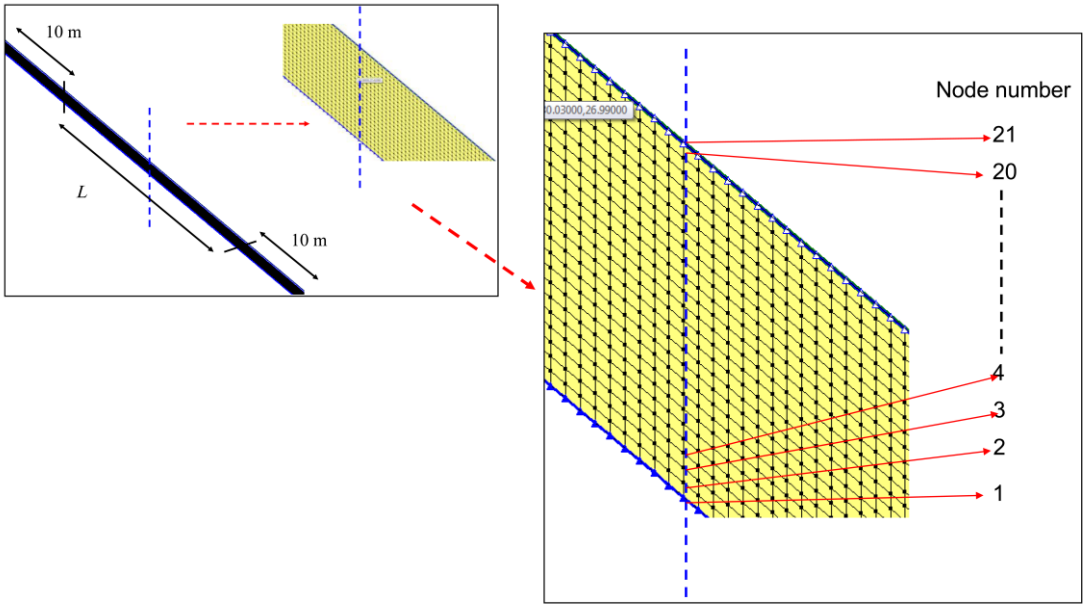

Figure 7.6 The porewater pressure profiles were measured at the middle of slope along dotted blue line after seepage modeling. Node numbers were assigned in increasing order from bottom to top along dotted blue line

7.4.4 Slope stability modeling

Slope stability modeling was performed in all slope profiles under the same conditions of hydrological and geo-mechanical parameters. Porewater pressure information was directly linked from SEEP/W. Slope inclination and soil depth were input from each hillslope profiles (Figure 7.2). A representative value of cohesion as C = 1 kN/m^2, angle of shearing resistance as ϕ = 34° and unit weight of soil as γ = 16.92 kN/m^3 were selected from Table 7.2. However, geo-mechanical parameters obtained from laboratory tests may vary from the actual field values as the laboratory tests were performed on the limited soil samples retrieved from field. To compensate variability in geo-mechanical parameters, slope stability modeling via sensitivity analysis was performed in this study. Sensitivity analysis examines the interrelationship of various parameters used in analysis, and then calculates factor of safety based on changes in given parameters. In sensitivity analysis, minimum and maximum values of cohesion, friction angle, unit weight, and ϕ^b (ϕ^b was assumed to be 2/3 of ϕ') were assigned as material properties in SLOPE/W environment. The exact location of triggering of hillslopes can not be predicted (von Ruette et al. 2013). The possible slip surface location, in this study, was defined by specifying range type entry and exit function. During rainfall, the factor of safety greatly reduces or the triggering of slope failure normally occurs either at the time of maximum rainfall intensity or after some hours of it no matter the geo-mechanical conditions of site. For this reason, porewater pressure developed at 14 pm of 20th October, 2004 (i.e., 223 time step of seepage modeling) which was two hours after the maximum hourly rainfall intensity (45 mm/hr at 12 pm on 20th October, 2004) was implemented in slope stability modeling. To determine the optimized factors of safety along the hillslopes during slope stability modeling, Morgenstern-Price (1965) method was used.

7.5 Results

7.5.1 Influence of slope inclination

Figure 7.7 (a) and (b) present porewater pressure distribution results with respect to various slope inclinations where soil depth is held constant. The slope profiles have undergone change in matric suction rather than positive porewater pressure. Matric suction is likely to completely vanish in all slope profiles with rainfall infiltration. Matric suction has disappeared quickly at bottom nodes of the slope profiles. The range of variation of matric suction is higher in lower slope inclinations compared to higher slope inclinations. Also the maximum value of matric suction is observed decreasing with increase in slope inclination for a given soil depth. The porewater profiles reveal that both the reduction in propagation

of matric suction and its maximum value are positively correlated with slope inclination. Matric suction propagation in unsaturated soil slope is related with rate of rainfall infiltration. However, rate of infiltration is influenced by slope inclination for the same rainfall flux. So, the cause of decrease in propagation of matric suction and its maximum value in Figure 7.7 (a) and (b) is that the rainfall flux infiltrated into slope decreases by cosine of the slope inclination (Zhan et al. 2013). The excess rainwater flows quickly down the slope as surface runoff or overland flow occurs. The studies, like Gofar et al. 2009, L'Heureux 2005 have presented similar effect of slope inclination on porewater pressure distribution.

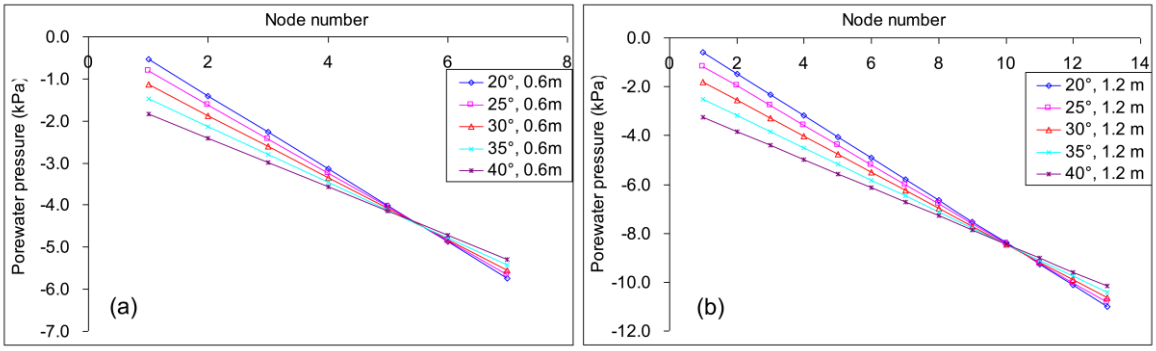

Figure 7.7 Examples of porewater pressure distribution with variation in slope inclination for (a) 0.6 m soil depth in 20 m slope profile, and (b) 1.2 m soil depth in 30 m slope profile after seepage modeling (the porewater pressure profiles were recorded at the middle of slope)

Figure 7.8 (a) and (b) show the variation in factors of safety with slope inclination after slope stability modeling. It can be seen from these figures that the factors of safety are maximum at the lowest slope inclination and these are decreasing exponentially with increase in slope inclination for all the values of soil depths. The trend in decrease in the factor of safety with increase in slope inclination is found sharper for relatively deep soil colluviums compared to shallow colluviums. For example, in Figure 7.8 (a), the factor of safety values at 20° and 25° for 0.3 m soil depth equal to 2.886 and 2.323 (a difference of 0.563, about 19.50 %), but the value of the same status drops to 2.288 and 1.825 (a difference of 0.463, about 20.20 %) for 0.6 m soil depth, and 2.102 and 1.665 (a difference of 0.437, about 20.78 %) for 0.9 m soil depth. It should be noted that the factor of safety is less than 1 after 38° for 1.8 m soil depth which implies that the hillslopes with soil depth greater than 1.8 m are prone to failure after 38°. Figure 7.8 (a) and (b) look similar, but the

factors of safety at consecutive points differ after decimal point. The results in Figure 7.8 (a) and (b) are consistent with those of some recent studies, such as Gofar et al. 2009, Cha and Kim 2011 and Zhan et al. 2013.

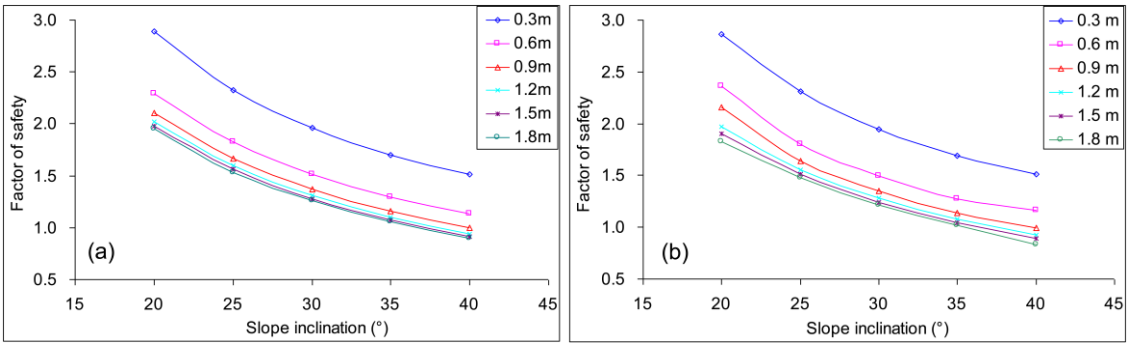

Figure 7.8 Typical examples of factor of safety distribution with variation in slope inclination at various constant soil depths in (a) 20 m slope profile, and (b) 30 m slope profile after slope stability modeling

On the other hand, with increase in slope inclination, the sliding component of the slope mass increases by sine of the slope inclination (or the resisting component of slope mass decreases by cosine of the slope inclination). This reduces static control on stability of slope mass whereby chance of sliding increases. Therefore, the decreasing trends in factor of safety (or increasing slope instability) with slope inclination in Figure 7.8 (a) and (b) can be attributed to two prime reasons: (i) gentler slope inclinations induce higher matric suction or porewater pressure, and (ii) steeper slope inclinations induce greater downslide force. The results indicate that instability of unsaturated soil slope is affected not only by mobilizing force of slope mass but also by matric suction.

7.5.2 Influence of soil depth

The variation in porewater pressure with respect to different soil depths is demonstrated in Figure 7.9 (a) and (b). In these figures, it can be seen that matric suction is decreasing in all soil depth colluviums with rainfall infiltration. But, the range of variation of matric suction is increasing with soil depth. Similarly, the value of matric suction at each node is noted increasing (or loss of matric suction at each node is noted decreasing) with increase in soil depth from 0.3 m to 1.2 m which implies that the seeping water is in course of reaching bottom of soil depth or it has just reached these depths within prescribed time (Garg et al. 2010). From 1.2 m to 2.4 m soil depth, the value of matric suction at corresponding nodes

is gradually decreasing (or the value of matric suction at corresponding nodes is increasing) which is due to marginal increase in volumetric water content with increase in soil depth. However, matric suction profiles are highly deepening from 1.2 m to 2.4 m for the same rainfall flux which points, in overall, less loss of matric suction at the deep soil colluviums. In shallow soil depths, matric suction may increase, decrease or remain constant (Travis et al. 2010) and similar interpretation for matric suction distribution can be understood in a couple of studies (Fredlund 1987, Tsaparas et al. 2002, Zhan and Ng 2004, Lee et al. 2009, Kassim et al. 2012). In case of much deeper soil colluviums (i.e., >2 m), however, the positive porewater pressure always increases with increase in soil depth and the relationship between porewater pressure increase and soil depth is linear (Fredlund and Rahardjo 1993).

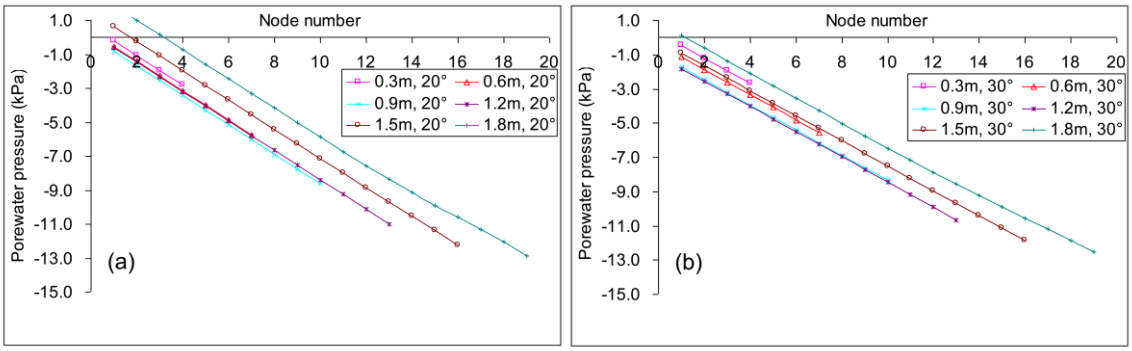

Figure 7.9 Examples of influence of soil depth on porewater pressure distribution for (a) 20° in 20 m slope profile, and (b) 30° in 30 m slope profile after seepage modeling (the porewater pressure profiles were recorded at the middle of slope)

In Figure 7.10 (a) and (b), the variations in factors of safety are clear with increase in soil depth at various constant slope inclinations. Increasing the soil depth from 0.3 m to 0.6 m in Figure 7.10 (a), factors of safety are significantly decreasing. From 0.6 m to 0.9 m, the trend in their decrement is gentle and for soil depth greater than 0.9 m, the factors of safety are insignificantly varying for all slope inclinations. The slowly decreasing factors of safety from 0.9 m to 1.8 m soil depths are consistent with less loss of matric suction or highly deepening matric suction profiles along same depths in Figure 7.9 (a) and (b). Also, the rate of decrease in the factor of safety with soil depth is observed faster with increase in slope inclination. As shown in Figure 7.10 (a) the factor of safety at 0.3 m and 0.6 m soil depth for 20° are 2.886 and 2.288 (a difference of 0.598, about 20.07 %), but the factors of safety under the same conditions for 25° and 30° are respectively 2.323 and 1.825 (a

difference of 0.498, about 21.43 %), and 1.996 and 1.511 (a difference of 0.449, about 22.90 %). With increase in soil depth, the slip surface deepens and the determined factors of safety are lower. The factor of safety has been observed to be less than 1 after 0.9 m for 40°. It indicates possibility of failure for slip surfaces deeper than 0.9 m. Effect of soil depth on slope instability has been fairly investigated in some significant studies (Dietrich et al. 2008, Griffiths et al. 2011) which have presented similar decreasing trends of factors of safety with soil depth as in Figure 7.10 (a) and (b).

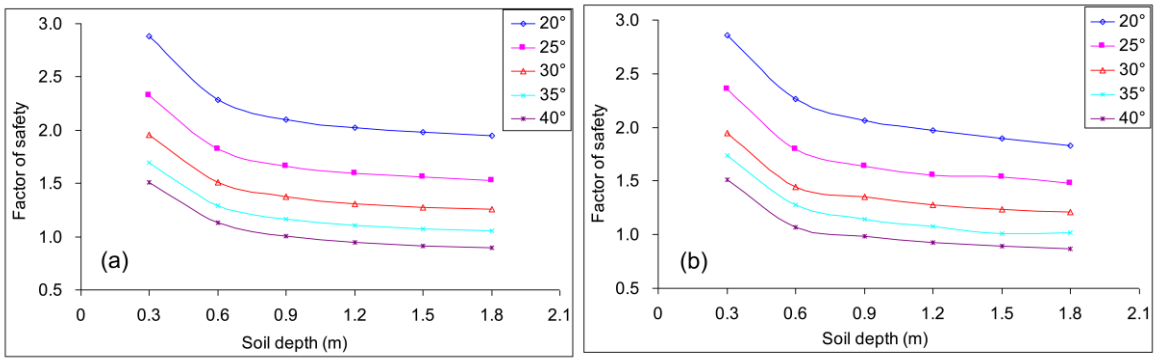

Figure 7.10 Typical examples of influence of soil depth on computed factors of safety at various constant slope inclinations in (a) 20 m slope profile, and (b) 30 m slope profile after slope stability modeling

Hence, there are two perspectives for decrease in the factor of safety (or increase in slope instability) with increase in soil depth in Figure 7.10 (a) and (b) as in the case of slope inclination. The first perspective is deepening of slip surface with increase in soil depth. This results in increased slope mass which, in turn, increases downward sliding component of force. The second perspective is increase in soil moisture content as thicker soil colluviums provide more space for storing water (or increase in marginal volumetric water content of soil with increase in soil depth). The increased moisture content due to addition of rainwater not only decreases shear strength at the slip surface by reducing matric suction but also increases the soil weight. Both phenomena enhance instability.

7.5.3 Influence of slope length

The porewater pressure distributions with respect to variation in slope length for various constant slope inclinations and 0.6 m soil depth are shown in Figure 7.11 (a) and (b). In these figures, there is no considerable change in matric suction distribution with increase in slope length. It means slope length does have no significant influence on matric suction

distribution. As the slope length increases, the chance for rainfall infiltration increases and more water enters into soil (Huang et al. 2013, Puigdefábregas et al. 1998). This brings change only in the quantity of surface runoff (De Bryan and Poesen 1989, Giesen et al. 2011). According to Aryal et al. 2005, hillslopes travel time for subsurface flow increases with increase in slope length, but the rate of infiltration does not change. The matric suction distribution in the hillslope is rather controlled by soil depth and slope inclination which is already mentioned in previous sections of result.

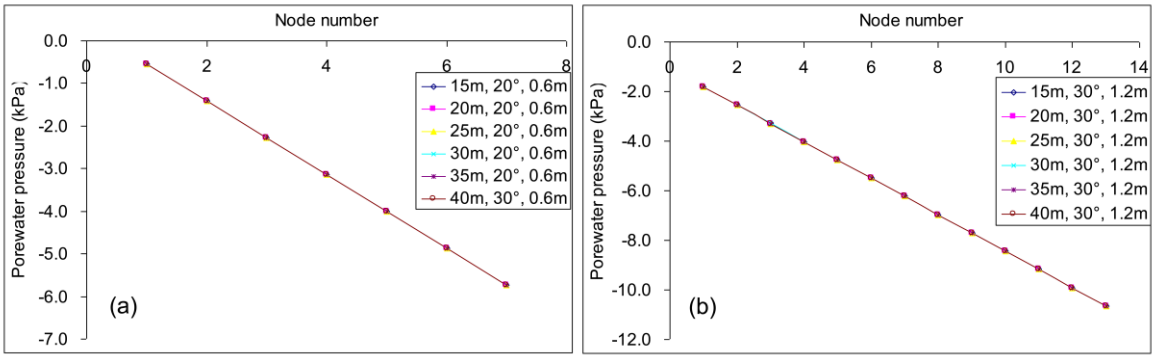

Figure 7.11 Examples of variation in porewater pressure with slope lengths at constant condition of (a) 20° and 0.6 m soil depth in 20 m slope profile, and (b) 30° and 1.2 m soil depth in 30 m slope profile (the porewater pressure profiles were recorded at the middle of slope)

The impact of slope length on factors of safety is illustrated in Figure 7.12 (a) and (b). In these figures, factors of safety are decreasing with increase in slope length at various constant slope inclinations and 0.6 m soil depths. Along short slope lengths, like from 15 m to 20 m, the decreasing trend in factor of safety can be easily noted. But, along relatively longer slope lengths; such as between 20 m and 40 m, the decreasing trend seems as it has almost diminished. Factors of safety between 20 m and 40 m slope lengths are varying in second and third decimal places. In short slope lengths, the slip surface does not pass parallel to the ground surface. Instead, it involves cutting at the top and bottom of the slope which results in higher factors of safety. But, in case of long slope lengths, the slip surface passes or failure mechanism occurs parallel to the ground surface and factor of safety gets lower (Griffiths et al. 2012). Factors of safety values are found below 1 for all slope lengths for 40° in Figure 7.12 (b). So, there is only one reason behind decrease in factors of safety (or increase in slope instability) with increase in slope length in Figure

7.12 (a) and (b): as the slope length increases, the mass of slope materials on sliding surface increases which results in increase in the downslide force and instability.

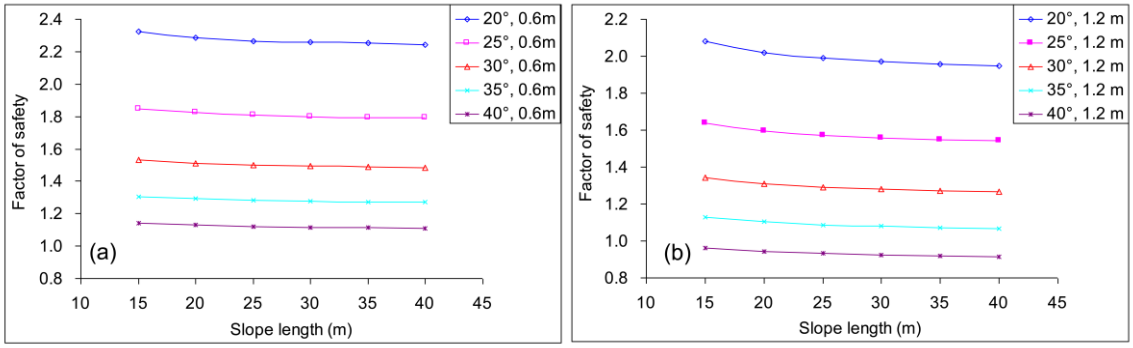

Figure 7.12 Examples of variation of factor of safety with slope length at various constant slope inclinations of (a) 0.6 m soil depth in 20 m slope profile, and (b) 1.2 m soil depth in 30 m slope profile

7.6 Discussion

Although hillslope instability occurs everywhere in mountainous areas, its nature is different as the subsurface hydrological and geo-mechanical phenomena vary over a short distance across different landscapes. Hence, hillslope instability is still not well understood topic of research and existing literatures are insufficient to describe its complex nature. In this study, hillslope instability was explicitly evaluated considering unsaturated soil slopes of Higashifukubegawa catchment in Shikoku Island of Japan under extreme rainfalls. The instability was observed through variation in porewater pressure response and factors of safety in slope profiles constructed by varying three basic parameters forming topography: slope inclination, soil depth and slope length across their explored range (Table 7.2) from seven slope failures of Higashifukubegawa. Finally, necessary explanations were provided for the role of resulting porewater pressure and mobilizing force of slope mass due to variation in values of employed parameters on determined factors of safety. There are some rationales which the present study follows. There are also some limitations. These should be explained here.

Influence of slope inclination on rainfall infiltration is an ambiguous topic: rainwater infiltration increases or decreases with increase in slope inclination (Fox et al. 1997). The raindrop impact breakdowns and compacts the thin surface layer into a hard crust or surface seal. The surface seal acts against rainwater infiltration. Therefore, with increase in surface sealing, rainwater infiltration decreases (West et al. 1992). But, the

development of surface seal is less in steeper slopes because of higher impact angle of the falling raindrops and the greater erosion rate. Rills may also form on the slope surface along with surface seal. The rate of formation of rills increases with increase in slope inclination (Poesen 1984). Luk et al. 1993 identified that the rate of infiltration increases with increase in slope inclination for shorter storms. But, in case of longer storms, the rainwater infiltration decreases with increase in slope inclination. For this, their justification was that during shorter storms, the development of surface seal is faster on gentle slopes while during longer storms, surface seal is completely formed at all the slope inclinations. SEEP/W does not take surface seal and rills into account and rainfall infiltration decreases normally with increase in slope inclination along slope profiles. Hence, unsaturated percolation, rapid response of porewater pressure increase, and overland flow of excess water from slope profile surface are the total hydrological processes that take place during seepage modeling in SEEP/W carried out in this study.

Also there has been a good argument for last two to three decades about what drives porewater pressure response which causes slope instability, such as lateral redistribution of water (Montgomery and Dietrich 1994, Montgomery et al. 2002, Milledge et al. 2012), vertical infiltration (Iverson 2000, 2004) or combination of both types (D'Odorico and Fagherazzi, 2003). The transient seepage modeling performed in this study is an example where porewater pressure increase is driven by vertical infiltration of rainwater. The transient seepage modeling was performed in deterministic approach (i.e., with defined soil permeability and porosity). In silty sand, rainflux quickly reaches the bottom of soil colluvium. Therefore, transient seepage modeling performed here gives exact range of expected change in porewater pressure. For example, matric suction varies between -1.82 kPa and -10.647 kPa in 1.2 m depth of silty sand at 30° under extreme rainfalls.

The porewater pressure profiles presented in result sections were subsurface hydrologic response of slope profiles to 223 time step rainflux. The value of applied rainflux/10 minute (q) at 223 time step was 1.62×10^{-6} m/s (i.e., $1/6^{th}$ of 9.72×10^{-6} m/s or 35 mm/hr at 14 pm of 20^{th} October, 2004) which is much greater than employed value of soil permeability (i.e., k as 9×10^{-8} m/s) in seepage modeling. Under such condition in coarse-grained shallow colluvial slopes, the infiltration front quickly meets underlying impervious bedrock and vertical flow of rainwater decreases. This phenomenon suppresses positive porewater pressure increase (McNamara et al. 2005, Rahardjo et al. 2005, Lanni et al. 2012). Instead, the porewater pressure and soil permeability increase based on the

relationship between matric suction head and unsaturated soil permeability. This is why matric suction was dominant or positive porewater pressure increase was insignificant in porewater pressure profiles at present study.

Griffiths et al. 2011, in stability analysis of an infinite slope, presented that factor of safety decreases, reaches a minimum and then increases with increase in slope inclination. They gave the term critical slope inclination at which minimum factor of safety was obtained and its value was 65° in their study. Their explanation for increase in the value of factor of safety after critical slope inclination was that the length of the potential failure surface available to resist sliding increases at a faster rate compared to down-slope component of the slope mass trying to cause sliding. However, instability process in natural hillslopes does not fully follow this trend. In natural slopes, instability always increases with increase in slope inclination and on steep slopes of greater than 65°, instability rarely occurs as there is no enough soil for sliding. In this study, factors of safety were found decreasing (or increasing instability) across full range of explored values of slope inclination of Higashifukubegawa catchment. In much deeper soil colluviums (i.e., >2 m), soil properties may change and rate of infiltration may not be effectively observed. So, localized failures may occur. On gentle hillslopes with deep soil colluviums, failure is attracted to crest whereas on relatively steeper hillslopes, toe failure is favored. Such types of instabilities were not noted at present study particularly due to limitation in employed value range of soil depth. The variations in factors of safety were regular with variation in values of all the three employed parameters across their permissible range. The parallel trend in porewater pressure and factor of safety distributions was due to coarse-grained nature of soil. Small grid size was used in finite element mesh since larger grids induce error in determination of factor of safety.

Hillslope is a three-dimensional morphological unit of topography. The three-dimensional geometry of a hillslope in a catchment can be represented by slope inclination, soil depth, slope length, slope width, profile curvatures [concave (hollow), convex (nose) and straight (side slopes) contours], and plan shapes (convergent, parallel, divergent) (Dietrich et al. 1987, Talebi et al. 2008a). The two-dimensional analyses of seepage and slope stability [GeoStudio (2005)] applied in this study might have slightly underestimated porewater pressure and overestimated factors of safety. However, these should not be significant since basic parameters of topography (slope inclination, soil depth and slope length) were captured in slope profiles and major controlling parameters of hillslope hydrologic response (soil permeability and porosity) were incorporated in dynamic

hydrological modeling in SEEP/W. Thus, two-dimensional seepage and slope stability analyses applied in this study is appropriate to investigate instability in a catchment with small-scale hillslope instability problems.

7.7 Conclusions

From this study, following conclusions were drawn.

(i) Slope instability increases with increase in slope inclination, soil depth and slope length with remarkable decreasing trend in factor of safety in Higashifukubegawa catchment. The failure process in hillslopes of other catchments in mountainous terrain should follow this trend.

(ii) Factors of safety were found exponentially decreasing with increase in slope inclination whereas the decrement was firstly exponential and then gentle (or nearly parallel) with soil depth and slope length across their permissible value range.

(iii) Slope inclination and soil depth impart significant impact on unsaturated zone moisture storage and sliding tendency of slope mass. Therefore, instability is controlled twofold by these two parameters.

(iv) The unsaturated zone moisture content does not considerably change with change in slope length, and only the changed sliding force of slope mass governs slope instability in case of slope length. Therefore, insignificant variation in unsaturated zone moisture content in relation to slope length can be neglected on stability analysis of catchment slopes.

(v) Among slope inclination, soil depth and slope length, the influence of a single parameter or combination of one with other two can be potential for predicting failure. Therefore, it is essential to properly consider these parameters in hillslope stability analysis.

(vi) How hillslope instability changes in relation to change in values of basic parameters of topography under same simulating conditions has been well studied and documented in this study. The comprehensive analyses performed in this study are believed to enhance the understanding on mechanism of extreme rainfall-induced instability or slope failure in

coarse-grained, shallow and unsaturated soil slopes of small catchments in mountainous terrain.

Chapter 8

Summary, conclusions, and limitations/recommendations

This chapter is based on summary of work and major results presented in **Chapter 5**, **6**, and **7**. Some limitations associated with methodology are also included together with recommendation.

Summary and Conclusions

The aim of this research was to evaluate rainfall-induced slope failures and potential instability during heavy rainfall in small catchment scale. For this, two-dimensional numerical modeling at hillslope scale and coupled deterministic-statistical modeling at landscape scale were performed in this study. The study was started with investigating triggering mechanism of slope failures in Higashifukbegawa catchment, Niihama of western Japan where the slope failures were induced by 2004 extreme typhoon-rainfalls. Seepage and slope stability modeling was performed in slope profiles passing through failure locations within the topographic hollows in Higashifukubegawa catchment, a part of tertiary sedimentary terrain in Niihama City of Shikoku Island. SEEP/W and SLOPE/W programs of GeoStudio (2005) can efficiently take the hydro-mechanical properties of soil into account from finite element mesh profile for numerical modeling. Hydrological and geo-mechanical processes associated with triggering of slope failures were analyzed and discussed in this part of research. After this, deterministic modeling was performed covering entire Higashifukubegawa catchment (landscape-scale analysis) employing infinite slope model and dynamic hydrological model. Parameter maps of hydrological and geo-mechanical properties of soil obtained from field/laboratory experiments were input to these models. A robust deterministic model was obtained as a result of deterministic slope failure hazard assessment. This model was then replicated into neighborhood test catchments of Higashifukubegeawa coupling it with discriminant function model through DEM-based morphometric parameters. In the last part of research, a parametric study in hillslope scale was performed numerically focusing on influence of basic parameters of topography on hillslope instability. The conclusions of this research are the following.

(i) Saturated-unsaturated interactions in soil slopes during heavy rainfall lead to fluctuation in subsurface zone moisture content which is one the major causes of triggering slope failure in topographic hollows.

(ii) One important dimension of this research is that it has related maximum porewater pressure with topographic hollow area through an empirical parametric equation so as to predict porewater pressure and potential instability in topographic hollows. The research emphasizes that topographic hollow size governs porewater pressure generation and it should be duly considered in the analysis of hillslope instability problems.

(iii) Major controlling parameters for hillslope instability have been outlined which were slope gradient, rainfall, saturated permeability of soil, porosity, and initial porewater pressure. These parameters directly affect/control rainfall infiltration through soil. Higher the rate of infiltration, higher is the soil moisture content or porewater pressure. When soil moisture content is much high, the slope mass fails regardless of the values of geotechnical parameters.

(iv) Hillslope subsurface hydrology was successfully linked to catchment subsurface hydrology (landscape-scale subsurface hydrology) which was then used for slope failure hazard assessment. By using SEEP/W, it was first done in this study.

(v) Realizing problems in existing methods of slope failure hazard assessment and replication in catchment-scale, the second part of this research utilized grey box approach [coupled deterministic-statistical method] to prepare and replicate a deterministic slope failure hazard model. The replicated hazard maps in neighborhood catchments of model catchment showed moderate to good prediction accuracy with existing inventories of 2004 slope failures. This reasonably validates the deterministic model and replication process presented in this study.

(vi) Even the variation in basic parameters of hillslope profiles significantly alters underlying hydro-mechanical mechanisms and instability which may eventually lead to slope failure.

(vii) The slope failure during extreme typhoon rainfalls can be realistically evaluated coupling hydro-geo-mechanical and statistical approaches.

Limitations and recommendations

(i) Evapotranspiration rate from the ground surface is a function of vegetation cover, soil moisture, and sunlight hour. But, it was neglected at present research.

(ii) Bedrock cracks play an important role on porewater pressure dynamics by acting as impedance for the downslope drainage of perched water. Influence of bedrock has been well studied in past studies of field and numerical investigation. This research has not considered drainage through bedrock in the analyses.

(iii) Antecedent rainfall affects slope stability by reducing soil suction and increasing transient porewater pressure. Most of the days of September and October had considerable antecedent rainfall. The antecedent rainfalls prior to major rainfall event (19-20 October 2004) were not considered in any of the analyses in this study.

(iv) There are some important aspects in porewater pressure profiles presented in **Chapter 5** which should be explained here. The trend in porewater pressure increase seems as it has converged or reached maximum before 7 am on 10/20 although it should reach peak only at 14 pm on 10/20 (i.e., at exactly at maximum hourly rainfall intensity, 45 mm/hr) or after some hours of maximum hourly rainfall intensity. In reality, the porewater pressure has not exactly converged. If it is closely observed, the increasing trend in porewater pressure from 7 am to 14 pm on 10/20 can be recognized and the porewater pressure has reached maximum only at 14 pm on 10/20 (i.e., at the 38th hour of two day continuous rainfall). However, the increasing trend in porewater pressure from 7 am to 14 pm on 10/20 is gentle or not sharp/significant compared to decrease in the factors of safety. Before performing seepage modeling, it was expected that there should be significant/sharp increase in porewater pressure with rainfall infiltration between 7 am and 14 pm on 10/20. Hundreds of trials were done in each slope profiles to get the expected porewater pressure increase by altering field values of hydrological parameters, such as hydraulic conductivity, volumetric water content across a reasonable range for silty sand. However, better results could not be obtained than presented in [i.e., Figure 7 (a, b, c, d, e, f, g)]. So, significant decrease in factors of safety was obtained between 7 am and 14 pm on 10/20. But, significant/sharp increase in porewater was not received during the same rainfall hours. From this, it is remarked that the significant decrease in factor of safety after 7 am on 10/20 is not mainly due to porewater pressure change but due to other parameters, such as

slope inclination, geo-mechanical parameters, soil depth etc. The next reason may be limitation of two-dimensional hydrological modeling program [SEEP/W plug-in of Geostudio (2005)] because the porewater pressure distribution was slightly overestimated between 7 am and 14 pm on 10/20. So, it is also recommended to use the other hydrological modeling programs for such kind of analysis and crosscheck the results.

(v) Although the two-dimensional seepage and slope stability modeling implemented in this study is considered appropriate to address simple instability problems in topographic hollows, it may not be sufficient. It is because a topographic hollow is a three-dimensional morphological unit, and seepage and slope stability mechanisms occurring on it must be three dimensional. The three dimensional geometry of a topographic hollow can be represented by hillslopes with slope shape [concave (hollow), convex (nose) and straight (side slopes) contours], slope inclination and slope profile (profile length, profile width, soil depth) (Dietrich et al. 1987). The present study has not considered plan shape and profile curvature in modeling. Apart from principle parameters of topography (slope inclination, soil depth, and slope length), plan shape and profile curvatures also significantly contribute to the subsurface hydrology of topographic hollow. Convex shape contributes water to concave and plane shape. Instability can occur in both concave and plane shape (Dietrich et al. 1987, May et al. 2002, Sidle et al. 1985, Thorne et al. 1987). Therefore, these parameters should also be incorporated in hydrological/slope stability modeling so to more realistically predict instability mechanism.

References

Acharya G, Smedt FDe, Long NT (2006) Assessing landslide hazard in GIS: a case study from Rasuwa, Nepal. Bulletin of Engineering Geology and the Environment 65: 99–107.

Aleotti P (2004) A warning system of rainfall-induced shallow failure. Engineering Geology 73: 247–265.

Aleotti P, Chowdhury R (1999) Landslide hazard assessment: summary review and new perspectives. Bulletin of Engineering Geology and the Environment 58: 21–44.

Alvioli M, Guzzetti F, Rossi M (2014) Scaling properties of rainfall induced landslides predicted by a physically based model. Geomorphology, http://dx.doi.org/10.1016/j.geomorph.2013.12.039.

Anderson H, Bengtsson P-E, Berglund C, Larsson C, Larsson R, Sällfors G, Öberg-Högsta A-L (2000) The landslide at Vagnharad in Sweden. In: Bromhead E, Dixon N, Ibsen M-L (eds) Landslides in research, theory and practice. Eighth international symposium on landslides. T. Telford, London, pp 65–70.

Anderson MG, Lloyd DM (1991) Using a combined slope hydrology-stability model to develop cut slope design charts. Proceedings of the Inst. of Civil Engineers 91: 705–718.

Ardizzone F, Cardinali M, Carrara A, Guzzetti F, Reichenbach P (2002) Impact of mapping errors on the reliability of landslide hazard maps. Natural Hazards and Earth System Sciences 2: 3–14.

Arnone E, Noto LV, Lepore C, Bras RL (2011) Physically-based and distributed approach to analyze rainfall-triggered landslides at watershed scale. Geomorphology: 133: 121–131.

Aryal SK, O'Loughlin EM, Mein RG (2005) A similarity approach to determine response times to steady-state saturation in landscapes. Advances in Water Resources 28 (2): 99-115.

ASTM (1999a) Standard Test Method for Particle-size Analysis of Soils: D422. Annual Book of ASTM standards, v. 04.08, West Conshohocken, Pa.

ASTM (1999b) Standard test method for liquid limit, plastic limit and plasticity index of soils: D4318. Annual Book of ASTM standards, v. 04.08, West Conshohocken, Pa.

Ayalew L (1999) The Effect of Seasonal Rainfall on Landslides in the Highlands of Ethiopia. Bulletin of Eng. Geology and the Environment: 58: 9 -19.

Ayalew L, Yamagishi H, Ugawa N (2004) Landslide susceptibility mapping using GIS-based weighted linear combination, the case in Tsugawa area of Agano River, Niigata Prefecture, Japan. Landslides 1(1): 73–81.

Baba K, Bahi L, Ouadif L, Akhssas A (2012) Slope Stability Evaluations by Limit Equilibrium and Finite Element Methods Applied to a Railway in the Moroccan Rif. Open Journal of Civil Engineering 2012 (2): 27-32.

Baeza C, Corominas J (2001) Assessment of shallow landslide susceptibility by means of multivariate statistical techniques. Earth Surface Processes Landforms 26: 1251–1263.

Baeza C, Lantada N, Moya J (2010) Validation and evaluation of two multivariate statistical models for predictive shallow landslide susceptibility mapping of the Eastern Pyrenees (Spain). Environmental Earth Sciences 61: 507–523.

Balaam NP (2001) Slope Stability Analysis – User´s Manual for Program XSlope for Windows. Centre for Geotecnhical Research – University of Sydney, 98p.

Barredo J, Benavides A, Hervas J, van Westen CJ (2000) Comparing heuristic landslide hazard assessment techniques using GIS in the Tirajana basin, Gran Canaria Island, Spain. International Journal of Applied Earth Observation and Geoinformation 2 (1): 9-23.

Baum RL, Godt JW, Savage, WZ (2010) Estimating the timing and location of shallow rainfall-induced landslides using a model for transient, unsaturated infiltration. Journal of Geophysical Research Earth Surface .115.Doi:10.1029/2009JF001321.

Bell R (2007) Lokale und regionale Gefahren- und Risikoanalyse gravitativer Massenbewegungen an der Schwäbischen Alb. University of Bonn, Germany.

Beven KJ, Kirkby MJ (1979) A physical based variable contributing area model of basin hydrology. Hydrological sciences Bulletin 24 (1): 43–69.

Bhandary NP (2003) Creep activation of landslides and related problems in active fault zones of Shikoku under the influence of expansive clay minerals, PhD Thesis, Graduate School of Science and Engineering, Ehime University, Chapter 3, pp. 27-57 (Unpublished).

Bhandary NP, Dahal RK, Timilsina M, Yatabe R (2013) Rainfall event-based landslide susceptibility zonation mapping. Natural Hazards DOI 10.1007/s11069-013-0715-x.

Bhandary NP, Yatabe R (2005) Influence of Precipitation Pattern on Triggering Surface-layer Failures of Slopes during 2004 Niihama Disasters, In: Proc. One-day Symposium on Geo-disasters and Geo-environment, Ehime University, Japan, 63–70.

Bijukchhen SM, Kayastha P, Dhital MR (2012) A comparative evaluation of heuristic and bivariate statistical modelling for landslide susceptibility mappings in Ghurmi–Dhad Khola, East Nepal. Arabian Journal of Geosciences, doi: 10.1007/s12517-012-0569-7.

Borga M, Fontana GD, Gregoretti C, Marchi L (2002) Assessment of shallow landsliding by using a physically based model of hillslope stability. Hydrological Processes 16: 2833 -2851.

Borga M, Fontana GD, Ros DD, Marchi L (1998) Shallow landslide hazard assessment using a physically based model and digital elevation data. Journal of Environmental Geology 35(2-3): 81-88.

Boussinesq J (1877) Essai sur la thorie des eaux courantes, Mm. Acad. Sci. Inst. France, 23: 1-680.

Bronstert A (1994) Modellierung der Abflussbildung und der Bodenwasserdynamik von Hangen, Universitat Karlsruhe, 46 pp.

Brooks SM, Richards KS (1994) The significance of rainstorm variations to shallow translational hillslope failure. Earth Surface Processes and Landforms 19(1): 85–94.

Brunetti MT, Peruccacci S, Rossi M, Luciani S, Valigi D, Guzzetti F (2010) Rainfall thresholds for the possible occurrence of landslides in Italy. Natural Hazards and Earth System Sciences 10: 447–458.

Bryan RB, Poesen J (1989) Laboratory experiments on the influence of slope length on overland flow, percolation, and rill development. Earth Surface Processes and Landforms 14: 211-231.

Burrough PA, McDonnell RA (1998) Principles of Geographical Information Systems. Oxford University Press.

Burton A, Bathurst JC (1998) Physically based modeling of shallow landslide yield at a catchment scale. Environmental Geology 35(2-3): 89-99.

Caine N (1980) The rainfall intensity: duration control of shallow landslides and debris flows. Geografiska Annaler. Series A, Phys Geog 62(1/2): 23–27. Accessed 18 Oct 2010.

Campbell RH (1975) Soil slips, debris flows, and rainstorms in the Santa Monica Mountains and vicinity, Southern California, U.S. Geological Survey Professional Paper 851, 1975, 51 p.

Cannon SH, Gartner JE, Rupert MG, Michael JA (2004) Emergency assessment of debris-flow hazards from basins burned by the Padua fire of 2003, southern, California. U.S. Geological Survey Open-File Report 2004-1072. pp. 14.

Cannon SH, Gartner JE (2005) Wildfire-related debris flow from a hazards perspective. In: Jakob M, Hungr O (eds) Debris flow hazards and related phenomena. Springer, Berlin, pp 363–385.

Capparelli G, Biondi D, De Luca DL, Versace P (2009) Hydrological and complete models for forecasting landslides triggered by rainfalls. In: Rainfall–induced landslides. Mechanisms monitoring techniques and nowcasting models for early warning systems. Proceedings of the first Italian workshop on landslides pp 8–10.

Cardinali M, Galli M, Guzzetti F, Ardizzone F, Reichenbach P, Bartoccini P (2006) Rainfall induced landslides in December 2004 in south-western Umbria, central Italy: types, extent, damage and risk assessment. Natural Hazards Earth and System Sciences 6: 237–260.

Carrara A, Cardinali M, Guzzetti F (1992) Uncertainty in assessing landslide hazard and risk. ITC Journal 2: 172– 83.

Carrara A, Crosta GB, Frattini P (2003) Geomorphological and historical data in assessing landslide hazard. Earth Surface Processes and Landforms 28(10): 1125–1142.

Carrara A, Guzzetti F, Cardinali M, Reichenbach P (1999) Use of GIS technology in the prediction and monitoring of landslide hazard. Natural Hazards 20 (2–3): 117–135.

Casagli N, Dapporto S, Ibsen ML, Tofani V, Vannocci P (2006) Analysis of the landslide triggering mechanism during the storm of 20th–21st November 2000, in Northern Tuscany. Landslides 3: 13–21

Cascini L, Cuomo S, Pastor M, Sorbino G (2010) Modeling of Rainfall-Induced Shallow Landslides of the Flow-Type. Journal of Geotechnical and Geoenvironmental Engineering, © ASCE, pp. 85-98.

Cascini L, Sorbino G, Cuomo S, Ferlisi S (2013) Seasonal effects of rainfall on the shallow pyroclastic deposits of the Campania region (southern Italy). Landslides DOI 10.1007/s10346-013-0395-3.

Cha K-S, Kim T-H (2011) Evaluation of Slope Stability with Topography and Slope Stability Analysis Method. KSCE Journal of Civil Engineering 15(2): 251-256.

Chandrasekaran SS, Owaise RS, Ashwin S, Jain RM, Prasanth S, Venugopalan RB (2013) Investigation on infrastructural damages by rainfall-induced landslides during November 2009 in Nilgiris, India. Natural Hazards 65: 1535–1557.

Chang K-T, Chiang S-H, Lei F (2007) Analysing the Relationship Between Typhoon-Triggered Landslides and Critical Rainfall Conditions. Earth Surface Processes and Landforms DOI: 10.1002/esp.1611.

Chen JC, Jan CD (2003) Probabilistic equation of critical slope for debris-flow occurrence, in Debris-Flow Hazards Mitigation: Mechanics, Prediction, and Assessment, edited by D. Rickenmann and C. Chen, pp. 83–89, Millpress, Rotterdam, Netherlands.

Ching J, Liao HJ, Lee JY (2011) Predicting rainfall-induced landslide potential along a mountain road in Taiwan. Geotechnique 61(2): 153–66.

Chugh AK, Stark TD (2006) Permanent seismic deformation analysis of a landslide. Landslides (2006) 3: 2–12.

Claessens L, Schoorl JM, Veldkamp A (2007) Modelling the location of shallow landslides and their effects on landscape dynamics in large watersheds: An application for Northern New Zealand. Geomorphology 87:16-27.

Clarizia M, Gullà G, Sorbino G (1996) Sui meccanismi di innesco dei soil slip. International conference Prevention of hydrogeological hazards: the role of scientific research 1: 585–597 (in Italian).

Clark GM (1987) Debris slide and debris flow historical events in the Appalachians south of the glacial border. Geological Society of America, Reviews in Engineering Geology, VII: 125-138.

Cole SJ, Moore RJ (2009) Distributed hydrological modelling using weather radar in gauged and ungauged basins. Advances in Water Resources 32: 1107–1120.

Comegna L, Urciuoli G, Picarelli L (2004) The role of pore pressures on the mechanics of mudslides. In: Lacerda W, Ehrlich M, Fontoura SAB, Sayao AS (eds) Landslides: evaluation and stabilization. Ninth international symposium on landslides. A.A. Balkema Publishers, Leiden, pp 1183–1188.

Corominas J (2001) Landslides and Climate, Keynote Lectures from the 8th International Symposium on Landslides, No 4, pp 1–33.

Crosta G (1998) Regionalization of rainfall thresholds: an aid to landslide hazard evaluation. Environmental Geology 35(2): 131–145.

Cotza G (2009) Geologische und geotechnische Verhältnisse der Massenbewegungen bei Pontives (Grödnertal, Südtirol). University of Vienna, Austria.

Crozier MJ (1999) Prediction of rainfall-triggered landslides: a test of the antecedent water status model. Earth Surface Processes and Landform 24(9): 825–833.

Crozier MJ, Preston NJ (1999) Modelling changes in terrain resistance as a component of landform evolution in unstable hill country. In: Hergarten S, Neugebauer HJ (eds) Process modelling and landform evolution. Springer, Berlin, pp 267–284.

Dai FC, Lee CF, Ngai YY (2002) Landslide risk assessment and management: an overview. Engineering Geology 64: 65–87.

Dai FC, Lee CF (2003) A spatiotemporal probabilistic modelling of storm-induced shallow landsliding using aerial photographs and logistic regression. Earth Surface Process and Landform 28(5): 527–545.

Dahal (2008) Evaluation of rainfall-induced landslides from the perspectives of stability analysis, rainfall threshold and hazard in the Nepal Himalaya and Shikoku, Japan. Ph.D. thesis. Kagawa University Japan.

Dahal RK, Hasegawa S (2008) Representative rainfall thresholds for landslides in the Nepal Himalaya. Geomorphology 100: 429–443.

Dahal RK, Hasegawa S, Yamanaka M, Dhakal S, Bhandary NP, Yatabe R (2009) Comparative analysis of contributing parameters for rainfall-triggered landslides in the Lesser Himalaya of Nepal. Environmental Geology 58: 567–586.

Dahal RK, Hasegawa S, Nonomura A, Yamanaka M, Masuda T, Nishino K (2008c) GIS-based weights-of-evidence modelling of rainfall-induced landslides in small catchments for landslide susceptibility mapping. Environmental Geology 54: 311–324.

Dahal RK, Hasegawa S, Nonomura A, Yamanaka Y, Dhakal S, Paudyal P (2008a) Predictive modelling of rainfall-induced landslide hazard in the Lesser Himalaya of Nepal based on weights-of-evidence. Geomorphology, 102, pp. 496–510.

Dahal RK, Hasegawa S, Nonomura A, Yamanaka M, Dhakal S (2008b) DEM-based deterministic landslide hazard analysis in the Lesser Himalaya of Nepal. Georisk: Assessment and Management of Risk for Engineered Systems and Geohazards, 2(3): 161-178.

Dahal RK, Hasegawa S, Yamanaka M, Nonomura A (2008d) Typhoon Rainfall and Landsliding in the Pacific Ocean Side of Japan. Proceedings of the Eighteenth International Offshore and Polar Engineering Conference Vancouver, BC, Canada, July 6-11, 2008. pp. 795-802.

Dahal RK, Hasegawa S, Yamanaka M, Bhandary NP, Yatabe R (2011) Rainfall-induced landslides in the residual soil of andesitic terrain, western Japan. Journal of Nepal Geological Society 42: 127–142.

Dahal RK, Hasegawa S, Yamanaka M, Nishino K (2006) Rainfall triggered flow-like landslides: understanding from southern hills of Kathmandu, Nepal and northern Shikoku, Japan. Proc 10th Int Congr of IAEG, The Geological Society of London, IAEG2006 Paper number 819, pp. 1–14 (CD-ROM).

Dahal RK, Hasegawa S, Yamanaka M, Dhakal S, Bhandary NP, Yatabe R (2009) Comparative analysis of contributing parameters for rainfall-triggered landslides in the Lesser Himalaya of Nepal. Environmental Geology 58: 567-586.

Dahal, R.K., Hasegawa, S., Bhandary, N.P., Poudel, P.P., Nonomura, A. and Yatabe, R., 2012, A replication of landslide hazard mapping at catchment scale. Geomatics, Natural Hazards and Risk 3(2): 161-192.

Daitou Techno Green, 2009, Hasegawa in situ permeability tester, operating manual. v. 3.1, available for download in http://www. daitoutg.co.jp/prd/pdf/tousui0703.pdf.

de Campos TMP, Andrade MHN, Vargas EA (1991) Unsaturated colluvium over rock slide in a forested site in Rio de Janeiro, Brazil, in Proc. 6th Int. Symp. On Landslides, Christchurch New Zealand pp. 1357-1364, Balkema, Rotterdam, Neatherlands.

De Giesen NV, Stomph T-J, Ajavi AE, Bagavoko F (2011) Scale effects in Hortonian surface runoff on agricultural slopes in West Africa: field data and models. Agriculture, Ecosystems and Environment 142: 95-101.

Dhakal AS, Sidle RC (2003) Long-term modelling of landslides for different forest management practices. Earth Surface Processes and Landforms 28: 853-868.

Dietrich WE, Dunne T (1978) Sediment budget for a small catchment in mountainous terrain, Z. Geomorphology 29: 191–206.

Dietrich WE, McKean J, Bellugi D, Perron T (2007) The prediction of shallow landslide location and size using a multidimensional landslide analysis in a digital terrain model. Proceedings of the Fourth International Conference on Debris-Flow Hazards Mitigation: Mechanics, Prediction, and Assessment (DFHM-4); Chengdu, China.

Dietrich WE, McKean J, Bellugi D, Perron T (2008) The prediction of shallow landslide location and size using a multidimensional landslide analysis in a digital terrain model. In Fourth International Conference on Debris-Flow Hazards Mitigation: Mechanics, Prediction, and Assessment (DFHM-4), Chengdu, China, September 10-13, 2007, Chen CL, Major JJ (eds). IOS Press: Amsterdam.

Dietrich WE, Real de Asua R, Coyle1 J, Orr B, Trso M (1998) A validation study of the shallow slope stability model, SHALSTAB, in forested lands of Northern California. Stillwater Ecosystem, Watershed & Riverine Sciences, Berkley, USA.

Dietrich WE, Reneau SL, Wilson CJ (1987) Overview: "zero-order basins" and problems of drainage density, sediment transport and hillslope morphology. Erosion and Sedimentation in the Pacific Rim (Proceedings of the Corvallis Symposium, August). IAHS Publ . no. 165.

Dikau R, Glade T (2003) Nationale Gefahrenhinweiskarte gravitativer Massenbewegungen. In:Liedtke H, Mäusbacher R, Schmidt K-H (eds) Relief, Boden und Wasser. Nationalatlas Bundesrepublik Deutschland. Spektrum Akademischer Verlag, Heidelberg, pp 98–99.

D'Odorico P, Fagherazzi S (2003) A probabilistic model of rainfall-triggered shallow landslides in hollows: A long-term analysis. Water Resources Research 39:1262. doi:10.1029/2002WR001595.

Dong JJ, Tung YH, Chen CC, Liao JJ, Pan YW (2009) Discriminant analysis of the geomorphic characteristics and stability of landslide dams. Geomorphology 110: 162–171.

Duman TY, Can T, Gokceoglu C, Nefeslioglu HA (2005) Landslide susceptibility mapping of Cekmece area (Istanbul, Turkey) by conditional probability. Hydrology and Earth System Sciences 2: 155–208.

Dunne T (1978) Field studies of hillslope flow processes. In Hillslope Hydrology, Kirkby MJ, (ed.). Wiley: Chichester pp.227–293.

Eeckhaut MVD, Reichenbach P, Guzzetti F, Rossi M, Poesen J (2009) Combined landslide inventory and susceptibility assessment based on different mapping units: an example from the Flemish Ardennes, Belgium. Natural Hazards and Earth System Sciences 9: 507–521.

Ekanayake JC, Phillips CJ (1999) A model for determining thresholds for initiation of shallow landslides under near-saturated conditions in the East Coast region, New Zealand. J Hydrol (NZ) 38(1): 1–28.

Fannin RJ, Jaakkola J (1999) Hydrological response of hillslope soils above a debris-slide headscarp. Canadian Geotechnical Journal 36: 1111–1122.

Fox DM, Bryan RB, Price AG (1997) The influence of slope angle on final infiltration rate for interrill conditions. Geoderma 80: 81- 194.

Frattini P, Crosta G, Sosio R (2009) Approaches for defining thresholds and return periods for rainfall-triggered shallow landslides. Hydrological Processes 23(10): 1444–1460.

Fredlund DG (1987) Slope stability analysis incorporating the effect of soil suction. Slope stability, Edited by M.G. Anderson and KS Richards, John Wiley and Sons Ltd.

Fredlund DG, Morgenstern NR, Widger RA (1978) The shear strength of unsaturated soils. Canadian Geotechnical Journal 15(3): 313-321.

Fredlund DG, Rahardjo H (1993) Soil Mechanics for Unsaturated Soils, John Wiley and Sons, New York.

Fredlund DG, Xing A (1994) Equations for the soil-water characteristics curve. Canadian Geotechnical Journal 31: 533–546.

Gabet EJ, Burbank DW, Putkonen JK, Pratt-Sitaula BA, Oiha T (2004) Rainfall thresholds for landsliding in the Himalayas of Nepal. Geomorphology 63: 131–143.

Garg A, Chetia M, Sreedeep S (2010) A Study on the Influence of Soil-Water Characteristic Curve on the Seepage Modeling of Unsaturated Soil. International Journal of Earth Sciences and Engineering 3 (2): 40-46.

Gasmo JM, Rahardjo H, Leong EC (2000) Infiltration effects on stability of a residual soil slope. Computers and Geotechnics 26: 145-165.

Glade TW (1997) The Temporal and Spatial Occurrence of Rainstorm-triggered Landslide Events in New Zealand, Unpublished Ph.D. Thesis, Victoria University of Wellington, Wellington, New Zealand.

Glade T (1998) Establishing the frequency and magnitude of landslide-triggering rainstorm events in New Zealand. Environmental Geology 35(2): 160–174.

Glade T, Crozier M, Smith P (2000) Applying probability determination to refine landslide-triggering rainfall thresholds using an empirical Antecedent Daily Rainfall Model. Pure and Applied Geophysics 157: 1059–1079.

GeoStudio (2005) GeoStudio Tutorials includes student edition lessons, 1st edition revised, Geo-Slope International Ltd., Calgary, Alberta, Canada.

Gessner K (2009) Coupled Models of Brittle-plastic Deformation and Fluid Flow: Approaches, Methods, and Application to Mesoproterozoic Mineralisation at Mount Isa, Australia. Surv Geophys 30: 211–232.

Ghimire M (2011) Landslide occurrence and its relation with terrain factors in the Siwalik Hills, Nepal: case study of susceptibility assessment in three basins. Natural Hazards 56: 299–320.

Ghosh S, van Westen CJ, Carranza EJM, Jetten VG, Cardinali M, Rossi M, Guzzetti F (2012) Generating event-based landslide maps in a data-scarce Himalayan environment for estimating temporal and magnitude probabilities. Engineering Geology 128: 49–62.

Giannecchini R, Galanti Y, Avanzi G. D'A (2012) Critical rainfall thresholds for triggering shallow landslides in the Serchio River Valley (Tuscany, Italy). Natural Hazards and Earth System Sciences 12: 829–842.

Godt JW, Baum RL, Chleborad AF (2006) Rainfall characteristics for shallow landsliding in Seattle, Washington, USA. Earth Surface Processes and Landform 31(1): 97–110.

Godt JW, Baum RL, Savage WZ, Salciarini D, Schulz WH, Harp EL (2008) Transient deterministic shallow landslide modeling: Requirements for susceptibility and hazard assessments in a GIS framework. Engineering Geology 102: 214–226.

Gofar N, Kassim KA, Kassim A, Lee LM (2009) The study on the development of saturation profile in soil. Fakultikejuruteraan Awam, Universiti Teknologi Malaysia.

Gotman AL (2007) Design experience with foundations at sites with combined karsting and landslide risk. Soil Mechanics and Foundation Engineering, Vol 44, No 5.

Griffiths DV, Huang J, deWolfe GF (2011) Numerical and analytical observations on long and infinite slopes. International Journal for Numerical and Analytical Methods in Geomechanics 35:569-585.

Guzzetti F, Cardinali M, Reichenbach P, Carrara A (2000) Comparing landslide maps: A case study in the Upper Tiber River Basin, Central Italy. Environmental Management 25(3): 247–263. Accessed 7 Oct 2010.

Guzzetti F, Cardinali M, Reichenbach P, Cipolla F, Sebastiani C, Galli M, Salvati P (2004) Landslides triggered by the 23 November 2000 rainfall event in the Imperia Province, Western Liguria, Italy. Engineering Geology 73: 229–245.

Guzzetti F, Reichenbach P, Ardizzone F, Cardinali M, Galli M (2006) Estimating the quality of landslide susceptibility models. Geomorphology 81: 166–184.

Guzzetti F, Reichenbach P, Cardinali M, Galli M, Ardizzone F (2005) Probabilistic landslide hazard assessment at the basin scale. Geomorphology 72: 272– 299.

Guzzetti F, Peruccacci S, Rossi M, Stark CP (2007) Rainfall thresholds for the initiation of landslides in central and southern Europe. Meteorology Atmospheric Physics 98(3–4): 239–267.

Guzzetti F, Peruccacci S, Rossi M, Stark CP (2008) The rainfall intensity–duration control of shallow landslides and debris flows: an update. Landslides 5(1): 3–17.

Hack JT, Goodlett JC (1960) Geomorphology and forest ecology of a mountain region in the central Appalachians. U.S. Geol. Surv. Prof. Pap., 347, 66 pp.

Hadmoko DS, Lavigne F, Sartohadi J, Hadi P and Winaryo (2010) Landslide hazard and risk assessment and their application in risk management and landuse planning in eastern flank of Menoreh Mountains, Yogyakarta Province, Indonesia. Natural Hazards 54(3): pp. 623–42.

Hammond C, Hall D, Miller S, Swetik P (1992) Level I Stability analysis (LISA), Documentation for Versito 2.0, Gen. Tech. Rep. INT-285, Ogden, UT: Department of Agriculture, Forest Service, Intermountain Research Station, pp. 190.

Harp EL, Reid ME, McKenna JP, Michael JA (2009) Mapping of hazard from rainfall-triggered landslides in developing countries: Examples from Honduras and Micronesia. Engineering Geology 104: 295–311.

Harris SJ, Orense RP, Itoh K (2012) Back analyses of rainfall-induced slope failure in Northland Allochthon formation. Landslides 9: 349–356.

Hashimoto M (1991) Geology of Japan. Springer, 249 p.

He MC, Feng JL, Sun XM (2008) Stability evaluation and optimal excavated design of rock slope at Antaibao open pit coal mine, China. International Journal of Rock Mechanics & Mining Sciences 45: 289–302.

He S, Pan P, Dai L, Wang H, Liu J (2012) Application of kernel-based Fisher discriminant analysis to map landslide susceptibility in the Qinggan River delta, Three Gorges, China. Geomorphology 171–172: 30–41.

Hilberts A, Troch P, Paniconi C (2005) Storage-dependent drainable porosity for complex hillslopes. Water Resources Research 41. W06001. doi:10.1029/2004WR003725.

Hilberts A, Troch PA, Paniconi C, Boll J (2007) Low-dimensional modeling of hillslope subsurface flow: the relationship between rainfall, recharge, and unsaturated storage. Water Resources Research 43. DOI: 10.1029/2006WR006496.

Hilberts A, Van Loon EE, Troch PA, Paniconi C (2004) The hillslope-storage Boussinesq model for non-constant bedrock slope. Journal of Hydrology 291: 160-173.

Hiura H, Kaibori K, Suemine A, Satofuka Y, Tsutumi D (2004) Sediment-related disaster in Kisawa Village and Kaminaka -Town in Tokushima Prefecture, Japan, induced by the heavy rainfall of the Typhoon Namtheun in 2004 (prompt report), Journal of the Japan Society of Erosion Control Engineering, Vol.57, No.4, p. 39-47 (in Japanese).

Hsu SM, Chiou LB, Lin GF, Chao CH, Wen HY, Ku CY (2010) Applications of simulation technique on debris-flow hazard zone delineation: a case study in Hualien County, Taiwan. Natural Hazards and Earth System Sciences10: 535-545.

Huang C-C (2013) Critical rainfall for typhoon-induced debris flows in the Western Foothills, Taiwan. Geomorphology 185: 87–95.

Huang J, Wu P, Zhao X (2013) Effects of rainfall intensity, underlying surface and slope gradient on soil infiltration under simulated rainfall experiments. Catena 104: 93-102.

Hubble TCT, Airey DW, Sealey HK, De Carli EV, Clarke SL (2013) A little cohesion goes a long way: Estimating appropriate values of additional root cohesion for evaluating slope stability in the Eastern Australian highlands. Ecological Engineering 61P: 621–632.

Hungr O (1995) A model for the run out analysis of rapid flow slides, debris flows and avalanches. Canadian Geotechnical Journal 32(4): 610–623.

Hungr O (2001) User's Manual: CLARA-W, Slope Stability. Oldrich Hungr Geotechnical Research, Inc., West Vancouver, British Columbia, Canada.

Hungr O, Evans SG (2004) Entrainment of debris in rock avalanches; an analysis of a long run-out mechanism. Geol Soc Amer Bull 116(9/10):1240–1252.

Iida T (1999) A stochastic hydro-geomorphological model for shallow landsliding due to rainstorm. Catena 34: 293-313.

Inne JL (1983) Debris flows. Prog Phys Geog 7: 469–501.

Iverson RM (2000) Landslide triggering by rain infiltration. Water Resources Research 36(7):1897-1910.

Iverson RM (2004) Comment on 'Piezometric response in shallow bedrock at CB1: implications for 'runoff generation and landsliding', by David R. Montgomery,William E. Dietrich, and John T. Heffner.Water Resources Research 40: W03801. DOI: 10.1029/2003WR002077.

Iverson RM, Reid ME, LaHusen RG (1997) Debris-flow mobilization from landslides. Annual Review of Earth and Planetary Sciences 25: 85–138.

Jagielko L, Martin YE, Sjogren DB (2012) Scaling and multivariate analysis of medium to large landslide events: Haida Gwaii, British Columbia. Natural Hazards 60: 321–344.

Jakob M, Weatherly H (2003) A hydroclimatic threshold for landslide initiation on the North Shore Mountains of Vancouver, British Columbia. Geomorphology 54: 137–156.

Jamaludin S, Huat B, Omar H (2006) Evaluation of slope assessment systems for predicting landslides of cut slopes in granitic and meta-sediment formations. American Journal of Environmental Sciences 2: 135–141.

Jia N, Mitani Y, Xie M, Djamaluddin I (2012) Shallow landslide hazard assessment using a three-dimensional deterministic model in a mountainous area. Computers and Geotechnics, 45, pp. 1–10.

JMA (2005) Rainfall Data of Japan as observed by the AMeDAS at 1300 points in Japan, Published by Japan Meteorological Society in 4 Compact Disc.

Johnson KA, Sitar N (1990) Hydrologic conditions leading to debris-flow initiations. Canadian Geotechnical Journal 27: 789–801.

Jorge LAB (2009) Soil erosion fragility assessment using an impact model and geographic information system. Sci. Agric. (Piracicaba, Braz.), September/October v.66 (5), pp. 658-666.

Kassim A, Gofar N, Lee LM, Rahardjo H (2012) Modeling of suction distributions in an unsaturated heterogeneous residual soil slope. Engineering Geology 131-132: 70-82.

Kasim F, Fredlund DG, Gan JK M (1998) Effect of Steady State Rainfall on Long Term Matric Suction Conditions in Slopes. Proceedings, 2nd Int. Conf. on Unsaturated Soils. Beijing, China pp. 78–83.

Kim SK, Hong W P, Kim YM (1991) Prediction of rainfall-triggered landslides in Korea, in: Proceedings of the 6th International Symposium on Landslides, edited by: Bell, D. H., Christchurch, New Zealand, Balkema, Rotterdam, pp. 989–994.

Kim SK, Hong WP, Kim YM (1992) Prediction of rainfall-triggered landslides in Korea. In Proc. 6th Int. Symp. (Bell, D.H., ed.) Christchurch, New Zealand, 989–994.

Krahn J (2003) The 2001 R.M. Hardy Lecture: The limits of limit equilibrium analyses. Canadian Geotechnical Journal 40: 643–660.

Krahn J (2004a) Seepage modeling with SEEP/W, An engineering Methodology, 1st edition, Geo-Slope International Ltd., Calgary, Alberta, Canada.

Krahn J (2004b) Stability modeling with SLOPE/W, An engineering Methodology, 1st edition, Geo-Slope International Ltd., Calgary, Alberta, Canada.

Lanni C (2012) Hydrological controls on the triggering of shallow landslides: from local to landscape scale. PhD thesis pp. 80.

Lanni C, Borga M, Rigon R, Tarolli P (2012) Modelling catchment-scale shallow landslide occurrence by means of a subsurface flow path connectivity index. Hydrology and Earth System Sciences 9: 4101-4134.

Larsen MC, Simon A (1993) A rainfall intensity–duration threshold for landslides in a humid-tropical environment, Puerto Rico. Geografiska Annaler 75: 13–23.

Lee CT, Huang CC, Lee JF, Pan KL, Kin ML, Dong JJ (2008) Statistical approach to earthquake induced landslide susceptibility. Engineering Geology 100: 43–58.

Lee LM, Gofar N, Rahardjo H (2009) A simple model for preliminary evaluation of rainfall-induced slope instability. Engineering Geology 108: 272–285.

Lee ML, Ng KY, Huang YF, Li WC (2014) Rainfall-induced landslides in Hulu Kelang area, Malaysia Natural Hazards 70: 353–375.

Leong EC, Rahardjo H (2012) Two and three-dimensional slope stability reanalyses of Bukit Batok slope. Computers and Geotechnics 42: 81–88.

Loague K, Heppner CS, Abrams RH, VanderKwaak JE, Carr AE, Ebel BA (2005) Further testing of the Integrated Hydrology Model (InHM): event-based simulations for a small

rangeland catchment located near Chickasha, Oklahoma. Hydrological Processes 19: 1373–1398.

Lu N, Godt J (2008) Infinite slope stability under steady unsaturated seepage conditions. Water Resources Research, Vol 44, W11404, doi:10.1029/2008WR006976.

Luk SH, Cai Q, Wang GP (1993) Effects of surface crusting and slope gradient on soil and water losses in the hilly loess region, North China. Catena Suppl. 24: 29-45.

Matshushi Y (2006) Triggering Mechanisms and Rainfall Thresholds of Shallow Landslides on Soil-mantled Hillslopes with Permeable and Impermeable Bedrocks. Ph.D. thesis. University of Tsukuba.

Matsushi Y, Matsukura Y (2007) Rainfall thresholds for shallow landsliding derived from pressure-head monitoring: cases with permeable and impermeable bedrocks in Boso Peninsula, Japan. Earth Surface Processes and Landform 32(9): 1308–1322.

May CL (2002) Debris flows through different forest age classes in the central Oregon Coast Range. Journal of American Water Resources Association 38: 1–17.

McNamara JP, Chandler D, Seyfried M, Achet S (2005) Soil moisture states, lateral flow, and streamflow generation in a semi-arid, snowmelt-driven catchment. Hydrological Processes 19(20): 4023-4038.

Meisina C, Scarabelli S (2007) A comparative analysis of terrain stability models for predicting shallow landslides in colluvial soils. Geomorphology 87: 207–223.

Milledge DG, Griffiths DV, Lane SN, Warburton J (2012) Limits on the validity of infinite length assumptions for modelling shallow landslides. Earth Surface Processes and Landforms 37: 1158-1166.

Miller DJ, Burnett KM (2007) Effects of forest cover, topography, and sampling extent on the measured density of shallow, translational landslides. Water Resources Research 43: 1–23.

Moon V, Blackstock H (2004) A Methodology for Assessing Landslide Hazard Using Deterministic Stability Models. Natural Hazards 32: 111–134.

Moon V, Bradshaw J, de Lange W (2009) Geomorphic development of White Island Volcano based on slope stability modeling. Engineering Geology 104: 16–30.

Montgomery DR, Dietrich WE (1994) A physically based model for the topographic control on shallow landsliding. Water Resources Research 30: 1153–1171.

Montgomery DR, Dietrich WE, Heffner JT (2002) Piezometric response in shallow bedrock at CB1: implications for runoff generation and landsliding. Water Resources Research 38(12): 1274. DOI: 10.1029/2002WR001429.

Montgomery DR, Dietrich WE, Torres R, Anderson SP, Heffner JT, Loague K (1997) Hydrologic response of a steep, unchanneled valley to natural and applied rainfall. Water Resources Research 33: 91–109.

Morgenstern NR, Price VE (1965) The analysis of the stability of general slip surfaces. Geotechnique 15(1): 79–93.

Muntohar AS, Liao HJ (2010) Rainfall infiltration: infinite slope model for landslides triggering by rainstorm. Natural Hazards 54: 967–984.

Nagarajan R, Roy A, Vinod Kumar R, Mukherjee A, Khire MV (2000) Landslide hazard susceptibility mapping based on terrain and climatic factors for tropical monsoon regions. Bulletin of Engineering Geology and the Environment 58 (4): 275– 287.

Neupane RR (2005) Experimental analysis of strength of local grass and shrub roots used for slope stabilization, Thesis No. 059/MSW/418, Master of Science in Water Resources Engineering, Institute of Engineering, Tribhuvan University, Nepal, pp. 85.

Ng CWW, Shi Q (1998) A Numerical Investigation of the Stability of Unsaturated Soil Slopes Subjected to Transient Seepage. Computer and Geotechnics 22(1): 1–28.

Norbiato D, Borga M, Esposti SD, Gaume E, Anquetin S (2008) Flash flood warning based on rainfall thresholds and soil moisture conditions: An assessment for gauged and ungauged basins. Journal of Hydrology 362: 274– 290.

Pachauri AK, Gupta PV, Chander R (1998) Landslide zoning in a part of the Garhwal Himalayas. Environmental Geology 36(3–4): 325–334. Accessed 25 Oct 2010.

Pack RT, Tarboton DG, Goodwin CN (1998) SINMAP—A stability index approach to terrain stability hazard mapping. http://www.neng.usu.edu/cee/faculty/dtarb/sinmap.pdf.

Pavel M, Fannin RJ, Nelson JD (2008) Replication of a terrain stability mapping using an Artificial Neural Network. Geomorphology 97: 356–373.

Persson H, Alén C, Lind BB (2007) Development of a pore pressure prediction model. In: McInnes R, Jakeways J, Fairbanks J, Mathie E (eds) Landslides and climate change. Challenges and solutions. Proceedings of the international conference on landslides and climate change. Taylor & Francis, Isle of Wight, UK, pp 21–24.

Poesen J (1984) The influence of slope angle on infiltration rate and Hortonian overland flow volume. Z. Geomorphology. N.F., Suppl.Bd. 49: 117-131.

Pradhan B, Oh H-J, Buchroithner M (2010a) Weights-of-evidence model applied to landslide susceptibility mapping in a tropical hilly area. Geomatics, Natural Hazards and Risk 1(3): 199-223.

Preuth T, Glade T, Demoulin A (2010) Stability analysis of a human-influenced landslide in eastern Belgium. Geomorphology 120: 38–47.

Puigdefábregas J, Barrio G, Boer M, Gutierrez L, Solé A (1998) Differential responses and channel elements to rainfall events in a semi-arid area. Geomorphology 23: 337-351.

Rahardjo H, Lee TT, Leong EC, Rezaur RB (2005) Response of a residual soil slope to rainfall. Canadian Geotechnical Journal 42(2): 340-351.

Rahardjo H, Li XW, Toll DG, Leong EC (2001) The Effect of Antecedent Rainfall on Slope Stability. Geotechnical and Geological Engineering 19: 371-399.

Rahardjo H, Ong TH, Rezaur RB, Leong EC (2007) Factors controlling instability of homogeneous soil slopes under rainfall. Journal of Geotechnical and Geoenvironmental Engineering ASCE 133(12): 1532-1543.

Rahardjo H, Satyanaga A, Leong E-C (2013) Effects of flux boundary conditions on porewater pressure distribution in slope. Engineering Geology 165: 133–142.

Rahimi A, Rahardjo H, Leong EC (2010) Effect of hydraulic properties of soil on rainfall-induced slope failure. Engineering Geology 114: 135–143.

Regmi AD, Devkota KC, Yoshida K, Pradhan B, Pourghasemi HR, Kumamoto T, Akgun A (2013) Application of frequency ratio, statistical index, and weights-of-evidence models and their comparison in landslide susceptibility mapping in Central Nepal Himalaya. Arabian Journal of Geosciences, DOI 10.1007/s12517-012-0807-z.

Reid ME (1994) A pore-pressure diffusion model for estimating landslide-inducing rainfall. The Journal of Geology 102(6): 709–717. Accessed 20 Oct 2010.

Reid ME, Iverson RM (1992) Gravity-driven groundwater flow and slope failure potential: 2. Effects of slope morphology, material properties, and hydraulic heterogeneity. Water Resources Research 28: 939–950.

Reid ME, Nielsen HP, Dreiss SJ (1988) Hydrologic factors triggering a shallow landslide failure, Bulletin of the Association of Engineering Geologists 25(3): 349-361.

Reneau SL, Dietrich WE, Donahue DJ, Jull AJT, Rubin M (1990) Late Quaternary history of colluvial deposition and erosion in hollows, central California Coast Ranges. The Geological Society of America. Bulletin 102: 969–982.

Rigon R, Bertoldi G, Over TM (2006) GEOtop: A distributed hydrological model with coupled water and energy budgets. Journal of Hydrometerology. 7(3): 371-388.

Ross SM (2004) Introduction to probability and statistics for engineers and scientists, 3rd ed. Delhi, India: Academic Press (an imprint of Elsevier), Elsevier Delhi.

Rosso R, Rulli MC, Vannucchi G (2006) A physically based model for the hydrologic control on shallow landsliding. Water Resources Research, Vol 42, W06410, doi: 10.1029/2005WR004369.

Saha AK, Gupta RP, Arora MK (2002) GIS-based landslide hazard zonation in the Bhagirathi (Ganga) valley, Himalayas. International Journal of Remote Sensing 23: 357–369.

Salciarini D, Godt JW, Savage WZ, Baum RL, Conversini P (2008) Modeling landslide recurrence in Seattle, Washington, USA. Engineering Geology 102: 227–237.

Santacana N, Baeza B, Corominas J, De Paz A, Marturia J (2003) A GIS-based multivariate statistical analysis for shallow landslide susceptibility mapping in La Pobla de Lillet Area (Eastern Pyrenees, Spain). Natural Hazards 30(3): 281– 295.

Sassa K (1986) The mechanism of debris flows and the forest effect on their prevention. Proc. of 18th IUFRO World Congress 1(1): 227–238.

Schnellmann R, Busslinger M, Schneider HR, Rahardjo H (2010) Effect of rising water table in an unsaturated slope. Engineering Geology 114: 71–83.

Segoni S, Rossi G, Catan F (2012) Improving basin scale shallow landslide modelling using reliable soil thickness maps. Natural Hazards 61: 85–101.

Shuguo Z, Weidong S, Wenbin X (2013) Study on Regularity of Stress Change for Quarry Wall Rock in Mining of Glacis Thin Orebody with the Long Wall Mining Based on FLAC. Proceedings of the 2012 International Conference on Communication, Electronics and Automation Engineering Advances in Intelligent Systems and Computing Volume 181:605-611.

Sidle RC (1987) A dynamic model of slope stability in zero-order basins. Erosion and Sedimentation in the Pacific Rim (Proceedings of the Corvallis Symposium, August) IAHS Publ . no. 165.

Sidle RC (1991) A conceptual model of changes in root cohesion in response to vegetation management. Journal of Environmental Quality 20 (1): 43–52.

Sidle RC, Dhakal AS (2002) Potential effects of environmental change on landslide hazards in forest environments, in: Environmental Change and Geomorphic Hazards in Forests, edited by: Sidle RC, IUFRO Research Series, No 9, pp123–165, CAB International Press, Oxen, UK.

Sidle RC, Ochiai H (2006) Landslides: Processes, Prediction, and Land Use. Water Resources Monographs Series 18. AGU: Washington, DC.

Sidle RC, Pearce AJ, O'Loughlin CL (Eds.) (1985) Hillslope Stability and Land Use. Water Resources Monograph Series, vol. 11, 140 pp., AGU, Washington, D. C.

Simoni S, Zanotti F, Bertoldi G, Rigon R (2008) Modelling the probability of occurrence of shallow landslides and channelized debris flows using GEOtop-FS. Hydrological Processes 22(4): 532-545.

Singh R, Umrao RK, Singh TN (2013) Stability evaluation of road-cut slopes in the Lesser Himalaya of Uttarakhand, India: conventional and numerical approaches. Bulletin of Engineering Geology and the Environment. DOI 10.1007/s10064-013-0532-1.

Skempton AW, Bjerrum L, Casagrande A, Peck RB (1960) From Theory to Practice in Soil Mechanics, chapter Significance of Terzaghi's concept of effective stress. Jhon Wiley and Sons.

Soeters R, Van Westen CJ (1996) Slope instability recognition, analysis, and zonation. In: Turner AK, Schuster RL (eds) Landslides: investigation and mitigation (Special Report). National Research Council, Transportation and Research Board Special Report 247, Washington, DC, USA, pp 129–177.

Sorbino G, Sica C, Cascini L (2010) Susceptibility analysis of shallow landslides source areas using physically based models. Natural Hazards 53: 313-332.

Swanson FJ, Fredriksen RL (1982) Sediment routing and budgets: Implications for judging impacts of forestry practices. In: Sediment Budgets and Routing in Forested Drainage Basins (USDA For. Serv. Gen. Tech. Rep. PNW-141), 129–137, Portland, Oregon, USA.

Talebi A, Uijlenhoet R, Troch PA (2007) Soil moisture storage and hillslope stability. Natural Hazards and Earth System Sciences 7: 523-534.

Talebi A, Uijlenhoet R, Troch PA (2008a) Application of a probabilistic model of rainfall-induced shallow landslides to complex hollows. Natural Hazards and Earth System Sciences 8: 733–744.

Talebi A, Uijlenhoet R, Troch PA (2008b) A low-dimensional physically based model of hydrologic control of shallow landsliding on complex hillslopes. Earth Surface Processes and Landforms 33: 1964-1976.

Tarolli P, Borga M, Chang KT, Chiang SH (2011) Modeling shallow landsliding susceptibility by incorporating heavy rainfall statistical properties. Geomorphology 133: 199–211.

Taylor DW (1948) Fundamentals of soil mechanics. Wiley, New York.

Terlien MTJ (1996) Modelling spatial and temporal variations in rainfall-triggered landslides. Thesis (PhD). ITC Publ. Nr. 32, Enschede, The Netherlands.

Terlien MTJ (1998) The determination of statistical and deterministic hydrological landslide-triggering thresholds. Environmental Geology 35(2): 124–130.

Terlien MTJ, Van Westen CJ, Van Asch TW (1995) Deterministic modelling in GIS-based landslide hazard assessment. In: Carrara, A. and Guzzetti, F. (Eds) Advances in Natural and Technological Hazard Research, Kluwer Academic Publishers, p. 51-77.

Terzaghi K (1943) Theoretical Soil Mechanics. New York: John Wiley & Sons, Inc. Bishop AW (1955) The use of slip circles in stability analysis of slopes. Geotechnique 5(1): 7-17.

Terzaghi K, Peck RB (1967) Soil Mechanics in Engineering Practice, Wiley Intersci., Hoboken, N. J.

Thiebes B (2011) Landslide analysis and early warning—local and regional case study in the Swabian Alb, Germany. Dissertation. University of Vienna, Austria.

Thorne CR, Zevenbergen LW, Burt TP, Butcher DP (1987) Terrain analysis for quantitative description of zero-order basins. Erosion and Sedimentation in the Pacific Rim (Proceedings of the Corvallis Symposium, August). IAHS Publ.no 165.

Tofani V, Dapporto S, Vannocci P, Casagli N (2005) Analysis of infiltration, seepage processes and slope instability mechanisms during the November 2000 storm event in Tuscany. Advances in Geosciences 2: 301-304.

Tofani V, Dapporto S, Vannocci P, Casagli N (2006) Infiltration, seepage and slope instability mechanisms during the 20-21 November 2000 rainstorm in Tuscany, central Italy. Natural Hazards and Earth System Sciences 6: 1025-1033.

Trandafir AC, Sidle RC, Gomi T, Kamai T (2008) Monitored and simulated variations in matric suction during rainfall in a residual soil slope. Environmental Geology 55: 951–961.

Travis Q, Houston S, Marinho, F, Schmeeckle M (2010) Unsaturated Infinite Slope Stability Considering Surface Flux Conditions. Journal of Geotechnical and Geoenvironmental Engineering 136(7): 963-974.

Troch PA, Paniconi C, Van Loon EE (2003) Hillslope-storage Boussinesq model for subsurface flow and variable source areas along complex hillslopes: 1. Formulation and characteristic response. Water Resources Research 39(11): 1316. DOI: 10.1029/2002WR001728.

Troch PA, Van Loon EE, Hillberts A (2002) Analytical solutions to a hillslope-storage kinematic wave equation for subsurface flow. Advance Water Resources 25: 637-649.

Tsai T-L (2010) Influences of soil water characteristic curve on rainfall-induced shallow landslides. Environmental Earth Sciences DOI 10.1007/s12665-010-0868-9.

Tsaparas I, Rahardjo H, Toll DG, Leong EC (2002) Controlling parameters for rainfall-induced landslides. Computers and Geotechnics 29: 1–27.

Tsukamoto Y (1973) Study on the growth of stream channel (I) —Relationship between stream channel growth and landslides occurring during heavy storm. Journal of Japan Society of Erosion Control Engineering 87:4–13 (in Japanese).

Tsukamoto Y, Minematsu H (1987) Hydrogeomorphological characteristics of a zero-order basin. Erosion and Sedimentation in the Pacific Rim (Proceedings of the Corvallis Symposium, August). IAHS Publ. no. 165.

Uchida T, Asano Y, Ohte N, Mizuyama T (2003) Analysis of flow path dynamics in a steep unchannelled hollow in the Tanakami Mountains of Japan. Hydrological Processes 17:417–430.

Van Asch TWJ, Buma J, Van Beek LPH (1999) A view on some hydrological triggering systems in landslides. Geomorphology 30: 25–32.

Van Den Eeckhaut M, Vanwalleghem T, Poesen J, Govers G, Verstraeten G, Vanderkerckhove L (2006) Prediction of landslide susceptibility using rare events logistic regression: a case-study in Flemish Ardennes (Belgium). Geomorphology 76: 392–410.

van der Spek JE, Bogaard TA, Bakker M (2013) Characterization of groundwater dynamics in landslides in varved clays. Hydrology and Earth System Sciences 17: 2171–2183.

Van Genuchten MT (1980) A closed-form equation for predicting the hydraulic conductivity of unsaturated soils. Soil Science Society of America Journal 48: 703–708.

van Schalkwyk A, Thomas MA (1991) Slope failures associated with the floods of September 1987 and February 1988 in Natal and Kwa-Zulu, Republic of South Africa. Proceedings of the 3rd international conference on tropical and residual soils, Lesotho, Rotterdam: Balkema, pp. 57-64.

van Westen CJ, Terlien TJ (1996) An approach towards deterministic landslide hazard analysis in GIS. A case study from Manizales (Colombia). Earth Surface Processes and Landforms 21: 853-868.

VanderKwaak JE (1999) Numerical simulation of flow and chemical transport in integrated surface-subsurface hydrologic systems. PhD dissertation, University of Waterloo, Ontario, Canada.

Varnes DJ (1978) Slope movement types and process. In Schuster RL, Krizek, RJ (Eds.), Landslides Analysis and Control. Special Report 176, Transportation Research Board, National Academy of Sciences, Washington D.C, pp.11–33.

Vaughan PR (1985) Pore pressures due to infiltration into partly saturated slopes. Proc. 1st International Conference on Geomechanics in Tropical Lateritic and Saprolitic soils. Brazil 2: 61-71.

von Ruette J, Lehmann P, Or D (2013) Rainfall-triggered shallow landslides at catchment scale: Threshold mechanics-based modeling for abruptness and localization. Water Resources Research 49: 1-20 doi:10.1002/wrcr.20418.

Villalobos SA, Oro´stegui PL, Villalobos FA (2013) Re-assessing a soil nailing design in heavily weathered granite after a strong earthquake. Bulletin of Engineering Geology and the Environment 72:203–212.

Wang G, Suemine A, Furuya G, Kaiboris M, And Sassa K (2005) Landslides in Kisawa area, Tokushima Prefecture during the 2004 Typhoon Namtheun, Annuals of Disas. Prey. Res. Inst., Kyoto Univ., No. 48 B, 1-8 p.

Ward TJ, Li RM, Simons DB (1981) Use of a mathematical model for estimating potential landslide sites in steep forested basin. In: T.R.H. Davis and A.J. Pearce, eds. Erosion and sediment transport in pacific Rim steep lands. International Hydrological Science Publ No. 132. Walliingford, Oxon: Institute of Hydrology, Wallingford, pp. 21-41.

Weiler M, McDonnell JJ, Tromp-van Meerveld I, Uchida T (2005) Subsurface stormflow, Encyclopedia of Hydrological Sciences, Wiley and Sons.

West L, Chiang S, Norton L (1992) The morphology of surface crusts. In: Sumner, M., Stewart, B. (Eds.), Soil Crusting: Chemical and Physical Processes. Lewis Publishing, Ann Arbor, Mich., pp. 73-92.

Weyman DR (1973) Measurements of the downslope flow of water in a soil. Journal of Hydrology 20(3):267-288. DOI: 10.1016/0022-1694(73)90065-6.

Wieczorek GF, Glade T (2005) Climatic factors influencing occurrence of debris flows. In: Jakob M, Hungr O (eds) Debris-flow hazards and related phenomena. Springer, Berlin, pp 325–362.

Wilson RC, Wieczorek GF (1995) Rainfall thresholds for the initiation of debris flows at La Honda, California: Environmental and Engineering Geoscience 1(1): 11-27.

Wu S, Jin Y, Zhang Y, Shi J, Dong C, Lei W, Shi L, Tan C, Hu D (2004) Investigations and assessment of the landslide hazards of Fengdu county in the reservoir region of the Three Gorges project on the Yangtze River. Environmental Geology 45 (4): 560–566.

Wu W, Sidle RC (1995) A distributed slope stability model for steep forested basins. Water Resources Research 31: 2097–2110.

Xiao-jun G, Peng CUI, Yong LI (2013) Debris Flow Warning Threshold Based on Antecedent Rainfall : a Case Study in Jiangjia Ravine, Yunnan, China. Journal of Mountain Science 10(2): 305–314.

Xueliang Wang X, Zhang L, Wang S, Lari S (2013) Regional landslide susceptibility zoning with considering the aggregation of landslide points and the weights of factors. Landslides DOI 10.1007/s10346-013-0392-6.

Yesilnacar E, Topal T (2005) Landslide susceptibility mapping: a comparison of logistic regression and neural networks methods in a medium scale study, Hendek region (Turkey). Engineering Geology 79(3–4): 251–266.

Zhan TLT, Ng CWW (2004) Analytical analysis of rainfall infiltration mechanism in unsaturated soils. International Journal of Geomechanics ASCE 4 (4): 273-284.

Zhan TLT, Jia GW, Chen YM, Fredlund DG, Li H (2013) An analytical solution for rainfall infiltration into an unsaturated infinite slope and its application to slope stability analysis. International Journal for Numerical and Analytical Methods in Geomechanics 37:1737-1760.

Zhang YJ, Chen LZ, Xing AG, Qi Chao (2013) Dynamic Simulation and Analysis of High-Speed and Long Run-Out Landslide Triggered by the Wenchuan Earthquake, China. Earthquake-Induced Landslides pp. 567-574.

Zolfaghari A, Heath AC (2008) A GIS application for assessing landslide hazard over a large area. Computers and Geotechnics 35(2): 278–85.

Zweig MH, Campbell G (1993) Receiver-operating characteristics (ROC) plots. Clinical Chemistry 39: 561–577.

Appendix A

Appendix A

Soil thickness at each location in Figure 5.2 after field measurement

1	Coordinate (y, x)	Soil depth (cm)
2	350367.96, 3760255.60	38.5
3	350330.65, 3760234.00	83.0
4	350330.13, 3760200.73	54.0
5	350320.54, 3760178.72	77.0
6	350301.53, 3760145.72	191.0
7	350359.07, 3760277.92	74.0
8	350358.90, 3760266.83	142.0
9	350339.89, 3760233.86	34.0
10	350366.91, 3760189.06	115.0
11	350350.53, 3760322.42	37.0
12	350303.99, 3760300.98	73.0
13	350462.46, 3760387.21	45.0
14	350442.75, 3760309.88	74.0
15	350405.27, 3760277.19	50.0
16	350423.22, 3760243.63	25.0
17	350451.64, 3760287.55	80.0
18	350469.59, 3760253.99	104.0
19	350459.30, 3760187.60	67.0
20	350431.94, 3760210.22	25.0
21	350413.46, 3760210.51	52.0
22	350443.28, 3760343.14	72.5
23	350440.30, 3760154.62	0.0
24	350458.43, 3760132.15	106.5
25	350514.21, 3760153.46	110.0
26	350531.99, 3760108.81	60.0
27	350513.34, 3760098.01	0.0
28	350532.17, 3760119.90	0.0
29	350458.08, 3760109.97	0.0
30	350515.09, 3760208.90	90.0
31	350487.72, 3760231.52	118.0
32	350543.33, 3760241.73	96.0
33	350506.90, 3760275.59	42.0
34	350479.36, 3760287.11	105.0
35	350369.54, 3760355.40	55.0
36	350341.82, 3760355.84	78.0
37	350305.22, 3760378.60	74.0
38	350248.90, 3760324.03	70.0
39	350606.43, 3760140.91	174.0
40	350489.65, 3760353.50	44.0
41	350489.47, 3760342.41	95.0
42	350369.01, 3760322.13	23.0
43	350599.29, 3760274.13	78.0
44	350412.23, 3760132.88	23.0

45	350596.49, 3760096.70	46.0
46	350578.36, 3760119.17	82.0
47	350559.88, 3760119.46	93.0
48	350457.55, 3760076.71	56.0
49	350447.79, 3760043.58	30.0
50	350429.83, 3760077.14	102.0
51	350373.87, 3760044.75	69.0
52	350318.44, 3760045.63	20.0
53	350300.66, 3760090.28	10.0
54	350507.95, 3760342.12	0.0
55	350617.07, 3760229.48	0.0
56	350356.09, 3760089.40	0.0
57	350388.42, 3760380.61	162.5
58	350369.74, 3760368.70	121.5
59	350361.05, 3760403.23	92.0
60	350360.56, 3760372.18	55.0
61	350331.28, 3760273.92	38.0
62	350322.62, 3760310.66	102.0
63	350313.54, 3760320.79	52.0
64	350286.10, 3760338.97	92.0
65	350266.75, 3760283.81	54.0
66	350257.37, 3760275.09	81.0
67	350230.09, 3760303.25	59.0
68	350183.07, 3760251.86	17.0
69	350210.49, 3760232.57	84.0
70	350246.95, 3760200.93	145.0
71	350283.58, 3760179.28	91.0
72	350329.14, 3760138.63	134.0

Appendix B

Appendix-B

Derivation of two-dimensional Richard's equation for rainwater infiltration through saturated/unsaturated soil

The rainfall-induced slope failure in saturated and unsaturated soils is directly connected with characteristics of water flow, porewater pressure distribution and shearing strength of soils (Rahardjo et al. 2005). Rainfall infiltration through both saturated and unsaturated soils follow the same physical laws such as law of motion, law of mass conservation, and Darcy's law. Also the partial differential flow equation is formulated in similar way for both cases. Still the water flow through saturated and unsaturated soils differs in two ways.
(1) Matric suction does not exist in saturated soils. The water retaining capacity of soil is more or less constant for a soil. But in unsaturated soils, matric suction alters the capacity to retain water [Soil water characteristics curve (SWCC) defines the relationship of matric suction with water content].
(2) The hydraulic conductivity of saturated soils is always constant. However, it increases with increase in the loss of matric suction in unsaturated soils.

The governing second order differential equation for flow through saturated and unsaturated soils is given by following relation.

$$\frac{\partial}{\partial x}\left(k_x \frac{\partial H}{\partial x}\right)+\frac{\partial}{\partial y}\left(k_y \frac{\partial H}{\partial y}\right)+q=\frac{\partial \theta_w}{\partial t} \qquad \text{(B-i)}$$

In which, H is the total hydraulic head and is defined by

$$H=z+\frac{u_w}{\rho_w.g} \qquad \text{(B-ii)}$$

Where z is the elevation measured from mean sea level; u_w is the pore water pressure, x and y are the Cartesian coordinates in x and y direction respectively, k_x is hydraulic conductivity in x direction, k_y is hydraulic conductivity in y direction, ρ_w is density of water; q is applied boundary flux, θ_w is volumetric water content; g is acceleration due to gravity, u_a is the pore air pressure and it is taken as atmospheric pressure, and t is time. Equation (B-i) is a water-mass balance equation. This equation implies that the rate of change of flows of water in the x-direction and y-direction plus an external applied flux is equal to the rate of change of the volumetric water content with respect to time.

The amount of water stored in soil depends on matric suction and moisture retention characteristics of the soil structure. Figure (B-a) is water retention characteristics curves or soil water characteristics curves (SWCC). The slope of the curves represents the water retention characteristics of the soils. The water retention characteristics denote the rate of change of water absorbed or released by the soil due to change in the porewater pressure with rainfall infiltraion. The total amount of water stored or the volumetric water content is equal to the soil porosity at 100 % saturation. A complete SWCC is shown in Figure (B-b). The drying curve denotes a continuous release of water from soil with increase in matric suction. The wetting curve denotes a continuous absorption of water by soil particles with decrease in matric suction. In SWCC, three distinct stages in soil desaturation can be recognized namely I, II, and III [Figure (B-a)]. Typical SWCC function used in seepage modeling in this research is shown in Figure (B-c)

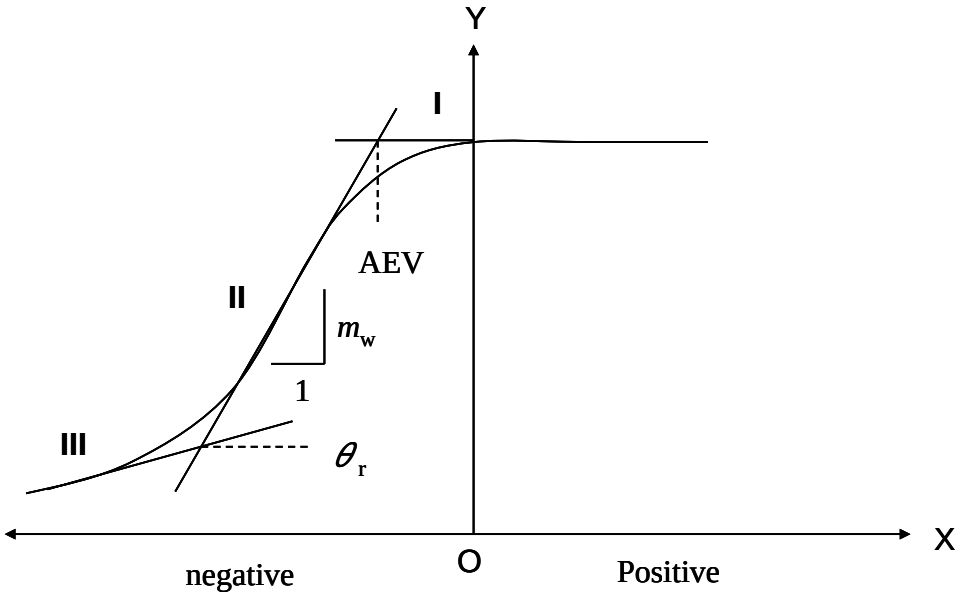

Figure (B-a) Soil water characteristics curve (GeoStudio 2005) (In this figure, AEV is air-entry value and Θ_r is residual water content.

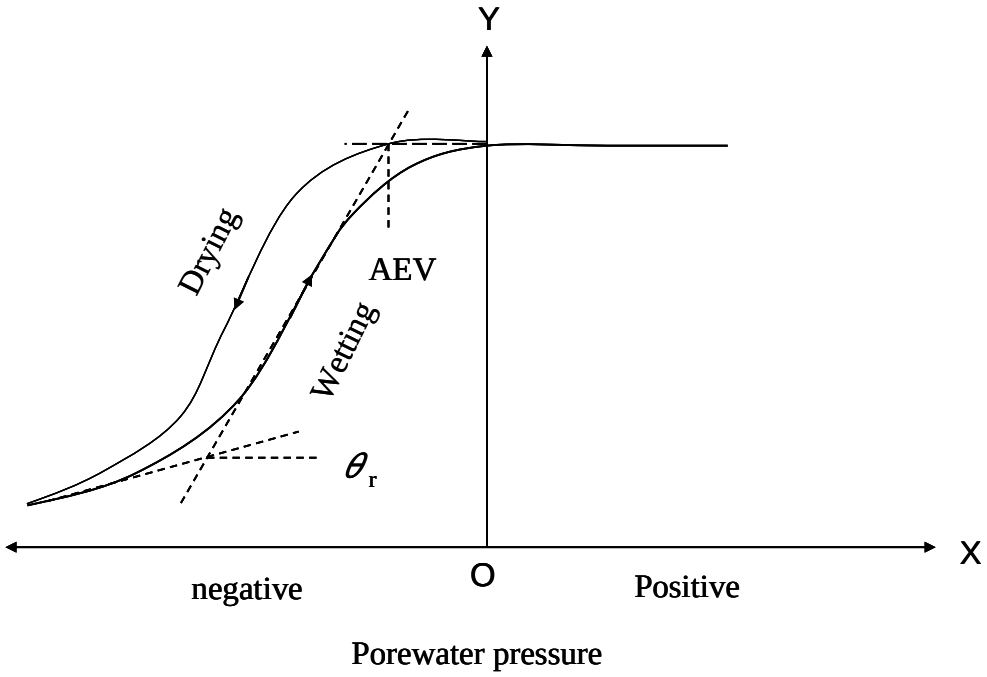

Figure (B-b) A complete soil water characteristics curve

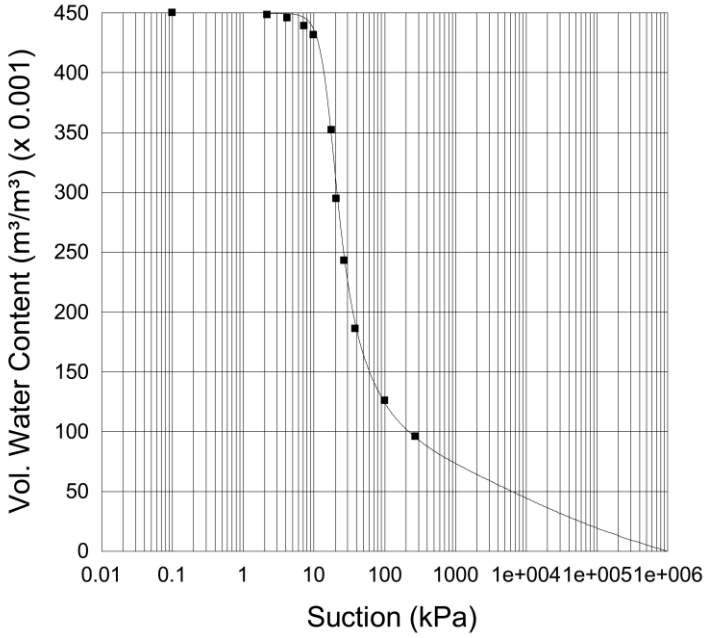

Figure (B-c) SWCC function used in seepage modeling.

The hydraulic conductivity of unsaturated soils depends on the water content of the soil. It is because of the heterogeneous distribution of water content in the soil mass (Ng and Shi 1998, Rahardjo et al. 2005). It is assumed that water flows along a web of interconnected but continuous conduits and with absorption of water in soil, the size and number of conduits increases thereby increasing the ability to conduct water through the soil. Therefore, hydraulic conductivity is a function of matric suction (or porewater pressure). Figure (B-d) shows variation of hydraulic conductivity with matric suction for

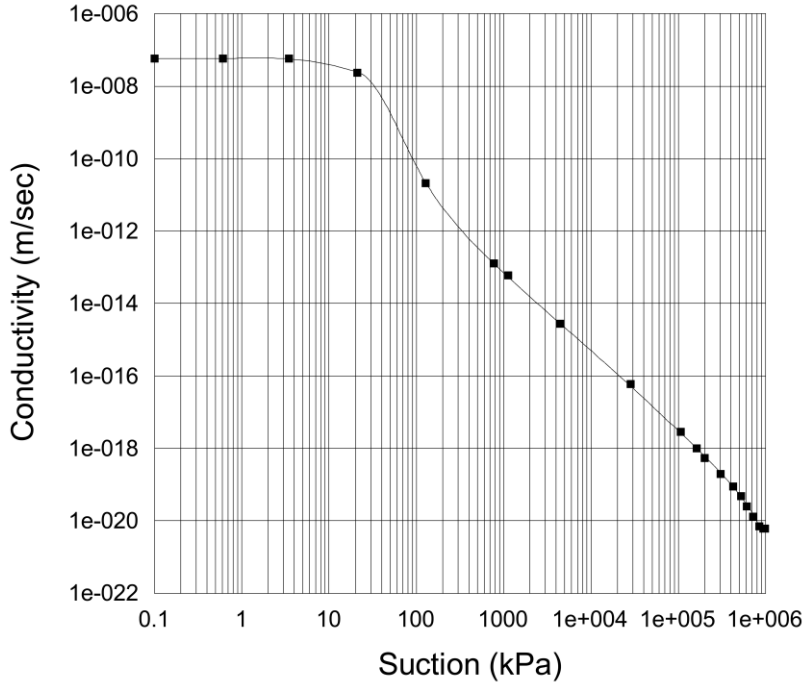

Figure (B-d) Hydraulic conductivity vs matric suction graph (log-log plot) for silty sand (GeoStudio2005) used in this research

silty sand. From this figure, it can be understood that the hydraulic conductivity decreases with increase in matric suction for unsaturated soils.

For an isotropic unsaturated soil element, the constitutive equation for the water phase is given below.

$$\partial\theta_w = m^2{}_a(\sigma - u_a) + m^2{}_w\partial(u_a - u_w) \qquad \text{(B-iii)}$$

Where m_a and m_w are the coefficient of volume change with respect to air and water respectively. During transient phenomenon, m_a and m_w are constant for a certain time step. m_a is nearly equal to m_v at saturated conditions. Also the total stress (σ) in the soil mass and the pore air pressure (u_a) remain constant during transient phenomenon. This implies that (σ - u_a) does not affect change in volumetric water content. If no hysteresis between drying and wetting paths in the SWCC [(Figure (B-a)], the change in porewater pressure can be linked to change in volumetric water content by following relationship.

$$\partial\theta_w = m^2{}_w\partial u_w \qquad \text{(B-iv)}$$

Rearranging equation (B-ii) we get,

$$\partial u_w = \gamma_w\partial(H - z) \qquad \text{(B-v)}$$

Substituting equation (B-v) into equation (B-iv) we get,

$$\partial\theta_w = m^2{}_w\gamma_w\partial(H - z) \qquad \text{(B-vi)}$$

Substituting equation (B-vi) into equation (B-i), we get

$$\frac{\partial}{\partial x}\left(k_x\frac{\partial H}{\partial x}\right) + \frac{\partial}{\partial y}\left(k_y\frac{\partial H}{\partial y}\right) + q = \frac{m^2{}_w\gamma_w\partial(H - z)}{\partial t} \qquad \text{(B-vii)}$$

Elevation (z) is constant and the derivative of z with respect to t becomes zero. The equation (B-vii) with remaining terms is given below.

$$\frac{\partial}{\partial x}\left(k_x\frac{\partial H}{\partial x}\right) + \frac{\partial}{\partial y}\left(k_y\frac{\partial H}{\partial y}\right) + q = \frac{m^2{}_w\gamma_w\partial H}{\partial t} \qquad \text{(B-vii)}$$

Equation (B-vii) is Richard's equation in two dimensions for saturated and unsaturated flow through soil.

Notes:
(1) For homogenous and isotropic condition, $k_x = k_y = k$ and Q = 0.
(2) Under steady state condition, the flux entering the elemental volume is equal to the flux leaving the elemental volume all the time. Then, the right hand side of equation (A-vii) disappears and equation (B-vii) reduces to following form.

$$\frac{\partial}{\partial x}\left(k_x\frac{\partial H}{\partial x}\right) + \frac{\partial}{\partial y}\left(k_y\frac{\partial H}{\partial y}\right) + q = 0$$

Appendix C

Appendix C

Hourly typhoon rainfall data of 19-20 October 2004 in Niihama of Shikoku Island, Japan

Date	Rainfall hour	Rainfall amount (mm)	One day rainfall accumulation (mm)
19/10/2004	0:00	0.0	78.0
	1:00	1.0	
	2:00	2.0	
	3:00	3.0	
	4:00	5.0	
	5:00	4.0	
	6:00	3.0	
	7:00	4.0	
	8:00	0.0	
	9:00	1.0	
	10:00	6.0	
	11:00	8.0	
	12:00	7.0	
	13:00	0.0	
	14:00	1.0	
	15:00	3.0	
	16:00	6.0	
	17:00	9.0	
	18:00	7.0	
	19:00	1.0	
	20:00	1.0	
	21:00	1.0	
	22:00	0.0	
	23:00	5.0	
20/10/2004	0:00	1.0	398.0
	1:00	4.0	
	2:00	0.0	
	3:00	2.0	
	4:00	5.0	
	5:00	13.0	
	6:00	13.0	
	7:00	11.0	
	8:00	19.0	
	9:00	20.0	
	10:00	27.0	
	11:00	45.0	
	12:00	43.0	
	13:00	35.0	
	14:00	22.0	
	15:00	26.0	
	16:00	15.0	
	17:00	14.0	
	18:00	2.0	
	19:00	1.0	
	20:00	0.0	
	21:00	2.0	
	22:00	0.0	
	23:00	0.0	

Appendix D

Appendix D

(i) Hydrological and geo-mechanical properties of soil at each location in Figure 5.2 (Appendix A) after field and laboratory investigation

1	Coordinate (y, x)	Soil type	C (kN/m^2)	ϕ (°)	γ_t (kN/m^3)	γ_{sat} (kN/m^3)	n	k (m/s)	C_r (kN/m^2)	Soil depth (cm)
2	350367.96, 3760255.60	SM fine	7.49	27.42	13.25	17.39	0.493	0.000025	0.00	38.5
3	350330.65, 3760234.00	SM coarse	6.46	36.86	12.41	17.08	0.532	0.000016	0.00	83.0
4	350330.13, 3760200.73	SM medium	4.09	34.55	12.23	16.84	0.559	0.000017	0.00	54.0
5	350320.54, 3760178.72	SM medium	5.11	40.39	12.99	16.93	0.560	0.000014	0.00	77.0
6	350301.53, 3760145.72	SM fine	4.92	31.04	10.71	15.57	0.642	0.000006	1.90	191.0
7	350359.07, 3760277.92	SM fine	1.57	30.37	13.72	16.99	0.547	0.000004	0.00	74.0
8	350358.90, 3760266.83	SM fine	5.22	31.00	15.00	17.62	0.504	0.000008	0.00	142.0
9	350339.89, 3760233.86	SM medium	4.52	39.58	12.02	15.74	0.622	0.000037	0.00	34.0
10	350366.91, 3760189.06	SM fine	3.30	28.12	11.11	15.66	0.628	0.000012	0.00	115.0
11	350350.53, 3760322.42	SM medium	2.19	31.83	10.74	15.33	0.653	0.000027	1.90	37.0
12	350303.99, 3760300.98	SM medium	0.90	42.59	12.20	16.33	0.559	0.000032	1.90	73.0
13	350462.46, 3760387.21	SM medium	3.30	39.85	13.49	16.52	0.550	0.000031	4.80	45.0
14	350442.75, 3760309.88	SM fine	8.21	37.87	11.95	16.23	0.576	0.000004	1.90	74.0
15	350405.27, 3760277.19	SM medium	7.96	37.28	11.33	15.67	0.602	0.00005	0.00	50.0
16	350423.22, 3760243.63	SM medium	7.73	39.20	15.04	17.59	0.484	0.000026	1.90	25.0
17	350451.64, 3760287.55	SM medium	13.37	32.78	12.74	16.86	0.548	0.000018	0.00	80.0
18	350469.59, 3760253.99	SM medium	14.11	27.89	13.88	16.71	0.551	0.000019	0.00	104.0
19	350459.30, 3760187.60	SM medium	8.32	30.54	13.42	16.35	0.548	0.000029	3.40	67.0
20	350431.94, 3760210.22	SM coarse	6.29	39.56	10.58	15.40	0.619	0.000039	1.90	25.0
21	350413.46, 3760210.51	SM medium	7.73	34.64	12.81	16.45	0.549	0.000019	1.90	52.0
22	350443.28, 3760343.14	SM coarse	0.31	40.41	11.82	15.54	0.623	0.000046	1.90	72.5
23	350440.30, 3760154.62	Bed rock	0.00	0.00	0.00	0.00	0.000	0	0.00	0.0
24	350458.43, 3760132.15	SM coarse	1.27	37.69	11.59	15.43	0.644	0.000021	4.30	106.5
25	350514.21, 3760153.46	SM medium	12.50	30.33	15.06	17.25	0.520	0.000015	1.90	110.0
26	350531.99, 3760108.81	SM fine	10.76	23.91	13.01	16.10	0.592	0.000046	4.30	60.0
27	350513.34, 3760098.01	Bed rock	0.00	0.00	0.00	0.00	0.000	0	0.00	0.0
28	350532.17, 3760119.90	Bed rock	0.00	0.00	0.00	0.00	0.000	0	0.00	0.0
29	350458.08, 3760109.97	Bed rock	0.00	0.00	0.00	0.00	0.000	0	0.00	0.0
30	350515.09, 3760208.90	SM medium	4.49	33.14	16.74	18.90	0.397	0.000016	1.90	90.0
31	350487.72, 3760231.52	SM coarse	4.49	24.70	14.44	16.83	0.540	0.000026	1.90	118.0
32	350543.33, 3760241.73	GM medium	10.85	21.92	15.07	17.19	0.521	0.000027	0.00	96.0
33	350506.90, 3760275.59	SM medium	0.85	33.06	13.71	16.79	0.548	0.000026	3.40	42.0
34	350479.36, 3760287.11	SM fine	2.37	31.45	12.98	16.37	0.591	0.000008	1.90	105.0
35	350369.54, 3760355.40	SM fine	0.85	31.04	14.57	16.52	0.565	0.000008	1.90	55.0
36	350341.82, 3760355.84	SM fine	4.87	29.10	14.25	17.30	0.525	0.000013	1.90	78.0
37	350305.22, 3760378.60	SM fine	1.48	28.50	11.94	15.88	0.610	0.000011	1.90	74.0
38	350248.90, 3760324.03	SM fine	5.33	27.20	13.55	17.06	0.540	0.000013	1.90	70.0
39	350606.43, 3760140.91	M	9.48	24.33	13.94	16.29	0.576	0.000016	4.80	174.0
40	350489.65, 3760353.50	SM medium	5.11	40.39	12.99	16.93	0.560	0.000014	4.30	44.0
41	350489.47, 3760342.41	SM coarse	1.27	37.69	11.59	15.43	0.644	0.000021	4.80	95.0
42	350369.01, 3760322.13	SM medium	0.90	42.59	12.20	16.33	0.559	0.000032	0.00	23.0
43	350599.29, 3760274.13	SM medium	7.73	34.64	12.81	16.45	0.549	0.000019	1.90	78.0
44	350412.23, 3760132.88	SM medium	0.90	42.59	12.20	16.33	0.559	0.000032	3.40	23.0
45	350596.49, 3760096.70	SM coarse	1.27	37.69	11.59	15.43	0.644	0.000021	4.30	46.0
46	350578.36, 3760119.17	SM coarse	1.27	35.69	11.59	15.43	0.644	0.000021	3.40	82.0
47	350559.88, 3760119.46	SM coarse	1.27	37.69	11.59	15.43	0.644	0.000021	4.30	93.0
48	350457.55, 3760076.71	SM coarse	1.27	37.69	11.59	15.43	0.644	0.000021	4.80	56.0
49	350447.79, 3760043.58	SM coarse	1.27	37.69	11.59	15.43	0.644	0.000021	4.80	30.0
50	350429.83, 3760077.14	SM coarse	1.27	37.69	11.59	15.43	0.644	0.000021	4.80	102.0
51	350373.87, 3760044.75	SM coarse	1.27	37.69	11.59	15.43	0.644	0.000021	4.80	69.0
52	350318.44, 3760045.63	SM medium	7.73	34.64	12.81	16.45	0.549	0.000019	4.30	20.0
53	350300.66, 3760090.28	SM coarse	0.31	40.41	11.82	15.54	0.623	0.000046	4.80	10.0
54	350507.95, 3760342.12	SM coarse	0.31	40.41	11.82	15.54	0.623	0.000046	4.30	0.0
55	350617.07, 3760229.48	SM coarse	0.31	40.41	11.82	15.54	0.623	0.000046	4.30	0.0
56	350356.09, 3760089.40	SM coarse	0.31	40.41	11.82	15.54	0.623	0.000046	4.80	0.0
57	350388.42, 3760380.61	None	None	None	None	None	None	None	None	162.5
58	350369.74, 3760368.70	None	None	None	None	None	None	None	None	121.5
59	350361.05, 3760403.23	None	None	None	None	None	None	None	None	92.0
60	350360.56, 3760372.18	None	None	None	None	None	None	None	None	55.0
61	350331.28, 3760273.92	None	None	None	None	None	None	None	None	38.0
62	350322.62, 3760310.66	None	None	None	None	None	None	None	None	102.0
63	350313.54, 3760320.79	None	None	None	None	None	None	None	None	52.0
64	350286.10, 3760338.97	None	None	None	None	None	None	None	None	92.0
65	350266.75, 3760283.81	None	None	None	None	None	None	None	None	54.0
66	350257.37, 3760275.09	None	None	None	None	None	None	None	None	81.0
67	350230.09, 3760303.25	None	None	None	None	None	None	None	None	59.0
68	350183.07, 3760251.86	None	None	None	None	None	None	None	None	17.0
69	350210.49, 3760232.57	None	None	None	None	None	None	None	None	84.0
70	350246.95, 3760200.93	None	None	None	None	None	None	None	None	145.0
71	350283.58, 3760179.28	None	None	None	None	None	None	None	None	91.0
72	350329.14, 3760138.63	None	None	None	None	None	None	None	None	134.0

(ii) Hydrological and geo-mechanical properties of soil at various points shown in Figure 5.2 (Appendix A) were fitted into 25 × 25 sq. m blocks based on nearness of block to the points for deterministic slope failure hazard modeling

Block No	C (kN/m^2)	ϕ (°)	γ_t (kN/m^3)	γ_{sat} (kN/m^3)	n	k (m/s)	C_r	Soil type
1	7.73	34.64	12.81	16.45	0.549	0.0000190	4.31	SM medium
2	7.73	34.64	12.81	16.45	0.549	0.0000190	4.31	SM medium
3	7.73	34.64	12.81	16.45	0.549	0.0000190	4.31	SM medium
4	1.27	37.69	11.59	15.43	0.644	0.0000210	4.79	SM coarse
5	1.27	37.69	11.59	15.43	0.644	0.0000210	4.79	SM coarse
6	1.27	37.69	11.59	15.43	0.644	0.0000210	4.79	SM coarse
7	1.27	37.69	11.59	15.43	0.644	0.0000210	4.79	SM coarse
8	0.31	34.64	12.20	16.63	0.548	0.0000320	1.92	SM coarse
9	0.31	34.64	12.20	16.63	0.548	0.0000320	1.92	SM coarse
10	7.73	34.64	12.81	16.45	0.549	0.0000320	4.31	SM coarse
11	7.73	34.64	12.81	16.45	0.549	0.0000190	4.31	SM medium
12	7.73	34.64	12.81	16.45	0.549	0.0000210	4.31	SM medium
13	1.27	37.69	11.59	15.43	0.644	0.0000210	4.79	SM coarse
14	1.27	37.69	11.59	15.43	0.644	0.0000210	4.79	SM coarse
15	1.27	37.69	11.59	15.43	0.644	0.0000210	4.79	SM coarse
16	1.27	37.69	11.59	15.43	0.644	0.0000210	4.79	SM coarse
17	1.27	37.69	11.59	15.43	0.644	0.0000210	4.79	SM coarse
18	1.27	37.69	11.59	15.43	0.644	0.0000210	4.79	SM coarse
19	1.27	37.69	11.59	15.43	0.644	0.0000210	4.79	SM coarse
20	6.46	27.42	10.71	15.70	0.628	0.0000060	1.92	SM fine
21	3.30	27.42	10.71	15.70	0.628	0.0000060	1.92	SM fine
22	3.30	40.39	12.20	15.70	0.628	0.0000320	1.92	SM coarse
23	3.30	40.39	12.20	16.63	0.548	0.0000320	1.92	SM coarse
24	3.30	34.64	12.20	16.63	0.548	0.0000460	1.92	SM coarse
25	0.31	40.41	11.82	15.54	0.623	0.0000460	4.79	SM coarse
26	0.31	40.41	11.82	15.54	0.623	0.0000460	4.79	SM coarse
27	0.31	40.41	11.82	15.54	0.623	0.0000460	4.79	SM coarse
28	0.31	40.41	11.82	15.54	0.623	0.0000460	4.79	SM coarse
29	0.31	37.69	11.82	15.54	0.623	0.0000460	4.79	SM coarse
30	1.27	37.69	11.59	15.43	0.644	0.0000210	4.79	SM coarse
31	1.27	37.69	11.59	15.43	0.644	0.0000210	4.79	SM coarse
32	1.27	37.69	11.59	15.43	0.644	0.0000210	4.79	SM coarse
33	1.27	37.69	11.59	15.43	0.644	0.0000210	4.79	SM coarse
34	10.76	23.91	13.01	16.10	0.592	0.0000210	4.31	SM coarse
35	10.76	23.91	13.01	16.10	0.592	0.0000210	4.31	SM coarse
36	1.27	37.69	11.59	15.43	0.592	0.0000210	4.31	SM coarse
37	1.27	37.69	11.59	15.43	0.644	0.0000210	4.31	SM coarse
38	1.27	37.69	11.59	15.43	0.644	0.0000210	4.31	SM coarse
39	6.46	27.42	10.71	15.57	0.628	0.0000060	1.92	SM fine
40	6.46	27.42	10.71	16.93	0.628	0.0000060	1.92	SM fine
41	6.46	36.86	15.07	16.83	0.619	0.0000270	3.35	SM coarse
42	3.30	40.39	15.07	16.83	0.819	0.0000270	3.35	SM coarse
43	0.31	40.41	15.07	16.83	0.619	0.0000270	3.35	SM coarse
44	0.31	40.41	11.82	15.54	0.623	0.0000460	4.79	SM coarse
45	0.31	40.41	11.82	15.54	0.623	0.0000460	4.79	SM coarse
46	0.31	40.41	11.82	15.54	0.623	0.0000460	4.79	SM coarse
47	0.31	40.41	11.82	15.54	0.623	0.0000460	4.79	SM coarse
48	0.31	40.41	11.82	15.54	0.623	0.0000460	4.79	SM coarse

49	0.90	37.69	11.59	16.33	0.644	0.0000460	4.79	SM coarse
50	1.27	37.69	11.59	15.43	0.644	0.0000210	4.79	SM fine
52	10.76	37.69	11.59	15.43	0.644	0.0000210	4.79	SM fine
54	10.76	23.91	11.59	16.40	0.592	0.0000460	4.31	SM fine
55	1.27	37.69	13.01	15.43	0.644	0.0000210	4.31	SM coarse
56	1.27	37.69	11.59	15.43	0.644	0.0000210	4.31	SM coarse
57	1.27	37.69	11.59	15.43	0.644	0.0000210	4.31	SM coarse
58	1.27	37.69	11.59	15.43	0.644	0.0000210	4.31	SM coarse
59	1.57	42.59	12.23	16.93	0.644	0.0000080	1.92	SM fine
60	1.57	42.59	10.58	16.93	0.559	0.0000080	1.92	SM fine
61	6.41	36.86	10.58	16.93	0.559	0.0000080	1.92	SM fine
62	6.41	32.86	15.07	16.83	0.619	0.0000270	3.35	SM coarse
63	4.92	40.39	15.07	16.83	0.619	0.0000270	3.35	SM coarse
64	4.92	31.01	10.79	15.57	0.842	0.0000060	1.92	SM fine
65	4.92	31.01	10.79	15.57	0.642	0.0000060	1.92	SM fine
66	0.31	24.70	13.42	18.90	0.530	0.0000160	1.92	SM medium
67	0.31	24.70	13.42	18.90	0.530	0.0000160	1.92	SM medium
68	0.90	42.59	13.42	16.33	0.559	0.0000320	3.35	SM medium
69	0.90	42.59	12.20	16.33	0.559	0.0000320	3.35	SM medium
70	1.27	37.69	11.59	15.43	0.644	0.0000210	4.31	SM coarse
71	1.27	37.69	11.59	15.43	0.644	0.0000210	4.31	SM coarse
72	1.27	30.33	11.59	17.25	0.644	0.0000210	1.92	SM coarse
74	10.76	30.33	11.59	16.10	0.592	0.0000210	4.31	SM fine
75	1.27	37.69	11.59	15.43	0.644	0.0000210	4.31	SM coarse
76	9.48	24.33	11.59	16.29	0.644	0.0000210	4.79	M
77	9.48	24.33	13.94	16.29	0.576	0.0000160	4.79	M
78	9.48	24.33	13.94	16.29	0.576	0.0000160	4.79	M
79	1.57	42.59	12.23	15.74	0.532	0.0000080	1.92	SM medium
80	1.57	42.59	12.23	15.74	0.559	0.0000080	1.92	SM medium
81	1.57	42.59	12.23	15.74	0.559	0.0000080	1.92	SM medium
82	5.22	27.42	15.04	16.86	0.484	0.0000260	1.92	SM fine
83	5.22	27.42	15.04	16.93	0.484	0.0000260	1.92	SM medium
84	4.92	31.04	10.71	15.57	0.642	0.0000060	1.92	SM fine
85	4.92	31.04	10.71	15.57	0.642	0.0000060	1.92	SM fine
86	6.20	28.12	13.42	18.90	0.530	0.0000160	1.92	SM medium
87	6.20	24.70	13.42	18.90	0.530	0.0000160	1.92	SM medium
88	6.20	24.70	13.42	18.90	0.548	0.0000160	3.35	SM medium
89	0.90	30.54	12.20	16.30	0.548	0.0000320	3.35	SM medium
91	1.27	37.69	11.59	15.43	0.644	0.0000210	4.31	SM coarse
92	12.50	30.33	15.06	17.25	0.520	0.0000150	1.92	SM coarse
93	12.50	30.33	15.06	17.25	0.520	0.0000150	1.92	SM medium
94	12.50	30.33	15.06	17.25	0.520	0.0000150	1.92	SM medium
95	12.50	34.64	14.11	15.43	0.644	0.0000210	4.31	SM medium
96	9.48	24.33	13.94	16.29	0.576	0.0000160	4.79	M
97	9.48	24.33	13.94	16.29	0.576	0.0000160	4.79	M
98	9.48	24.33	13.94	16.29	0.576	0.0000160	4.79	SM coarse
99	1.57	31.83	13.72	17.08	0.532	0.0000250	4.31	SM medium
100	1.57	31.83	13.72	17.08	0.532	0.0000250	4.31	SM medium
101	1.57	39.85	15.00	17.39	0.493	0.0000180	1.92	SM medium
102	5.22	39.85	15.00	16.86	0.484	0.0000260	3.35	SM medium
103	5.22	27.42	15.04	16.86	0.484	0.0000260	3.35	SM medium
104	5.11	27.42	15.04	16.86	0.560	0.0000260	1.92	SM medium
105	5.11	40.39	12.99	16.93	0.628	0.0000140	0.00	SM medium
106	5.11	40.39	12.99	15.66	0.560	0.0000120	1.92	SM medium
107	3.30	28.12	11.11	15.66	0.628	0.0000120	0.00	SM fine
108	3.30	28.12	11.11	18.90	0.530	0.0000120	1.92	SM fine
109	6.20	30.54	12.81	16.45	0.549	0.0000160	1.92	SM fine
110	8.32	30.54	13.42	16.35	0.548	0.0000290	1.92	SM medium

111	8.32	30.54	13.42	16.35	0.548	0.0000290	3.35	SM medium
112	4.49	30.54	13.42	16.35	0.548	0.0000290	3.35	SM medium
113	12.50	30.33	15.06	18.90	0.520	0.0000150	1.92	SM medium
114	12.50	34.64	11.82	15.43	0.644	0.0000210	4.31	SM medium
115	0.31	34.64	11.82	15.43	0.644	0.0000210	4.31	SM medium
116	0.31	34.64	11.82	15.43	0.644	0.0000210	4.31	SM medium
117	0.31	34.74	11.82	15.43	0.576	0.0000160	1.92	SM medium
118	0.90	31.83	13.72	15.54	0.644	0.0000040	4.79	SM medium
119	1.57	42.59	13.72	17.39	0.644	0.0000250	4.79	SM medium
120	1.57	39.85	15.00	17.39	0.493	0.0000180	1.92	SM fine
121	1.57	39.85	15.00	17.39	0.493	0.0000180	1.92	SM fine
122	5.22	27.42	15.00	16.86	0.484	0.0000190	1.92	SM medium
123	5.22	34.55	12.23	16.86	0.484	0.0000170	4.31	SM medium
124	4.09	34.55	12.23	16.84	0.559	0.0000170	0.00	SM medium
125	4.09	28.12	12.23	16.84	0.559	0.0000170	1.92	SM medium
126	3.30	28.12	11.11	15.66	0.628	0.0000120	1.92	SM medium
127	3.30	34.64	12.81	16.45	0.549	0.0000190	1.92	SM medium
128	7.73	34.64	10.58	16.45	0.549	0.0000190	1.92	SM coarse
129	6.29	39.56	12.81	15.40	0.619	0.0000390	1.92	SM coarse
130	8.32	35.44	13.42	16.35	0.548	0.0000290	3.35	SM medium
131	4.49	33.14	16.74	18.90	0.397	0.0000160	3.35	SM medium
132	4.49	33.14	16.74	18.90	0.397	0.0000160	1.92	SM medium
133	4.49	33.14	11.82	15.43	0.397	0.0000210	4.31	SM medium
134	0.31	34.64	11.82	15.43	0.644	0.0000210	4.31	SM medium
135	0.31	34.64	11.82	15.40	0.644	0.0000460	4.31	SM coarse
136	0.31	40.41	11.82	15.40	0.644	0.0000460	1.92	SM coarse
137	0.90	42.59	12.20	15.54	0.644	0.0000040	4.79	SM coarse
138	0.90	42.59	12.20	15.54	0.644	0.0000040	4.79	SM coarse
139	4.87	39.85	15.00	17.39	0.644	0.0000180	1.92	SM coarse
140	4.87	39.85	10.74	17.39	0.653	0.0000040	1.92	SM coarse
141	0.90	42.59	11.95	15.74	0.576	0.0000040	4.79	SM coarse
142	0.90	42.59	11.95	16.23	0.559	0.0000040	4.79	SM coarse
143	6.46	36.86	12.41	17.08	0.532	0.0000160	0.00	SM coarse
144	4.52	39.58	12.02	15.74	0.622	0.0000370	0.00	SM medium
145	4.52	39.58	12.02	15.74	0.622	0.0000370	3.35	SM medium
146	7.73	34.64	15.04	17.69	0.484	0.0000190	3.35	SM medium
147	7.73	39.20	15.04	17.59	0.484	0.0000260	1.92	SM medium
148	7.73	34.64	15.04	15.40	0.619	0.0000390	1.92	SM medium
149	4.49	24.70	14.44	16.83	0.540	0.0000260	1.92	SM coarse
150	4.49	24.70	15.07	16.83	0.540	0.0000260	1.92	SM coarse
151	4.49	22.15	15.07	16.83	0.521	0.0000160	1.92	SM coarse
152	10.85	21.92	15.07	17.19	0.521	0.0000270	0.00	GM medium
153	10.85	21.92	15.07	17.19	0.521	0.0000270	4.31	GM medium
154	0.31	40.41	11.82	15.54	0.623	0.0000460	4.31	SM coarse
155	0.31	40.41	11.82	15.54	0.623	0.0000460	4.31	SM coarse
156	0.90	42.59	12.20	15.54	0.644	0.0000040	4.79	SM coarse
157	4.84	42.59	12.20	15.54	0.559	0.0000040	4.79	SM coarse
158	4.84	31.04	10.74	15.33	0.559	0.0000320	1.92	SM coarse
159	4.84	31.04	10.74	15.33	0.559	0.0000320	1.92	SM coarse
160	4.84	42.59	10.74	16.25	0.540	0.0000320	4.79	SM coarse
161	0.90	42.59	11.95	16.23	0.576	0.0000040	4.79	SM coarse
162	6.46	40.03	11.95	16.23	0.576	0.0000040	4.79	SM coarse
163	5.22	36.86	13.25	7.62	0.504	0.0000080	1.92	SM medium
164	7.49	27.42	13.25	17.32	0.493	0.0000250	0.00	SM fine
165	7.49	27.42	11.23	17.39	0.493	0.0000250	1.92	SM fine
166	7.73	39.20	15.04	17.59	0.484	0.0000260	1.92	SM medium
167	7.73	36.25	15.04	17.59	0.484	0.0000260	1.92	SM medium
168	14.11	27.89	13.88	16.71	0.551	0.0000190	0.00	SM medium
169	14.11	27.89	14.44	16.71	0.540	0.0000190	3.35	SM medium
170	10.85	21.92	14.44	16.79	0.540	0.0000190	3.35	SM medium
171	10.85	21.92	15.07	17.19	0.521	0.0000270	1.92	SM medium
172	10.85	34.64	12.81	16.45	0.549	0.0000190	1.92	SM medium

173	7.73	34.64	12.81	16.45	0.549	0.0000190	1.92	SM medium
174	4.87	29.55	13.42	15.33	0.550	0.0000060	1.92	SM coarse
175	4.87	29.55	14.25	15.33	0.559	0.0000060	1.92	SM coarse
176	4.87	31.04	14.25	15.33	0.559	0.0000320	1.92	SM medium
177	4.87	31.04	10.74	15.33	0.559	0.0000320	1.92	SM medium
178	0.90	42.59	10.74	16.33	0.559	0.0000320	4.79	SM fine
179	0.90	42.59	12.20	16.33	0.576	0.0000320	4.79	SM fine
180	1.57	30.37	13.72	16.99	0.547	0.0000040	1.92	SM fine
181	1.57	30.37	11.33	16.99	0.084	0.0000080	0.00	SM fine
182	7.96	37.28	11.33	15.67	0.602	0.0000500	0.00	SM medium
183	7.96	37.28	11.33	15.67	0.602	0.0000180	1.92	SM medium
184	13.37	32.78	12.74	16.86	0.548	0.0000080	0.00	SM medium
185	2.37	31.45	12.98	16.37	0.591	0.0000080	1.92	SM medium
186	0.85	33.06	13.71	16.37	0.591	0.0000260	3.35	SM fine
187	0.85	33.06	13.71	16.79	0.548	0.0000260	3.35	SM medium
188	0.85	34.64	13.71	16.79	0.549	0.0000190	1.92	SM medium
189	7.73	34.64	12.81	16.45	0.549	0.0000190	1.92	SM medium
190	7.73	34.64	12.81	16.45	0.549	0.0000080	1.92	SM medium
191	4.87	29.10	14.25	15.74	0.550	0.0000080	1.92	SM medium
192	4.87	29.10	14.25	15.74	0.550	0.0000080	1.92	SM medium
193	4.87	29.10	14.25	15.74	0.550	0.0000320	1.92	SM medium
194	0.90	42.59	12.20	16.33	0.559	0.0000320	1.92	SM medium
195	0.90	42.59	12.20	16.33	0.652	0.0000040	1.92	SM medium
196	2.19	31.83	10.74	15.33	0.559	0.0000040	1.92	SM medium
197	0.90	42.59	12.20	16.33	0.559	0.0000140	4.31	SM medium
198	0.31	39.85	12.20	16.93	0.484	0.0000040	4.31	SM medium
199	0.31	37.87	11.95	16.23	0.484	0.0000040	4.31	SM fine
200	8.21	37.87	11.95	16.23	0.576	0.0000040	1.92	SM fine
201	8.21	32.78	12.98	16.23	0.548	0.0000040	1.92	SM fine
202	13.37	31.45	11.95	16.37	0.591	0.0000080	1.92	SM medium
203	13.37	33.06	13.71	16.79	0.548	0.0000080	1.92	SM medium
204	13.37	34.64	13.71	15.54	0.548	0.0000260	1.92	SM medium
205	4.87	27.20	13.55	17.06	0.540	0.0000130	1.92	SM fine
206	5.33	27.20	13.55	17.06	0.540	0.0000130	1.92	SM fine
207	5.33	29.20	13.55	17.06	0.540	0.0000130	1.92	SM fine
208	5.33	28.50	14.25	15.74	0.550	0.0000320	1.92	SM medium
209	0.90	42.59	12.20	17.30	0.559	0.0000320	1.92	SM medium
210	2.19	31.83	10.74	15.33	0.653	0.0000270	1.92	SM medium
211	0.90	42.59	12.20	16.33	0.559	0.0000320	0.00	SM medium
212	0.90	42.59	12.20	16.93	0.559	0.0000140	4.31	SM medium
213	0.31	39.85	12.20	16.93	0.484	0.0000140	4.31	SM medium
214	0.31	40.41	11.82	15.54	0.623	0.0000460	1.92	SM coarse
215	1.27	37.69	11.59	15.43	0.644	0.0000210	1.92	SM coarse
216	1.27	37.69	11.59	15.43	0.644	0.0000210	4.79	SM coarse
217	0.31	40.41	11.82	15.54	0.623	0.0000460	4.31	SM coarse
218	0.31	40.41	11.82	15.54	0.623	0.0000460	4.31	SM coarse
219	5.33	27.20	13.55	17.06	0.540	0.0000130	1.92	SM fine
220	5.33	27.20	13.55	17.06	0.540	0.0000130	1.92	SM fine
221	1.48	28.50	11.94	15.88	0.610	0.0000130	1.92	SM fine
222	4.87	29.10	11.94	15.88	0.610	0.0000110	1.92	SM fine
223	4.87	31.04	14.25	17.30	0.530	0.0000110	1.92	SM fine
224	0.85	31.04	14.57	16.52	0.565	0.0000130	1.92	SM fine
225	0.31	31.04	14.57	16.52	0.565	0.0000080	1.92	SM fine
226	0.31	40.41	11.82	15.54	0.623	0.0000460	1.92	SM coarse
227	0.31	40.41	11.82	15.54	0.623	0.0000460	1.92	SM coarse
228	5.11	40.41	12.99	15.54	0.560	0.0000140	4.31	SM coarse
229	5.11	40.39	12.99	16.93	0.644	0.0000210	4.31	SM medium
230	0.31	40.41	11.82	15.54	0.623	0.0000460	4.31	SM coarse
231	1.48	28.50	11.94	15.88	0.610	0.0000110	1.92	SM fine
232	1.48	28.50	11.94	15.88	0.610	0.0000110	1.92	SM fine
233	4.87	29.10	14.25	16.52	0.530	0.0000130	1.92	SM fine
234	4.87	27.20	14.57	16.52	0.365	0.0000080	1.92	SM medium

235	0.85	31.04	14.57	15.54	0.540	0.0000130	1.92	SM medium
236	3.30	32.04	13.55	15.54	0.525	0.0000080	4.79	SM coarse
237	3.30	39.85	13.49	16.52	0.550	0.0000310	4.79	SM medium
238	3.30	39.85	13.49	16.52	0.550	0.0000310	4.79	SM medium
239	3.30	39.85	12.99	16.52	0.623	0.0000180	4.31	SM coarse
240	3.30	37.69	11.82	15.54	0.623	0.0000180	4.31	SM coarse
241	1.48	27.20	11.94	15.88	0.565	0.0000090	1.92	SM medium
242	1.48	27.20	11.82	16.52	0.565	0.0000090	1.92	SM medium
243	1.48	27.20	11.82	16.52	0.565	0.0000130	1.92	SM medium
244	0.90	27.20	13.55	15.54	0.525	0.0000130	1.92	SM coarse
245	0.90	28.50	14.25	15.54	0.525	0.0000130	1.92	SM coarse
246	0.90	29.10	14.25	15.54	0.550	0.0000130	1.92	SM medium
247	3.30	29.10	13.49	15.54	0.550	0.0000080	1.92	SM medium
248	3.30	34.50	13.49	15.54	0.623	0.0000310	1.92	SM medium
249	1.42	27.20	11.82	16.52	0.565	0.0000460	1.92	SM medium
250	5.33	27.20	13.55	16.52	0.565	0.0000090	4.79	SM coarse
251	5.33	27.20	13.55	15.54	0.525	0.0000130	4.79	SM coarse
252	0.90	29.10	13.55	15.54	0.525	0.0000130	4.79	SM coarse
253	0.90	29.10	14.25	15.54	0.540	0.0000080	1.92	SM medium
254	0.90	27.20	14.25	15.54	0.540	0.0000080	4.13	SM medium
255	0.90	27.20	14.25	15.54	0.540	0.0000080	1.92	SM medium
256	5.33	28.50	13.49	16.79	0.623	0.0000310	4.79	SM medium
257	5.33	28.50	13.49	16.79	0.623	0.0000310	4.79	SM medium
258	5.33	28.50	13.49	17.08	0.623	0.0000160	1.92	SM coarse
259	0.90	27.20	14.25	15.54	0.540	0.0000080	1.92	SM medium
260	0.90	28.50	14.25	15.54	0.540	0.0000160	1.92	SM medium
261	4.87	28.50	15.07	15.54	0.540	0.0000160	3.35	SM coarse
258	5.33	28.50	13.49	17.08	0.623	0.0000160	1.92	SM coarse
259	0.90	27.20	14.25	15.54	0.540	0.0000080	1.92	SM medium
260	0.90	28.50	14.25	15.54	0.540	0.0000160	1.92	SM medium
261	4.87	28.50	15.07	15.54	0.540	0.0000160	3.35	SM coarse

Appendix E

Appendix-E

Derivation of infinite slope stability model for stability analysis of saturated/unsaturated soil slopes

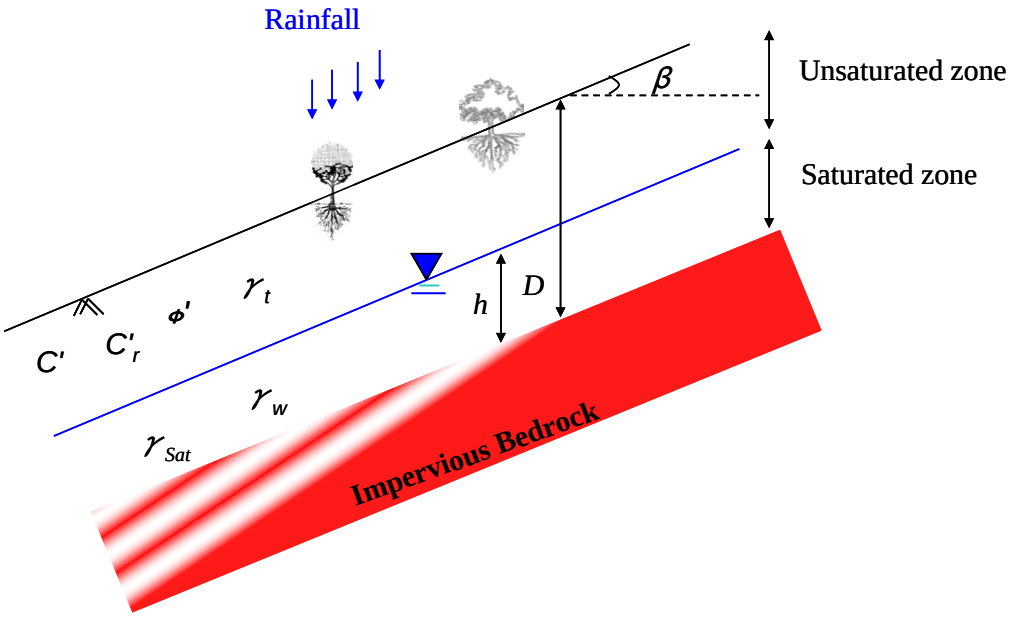

Figure (C-a) Infinite slope stability model

The assumptions of infinite slope stability model (Skepmton and Delory1959, Hammond et al. 1992) are given below.

1. Ground surface and subsurface water run parallel to bedrock.
2. Failure plane is parallel bedrock or translational.
3. Depth of failure is very less compared to the length of slope.
4. Slope is constant throughout the length.
5. End conditions of the slopes are neglected.
6. The slopes can be easily destabilized by widespread areas of positive pore water pressure.

Figure (E-a) the schematic diagram of Infinite slope stability model. In fact, this is a finite slope. But it is made infinite by removing the end conditions and it fulfils all other assumptions of infinite slope stability model which are listed above. The infinite slope stability model is formulated based on law of static friction for a rigid block on an inclined plane and forces are resolved into normal and sliding components. Let us consider a small soil element IJKL in the infinite slope as shown in Figure (E-b). In Figure (E-b), C' is effective soil cohesion, C'_r is effective root strength; β is slope inclination (°); γ_{sat} (kN/m^3) is saturated unit weight of soil; γ_t (kN/m^3) is bulk unit weight of soil; h is vertical saturation depth (m); and D is vertical soil depth (m). When factor of safety is greater than 1, the hillslope is stable and when it is equal to 1, the slope mass is in verge of failure (limit equilibrium state). Let us consider a small soil element IJKL in infinite slope.

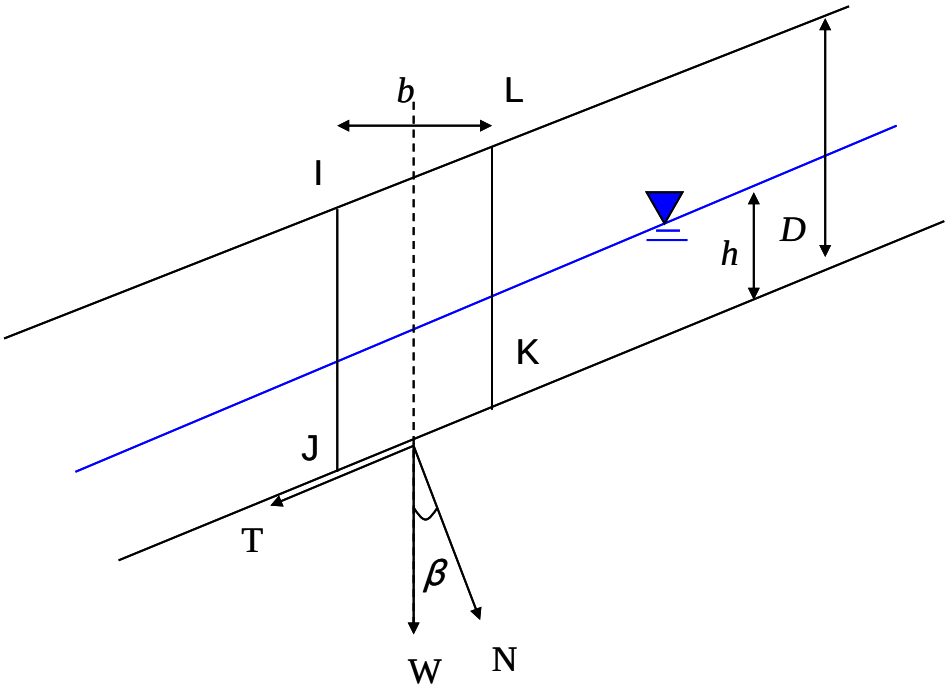

Figure (E-b) Showing considered forces in soil element IJKL

Saturated zone

Suppose A_1 is area of soil element in saturated zone; b is width of soil element; A_{11} is the base area occupied by weight of soil element; W_w is weight of water; W_{Sat} is saturated unit weight; m_w is mass of water; g is acceleration due to gravity; V_w is volume of water; V_{Sat} is saturated volume of soil; N_1 is normal force; T_1 is driving force; σ_{n1} is normal stress; and T_{n1} is shear stress.

Then,

$$A_1 = h.b$$

$$A_{11} = \left(\frac{b}{\cos\beta}.1\right)$$

$$W_{Sat} = m_{Sat}.g = \gamma_{Sat}.V_{Sat} = \gamma_{Sat}.A_1.1 = \gamma_{Sat}.h.b.1 = \gamma_{Sat}.h.b$$

$$N1 = W_{Sat}.\cos\beta = \gamma_{Sat}.h.b\cos\beta$$

$$T1 = W_{Sat}\sin\beta = \gamma_{Sat}.h.b\sin\beta$$

$$\sigma_{n1} = \frac{N_1}{A_{11}} = \frac{\gamma_{Sat}.h.b\cos\beta}{\left(\frac{b}{\cos\beta}.1\right)} = \gamma_{Sat}.h.\cos^2\beta$$

$$T_{n1} = \frac{T_1}{A_{11}} = \frac{\gamma_{Sat}.h.b\sin\beta}{\left(\frac{b}{\cos\beta}.1\right)} = \gamma_{Sat}.h.b\sin\beta\cos\beta$$

$$W_w = m_W.g = \gamma_W.V_W = \gamma_W.A_1.1 = \gamma_W.h.b.1 = \gamma_W.h.b$$

$$u_a = \frac{W_w\cos\beta}{A} = \frac{\gamma_W.h.b\cos\beta}{\left(\frac{b}{\cos\beta}.1\right)} = \gamma_W.h\cos^2\beta$$

Net effective stress in saturated zone is given by

$$= \gamma_{Sat}.h.\cos^2\beta - \gamma_W.h\cos^2\beta = (\gamma_{Sat} - \gamma_W).h\cos^2\beta \quad \text{(E-i)}$$

Net tangential stress in saturated zone is given by

$$= \gamma_{Sat}.h.b\sin\beta\cos\beta \quad \text{(E-ii)}$$

Unsaturated zone

Suppose A_2 is area of soil element in unsaturated zone; A_{11} is the base area occupied by weight of soil element; W_t is bulk unit weight; V_t is bulk volume; N_2 is normal force; T_2 is driving force; σ_{n2} is normal stress; and T_{n2} is shear stress.

The area of soil element in unsaturated zone is given area of parallelogram as below

$$A_2 = (D-h).b$$

The base area on which weight of soil element in unsaturated zone (W_t) acts is given by

$$A_{11} = \left(\frac{b}{Cos\beta}.1\right)$$

$$W_t = m_t.g = \gamma_t.V_t = \gamma_t.A_2.1 = \gamma_t.(D-h).b.1 = \gamma_{Sat}.(D-h).b$$

$$N_2 = W_t Cos\beta = \gamma_t.(D-h).bCos\beta$$

$$T_2 = W_t Sin\beta = \gamma_t.(D-h).bSin\beta$$

$$\sigma_{n2} = \frac{N_2}{A_{11}} = \frac{\gamma_t.(D-h).bCos\beta}{\left(\frac{b}{Cos\beta}.1\right)} = \gamma_t.(D-h).Cos^2\beta$$

$$T_{n2} = \frac{T_2}{A_{11}} = \frac{\gamma_t.(D-h).bSin\beta}{\left(\frac{b}{Cos\beta}.1\right)} = \gamma_t.(D-h).bSin\beta Cos\beta$$

Net effective stress in unsaturated zone is given by

$$= \gamma_t.(D-h).Cos^2\beta - 0 = \gamma_t.(D-h).Cos^2\beta \qquad \text{(E-iii)}$$

Net tangential stress in unsaturated zone is given by

$$= \gamma_t.(D-h).bSin\beta Cos\beta \qquad \text{(E-iv)}$$

From equation (E-i) and (E-iii), net effective stress is given by

$$\bar{\sigma}_n = (\gamma_{Sat} - \gamma_W).hCos^2\beta + \gamma_t.(D-h).Cos^2\beta = Cos^2\beta\left[h(\gamma_{Sat} - \gamma_W) + \gamma_t.(D-h)\right] \qquad \text{(E-v)}$$

Net resisting stress or shear strength is given by Mohr-Coulomb Criteria

$$\tau = C' + \bar{\sigma}Tan\phi' = C' + Cos^2\beta\left[h(\gamma_{Sat} - \gamma_W) + \gamma_t.(D-h)\right]Tan\phi' \qquad \text{(E-vii)}$$

Including root cohesion, net resisting stress or shear strength is given by

$$\tau = C' + C_r' + \bar{\sigma}Tan\phi' = C' + C_r' + Cos^2\beta\left[h(\gamma_{Sat} - \gamma_W) + \gamma_t.(D-h)\right]Tan\phi' \qquad \text{(E-viii)}$$

From equation (E-ii) and (E-iv), total tangential or driving stress is given by

$$T = \gamma_{Sat}.h.bSin\beta Cos\beta + \gamma_t.(D-h).bSin\beta Cos\beta = Sin\beta.Cos\beta\left(h\gamma_{Sat} + \gamma_t(D-h)\right) \qquad \text{(E-ix)}$$

Using equation (E-vii) and (E-ix), factor of safety (FS) can be expressed as

$$FS = \frac{\tau}{T} = \frac{C' + C_r' + Cos^2\beta\left[h(\gamma_{Sat} - \gamma_W) + \gamma_t.(D-h)\right]Tan\phi'}{Sin\beta.Cos\beta\left(h\gamma_{Sat} + \gamma_t(D-h)\right)} \qquad \text{(E-x)}$$

Equation (E-x) represents infinite slope stability model (Skepmton and Delory 1959 and Hammond et al. 1992) used in **Chapter 6**. Surcharge has not been included in the model equation in this chapter.